Ministère de l'Enseignement Supérieur et de la Recherche Scientifique

Université Hassiba Benbouali de Chlef

Faculté Technologie

Département d'Electrotechnique

THÈSE

Présentée pour l'obtention du diplôme de

DOCTORAT LMD

Filière : Electrotechnique

Spécialité : commande électrique

Par

KACEMI Walid Mohammed

Thème :

Contribution à la commande des générateurs synchrones à excitation hybride pour la conversion d'énergie Eolienne

"***Contribution to the Control of Hybrid Excitation Synchronous Generators for Wind Energy Conversion*** "

Soutenue le **17/12/2024**, devant le jury composé de:

Dr. MOSTEFAOUI Mohamed	MCA	Université de Chlef	Président
Dr. BOUNADJA Elhadj	MCA	Université de Chlef	Directeur de thèse
Dr. BELHADJ DJILALI Abdelkadir	MCA	Université de Chlef	Co- directeur de thèse
Pr. BELMADANI Bachir	Professeur	Université de Chlef	Examinateur
Dr. BESSAAD Taieb	MCA	Université de Chlef	Examinateur
Dr. MELIANI Bouziane	MCA	Université de Relizane	Examinateur
Pr. TALEB Rachid	Professeur	Université de Chlef	Invité

Acknowledgments

All the work presented in this thesis was carried out in the Laboratory of Electrical Engineering and Renewable Energy (LGEER) at Hassiba Benbouali University - Chlef.

Firstly, I would like to express my deepest gratitude and my sincere thanks to my thesis director, Dr Elhadj Bounadja, MCA at Hassiba Benbouali University - Chlef, and my co-director, Dr Abdelkadir Belhadj Djilali MCA at Hassiba Benbouali University - Chlef, for the valuable advice, ideas, encouragement, guidance, trust and support they gave me to complete this work. I have learned a lot working with them. I particularly appreciate their scientific skills and their remarkable human qualities.

Similarly, I am indebted to the board of examiners for taking from their time to read and assess this humble work, namely, Dr. MOSTEFAOUI Mohamed (the chairman), Prof. BELMADANI Bachir (examiner), Dr. BESSAAD Taieb (examiner), Dr. MELIANI Bouziane (examiner), Pr. TALEB Rachid (guest).

I would also like to thank my teachers and colleagues at Hassiba Benbouali University - Chlef, each by name, for their constant encouragement in the development of this work.

My thanks also go to all those who have helped, directly or indirectly, to the completion of this work.

Finally, I would like to thank all those I may have forgotten to mention and who have helped and supported me from near or far.

Dedication

I have the honor of dedicating this work:

To my very dear parents, may Allah keep them and protect them for their moral and financial support, for their encouragement and the sacrifices they have endured.

To my grandfather Ahmed, may Allah bless him.

To the soul of grandparents Fatima, Zohra and Mohammed.

To my brother SID AHMED and my dear sisters FATIMA and KAWTER.

To all the teachers and educators who have contributed to my training throughout my studies to this day.

To my family and friends and everyone who knows and loves me.

Abstract

ملخص- يجمع المولد التزامني ذو الإثارة الهجينة (HESG) بين مزايا المولد التزامني ذو المغناطيس الدائم، مثل الكفاءة العالية في استغلال الطاقة، ومزايا المولد ذو الإثارة القابلة للتحكم، مما يوفر مرونة كبيرة في التشغيل بسرعات متغيرة. يجعل هذا المزيج منه بديلاً واعدًا للآلات التقليدية في تطبيقات التحويل الكهربائي. تركز هذه الأطروحة على التحكم في المولد التزامني ذو الإثارة الهجينة المدمج في نظام تحويل طاقة الرياح المتصل بالشبكة. أولا، تم تطوير تقنية تحكم متقدمة تعتمد على "التحكم التدريجي (Backstepping Control - BSC)" على جانب المولد لتحسين تتبع نقطة الطاقة القصوى (MPPT) من خلال التدفق الناتج عن ملف الإثارة الإضافي، مما يحسن الأداء العام للمولد.
الجزء الثاني من الأطروحة يقترح طوبولوجيا جديدة حيث يتم توصيل المولد بالشبكة عبر هيكل يتكون من مقوم متتابع – رابط تيار مستمر – عاكس. وعلى عكس الطوبولوجيا التقليدية، تتطلب هذه البنية الجديدة التحكم في العاكس فقط. لهذا الغرض، تم تطوير تقنية تحكم متقدمة تعتمد على خوارزمية الالتواء الفائق المعدلة (ASTC). على عكس تقنية الالتواء الفائق التقليدية (STC)، تعد الطريقة المقترحة، المسماة ASTC، امتدادًا من الدرجة الثالثة لـ STC، حيث يتم استبدال العنصر غير المتصل بوظيفة سلسة ومستمرة. يوفر هذا النهج توازنًا جيدًا بين الدقة ووقت الحساب، مع تقليل تأثير الاهتزاز. أظهرت نتائج هذا البحث إمكانيات HESG في تحسين تحويل طاقة الرياح، مما يقدم حلاً مبتكرًا لاستقرار وكفاءة أنظمة الطاقة. تم التحقق من فعالية تقنيات التحكم المتقدمة المقترحة وتطبيقها في سيناريوهات العالم الواقعي من خلال عمليات محاكاة مفصلة باستخدام بيئة. .MATLAB/Simulink

الكلمات المفتاحية :المولد المتزامن ذو الإثارة الهجينة(HESG) ، تيار الإثارة القابل للتحكم، التحكم بالتراجع(BSC) ، التحكم المتقدم بالالتواء الفائق(ASTC) ، نظام تحويل طاقة الرياح.

Résumé - La Génératrice Synchrone à Excitation Hybride (GSEH) combine les avantages de la génératrice synchrone à aimants permanents, tels qu'un excellent rendement énergétique, et ceux de la génératrice à excitation contrôlable, offrant ainsi une grande flexibilité de fonctionnement à vitesse variable. Cette combinaison en fait une alternative prometteuse aux machines conventionnelles pour les applications de conversion électrique. Cette thèse se concentre sur la commande de la GSEH intégrée dans un système de conversion éolien connecté au réseau. Dans un premier temps, une commande avancée de type "backstepping control (BSC)" est développée pour le côté générateur afin d'optimiser le suivi du point de puissance maximale (MPPT) via le flux généré par la bobine d'excitation supplémentaire, améliorant ainsi les performances globales du générateur. La seconde partie de la thèse propose une nouvelle topologie où la GSEH est connectée au réseau via une structure en cascade redresseur à ponts-bus continu-onduleur. Contrairement aux topologies conventionnelles, cette nouvelle structure ne nécessite que la commande de l'onduleur. Pour cela, une commande avancée basée sur un algorithme de super-twisting (ASTC) modifié a été développée. Contrairement au STC classique, la méthode proposée, appelée ASTC, est une extension au troisième ordre du STC tout en remplaçant le terme discontinu par une fonction douce continue. Cette approche offre un bon compromis entre précision et temps de calcul, tout en réduisant l'effet de chattering. Les résultats de cette recherche démontrent le potentiel de la GSEH à améliorer la conversion d'énergie éolienne, offrant une solution innovante pour la stabilisation et l'efficacité des systèmes énergétiques. L'efficacité des techniques de commande avancées proposées et leur application dans des scénarios réels ont été validées par des simulations détaillées dans l'environnement MATLAB/Simulink.

Mots clés : Génératrice Synchrone à Excitation Hybride (GSEH), Courant d'excitation contrôlable, Control par Backstepping control (BSC), Commande par supertwisting avancée (ASTC), Système de Conversion éolien.

Abstract -The Hybrid Excitation Synchronous Generator (HESG) combines the advantages of a permanent magnet synchronous generator, such as excellent energy efficiency, with those of a controllable excitation generator, offering great flexibility in variable-speed operation. This combination makes it a promising alternative to conventional machines for electrical conversion applications. This thesis focuses on the control of the HESG integrated into a wind energy conversion system connected to the grid. First, an advanced control based on "backstepping control (BSC)" is developed for the generator side to optimize the maximum power point tracking (MPPT) via the flux generated by the additional excitation coil, thereby improving the overall performance of the generator. The second part of the thesis proposes a new topology where the HESG is connected to the grid via a cascaded rectifier-dc link-inverter structure. Unlike conventional topologies, this new structure only requires the control of the inverter. For this, an advanced control based on a modified super-twisting algorithm (ASTC) was developed. Unlike the classical STC, the proposed method, called ASTC, is a third-order extension of the STC, replacing the discontinuous term with a smooth continuous function. This approach offers a good compromise between precision and computation time, while reducing the chattering effect. The results of this research demonstrate the potential of the HESG to improve wind energy conversion, offering an innovative solution for the stabilization and efficiency of energy systems. The effectiveness of the proposed advanced control techniques and their application in real-world scenarios were validated through detailed simulations in the MATLAB/Simulink environment.

Keywords: Hybrid Excitation Synchronous Generator (HESG), Controllable Excitation Current, Backstepping Control (BSC), Advanced Super-Twisting Control (ASTC), Wind Energy Conversion System.

Table of Contents

Nomenclature

Acronyms

HESG	Hybrid excitation synchronous Generator
WECS	Wind Energy Conversion Systems
MPPT	Maximum Power Point Tracker
WT	Wind Turbine
THD	Total Harmonic Distortion
DC	Direct Current
POR	Point Of Regulation
PLL	Phase Locked Loop
GSC	Grid Sid control
MSC	Machine Sid control
BSC	Backstepping control
STC	Super twisting control
ASTC	Advanced super twisting

Turbine

C_p	Power coefficient
V	Wind speed
P_t	Aerodynamic power
T_t	Aerodynamic torque
T_g	Generator torque
Λ	Tip-speed ratio
P	Air density
R	Radius of the turbine
Ω_t	Mechanical speed of the turbine
Ω_g	Mechanical speed of the generator
B	Blade-pitch angle
G	Gearbox ratio
J	Total inertia

Generator

I_s	Stator current
Ψ_5	Excitation flux
M_e	Mutual inductance vector between stator and excitation coil
L_f	Excitation inductance
L_s	Stator inductance matrix
R	Armature resistance
R_f	Excitation coil resistance
R	Electrical pulsation
σ	Blondel coefficient
P	Number of pole pairs
L_d	d-axis armature inductance
Lq	q-axis armature inductance
M	Mutual inductance between d-axis

List of Figures

Chapiter I An Overview of WECS Technologies

Chapter II Principles and Tools for Modeling HESG -based WECS

Chapter III Backstepping Control for MPPT in HESG-Based WECS with Isolated Load

Chapiter IV Advanced Super-Twisting Control for Grid-Connected HESG-Based WECS

List of Tables

Chapter I An Overview of WECS Technologies

Chapter IV Advanced Super-Twisting Control for Grid-Connected HESG-Based WECS

Appendix

General Introduction

1. General introduction

The exploitation of wind energy has a deep-rooted history, tracing back thousands of years, where it initially served fundamental purposes. Around 200 BC, simple vertical-axis windmills were developed along the Perso-Afghan borders for essential tasks such as grinding grains and pumping water [1]. These rudimentary windmills demonstrated the potential of wind power as a mechanical energy source. As wind-powered devices spread to other regions, especially Europe, their design and applications evolved to accommodate more complex needs. Between 1300 and 1875, horizontal-axis windmills became prominent in Europe, particularly in the Netherlands and Mediterranean regions. These windmills facilitated tasks like draining wetlands and milling grain, making wind energy an invaluable resource for agriculture and community needs [1].

The 19th century marked a notable development in wind energy technology, especially in the United States. During this period, over six million small wind machines were installed in rural areas, primarily for water pumping [2]. This application demonstrated wind energy's feasibility as a distributed, localized power source. In 1888, a critical milestone was reached when the first electricity-generating wind turbine was installed in Cleveland, Ohio. This turbine had a capacity of 12 kW and marked the transition of wind energy from mechanical applications to electrical power generation [1]. This shift highlighted the potential of wind energy to support the increasing demand for electricity, setting the stage for modern wind energy systems.

The 1970s introduced a renewed interest in wind energy as the oil crises and environmental awareness heightened the need for clean, renewable energy sources. Governments and industries globally started to invest in wind energy research, leading to advancements in aerodynamics, materials science, and turbine design by the 1990s. These developments, supported by policy incentives and rising environmental concerns, allowed wind energy to emerge as a competitive resource in the global energy market. Modern Wind Energy Conversion Systems (WECS) incorporate innovative technologies to improve efficiency, reliability, and scalability, underscoring wind energy’s role in reducing greenhouse gas emissions and facilitating the transition to a sustainable energy future [3].

2. Background of wind energy conversion systems (WECS)

Wind Energy Conversion Systems (WECS) are engineered to capture the kinetic energy of the wind and convert it into usable electrical power through the integrated use of turbines, generators, and control systems. The turbine acts as the initial point of energy capture, converting the wind's kinetic energy into mechanical power. This mechanical energy is then transformed into electrical power through the generator. WECS have evolved significantly over time, incorporating advanced technologies in turbine aerodynamics, generator materials, and sophisticated control mechanisms to maximize their efficiency and adaptability to varying wind conditions.

A critical aspect of WECS performance is the type of generator employed, as it dictates efficiency, robustness, and adaptability. Traditional generators, such as asynchronous (induction) and synchronous machines, have been widely used in WECS. However, advancements in generator technology have introduced Permanent Magnet Synchronous Generators (PMSG) and, more recently, Hybrid Excited Synchronous Generators (HESG). The HESG represents a significant advancement in generator technology as it combines the benefits of permanent magnets and wound-field excitations. This combination enables better control over magnetic flux, making it adaptable to fluctuating wind speeds. Such adaptability is essential in environments where wind patterns are inconsistent, as it allows HESG-based WECS to maintain high efficiency and stability under varying conditions [4].

The flexibility provided by HESG in controlling magnetic flux distinguishes it from traditional generator types, which may struggle to maintain efficiency under variable wind conditions. HESG technology allows for dynamic adjustments to magnetic flux, optimizing power output while reducing mechanical stresses on turbine components. This adaptability not only increases energy capture but also contributes to the system's durability by minimizing wear on mechanical parts. By incorporating HESG, WECS are better equipped to handle real-world wind conditions, making them a reliable option for both onshore and offshore wind installations where environmental variables play a significant role.

3. Research problem

Despite the technological advancements in wind energy, WECS face several persistent challenges that limit their operational efficiency and longevity. One of the

primary issues is the variability in wind speed, which leads to fluctuating power output. This fluctuation affects the stability of the power grid and poses challenges for maintaining consistent efficiency within WECS. Additionally, the mechanical components of WECS, especially the drive shaft and blade root, are subject to mechanical fatigue due to constant wind-induced loads. This fatigue leads to premature wear, increasing the frequency of maintenance and decreasing the system's operational life.

Addressing these challenges requires advanced control strategies that can optimize energy capture while minimizing the physical stresses imposed on WECS components. Traditional generators like asynchronous and synchronous machines have limitations when exposed to these conditions, especially in environments with unpredictable wind patterns. The introduction of the HESG offers a potential solution to these issues, but its applications in WECS are still relatively unexplored. The primary research question for this study is to determine whether HESG technology can enhance WECS by improving efficiency, stability, and mechanical durability. By developing and testing control strategies tailored for HESG, this study seeks to contribute to the advancement of resilient and efficient wind energy systems that can meet modern energy demands.

4. Objectives of the research

The main objective of this thesis is to validate the feasibility and advantages of integrating HESG technology within WECS and to develop control strategies that maximize energy capture, reduce mechanical fatigue, and enhance system robustness. The objectives can be broken down as follows:

- **Maximizing energy efficiency**: This study aims to optimize WECS performance across all operational zones, from partial load regions—where maximizing power capture is essential—to full load regions—where power regulation and system stability are prioritized. Achieving this objective involves designing control strategies capable of dynamically adjusting system parameters in response to changing wind conditions to ensure continuous high-efficiency operation.
- **Reducing mechanical fatigue:** Mechanical fatigue is particularly significant in high-stress components like the drive shaft and blade root. The study aims to implement control laws that mitigate vibrations and mechanical stresses associated with fluctuating wind loads. By minimizing these stresses, the control strategies are

expected to extend the lifespan of these components, reducing maintenance requirements and improving overall system reliability.

- **Enhancing system robustness:** Given the inherent variability in wind and the susceptibility of WECS to environmental disturbances, the control system must be resilient enough to maintain stable performance under diverse conditions. The study aims to develop robust control strategies that can handle parameter variations and external disturbances, ensuring consistent performance across a range of wind conditions.

5. Methodology overview

The methodology employed in this research is designed to optimize WECS performance through the application and testing of advanced control strategies tailored specifically to HESG-based systems. The methodology encompasses several key elements, including the design of control systems, development of a simulation model, and scalability testing to evaluate performance under realistic operating conditions.

- ✓ **Control strategies:** This study proposes two primary control techniques—the backstepping controller (BSC) and an advanced super twisting control (ASTC). The BSC offers a step-by-step design approach that allows for precise control over generator speed, facilitating optimal energy capture. On the other hand, the ASTC is known for its robustness against parameter uncertainties and environmental disturbances, making it ideal for managing variability in wind conditions. Together, these control strategies are designed to maintain smooth and efficient operation of the HESG, ensuring optimal performance across different wind scenarios.
- ✓ **Simulation platform:** A comprehensive MATLAB/Simulink simulation model was developed to test the control strategies' effectiveness. This model includes critical elements of WECS, such as converter switching effects, generator space harmonics, and mechanical coupling, to simulate the behavior of a 2-kW wind turbine equipped with an HESG. The simulation provides a controlled environment to assess the performance of each control strategy in terms of energy production efficiency, mechanical stress reduction, and system stability.
- ✓ **Scaling to larger systems:** Following successful validation in a small-scale setting, the study expands to a 1.5 MW wind turbine model. This larger model allows for testing the scalability of HESG technology and the robustness of the control

strategies under conditions typical of commercial wind farms. This scale-up offers insights into the feasibility of deploying HESG in large-scale WECS and examines the adaptability of the control strategies for grid-connected applications, ensuring that the proposed solutions are practical for real-world deployment.

6. Significance of the study

This research is significant for several reasons:

1. **Enhanced WECS efficiency**: By developing control strategies tailored specifically to HESG, this study enhances the efficiency of WECS, contributing to the global goal of reducing reliance on fossil fuels. Increased efficiency enables WECS to capture wind energy more effectively, particularly in regions with variable wind conditions where traditional systems may struggle to maintain consistent performance.

2. **Reduction of operational Costs**: Advanced control strategies that reduce mechanical fatigue can extend the operational lifespan of critical WECS components, thereby lowering maintenance and replacement costs. This benefit is especially relevant for large-scale wind farms, where operational expenses are a significant consideration in the financial viability of wind energy projects. By lowering these costs, the study supports the economic sustainability of wind energy as a renewable resource.

3. **Advancement in control methodologies**: The application of backstepping and super twisting control strategies in HESG-based WECS introduces a novel approach to managing the challenges of wind energy systems. This advancement in control methodology contributes to the ongoing development of high-performance, resilient renewable energy systems, setting a foundation for future research on HESG technology and its potential applications in wind energy and other renewable fields.

7. Thesis structure

This thesis is organized into four main chapters:

- **Chapter I: An Overview of WECS Technologies**: This chapter provides a comprehensive overview of wind turbine technology, including the operational principles of horizontal-axis and vertical-axis turbines. It also discusses various types of generators, such as asynchronous, synchronous, and HESG, emphasizing their advantages and disadvantages. Special attention is given to HESG, which combines the benefits of permanent magnet and wound-field excitations, making it particularly well-suited to varying wind conditions.

- **Chapter II: Principles and Tools for Modeling HESG -based WECS**: This chapter presents the principles and methodologies used for modeling WECS, incorporating aerodynamic, mechanical, and electrical dynamics specific to HESG. Matlab/Simulink is used to develop a realistic simulation model, providing a foundation for testing the proposed control strategies under conditions that closely resemble real-world WECS operations. The chapter also addresses the challenges associated with accurately modeling the unique characteristics of HESG within WECS.

- **Chapter III: Backstepping Control for MPPT in HESG-Based WECS with Isolated Load**: This chapter focuses on the design and implementation of the control strategies employed in this study. It covers the inner current loop, which is regulated by a proportional-integral (PI) controller, and the outer speed loop, which is managed by a backstepping controller (BSC). A comparative study of PI and BSC controllers is conducted to evaluate their performance under different wind conditions, providing insights into each controller's strengths and limitations.

- **Chapter IV: Advanced Super-Twisting Control for Grid-Connected HESG-Based WECS**: In this chapter, the study addresses the challenges of integrating HESG-based WECS into the electrical grid. Using a 1.5 MW model, the chapter examines grid connectivity requirements, including synchronization, voltage regulation, and reactive power management. An advanced super twisting control (ASTC) strategy is implemented for regulating active and reactive power, focusing on pitch regulation to maximize aerodynamic efficiency and reduce structural loads on turbine components. This chapter also discusses the potential for HESG-based WECS to contribute to grid stability, particularly in terms of frequency and voltage support.

Chapter I: An Overview of WECS Technologies

I.1 Introduction

The exploitation of wind energy has a deep-rooted history, tracing back thousands of years, where it initially served fundamental purposes. Around 200 BC, simple vertical-axis windmills were developed along the Perso-Afghan borders for essential tasks such as grinding grains and pumping water [1]. These rudimentary windmills demonstrated the potential of wind power as a mechanical energy source. As wind-powered devices spread to other regions, especially Europe, their design and applications evolved to accommodate more complex needs. Between 1300 and 1875, horizontal-axis windmills became prominent in Europe, particularly in the Netherlands and Mediterranean regions. These windmills facilitated tasks like draining wetlands and milling grain, making wind energy an invaluable resource for agriculture and community needs [1].

The 19th century marked a notable development in wind energy technology, especially in the United States. During this period, over six million small wind machines were installed in rural areas, primarily for water pumping [2]. This application demonstrated wind energy's feasibility as a distributed, localized power source. In 1888, a critical milestone was reached when the first electricity-generating wind turbine was installed in Cleveland, Ohio. This turbine had a capacity of 12 kW and marked the transition of wind energy from mechanical applications to electrical power generation [1]. This shift highlighted the potential of wind energy to support the increasing demand for electricity, setting the stage for modern wind energy systems.

This chapter provides an overview of the overall context in which the thesis is situated. We start by establishing the significance of wind energy and its overall expansion. Next, a comprehensive examination of the generators employed in contemporary wind systems is provided. Subsequently, we suggest an alternative to traditional generators using the HESG.

I.2 History of wind energy

Humans have been utilizing wind energy for a very long time. Approximately 3000 years ago, the Egyptians used this energy source for water pumping, predating the discovery of coal and refined oil. Vertical axis windmills were utilized in the Afghan highlands as early as the 7th century BC to grind wheat and rice. Thus, at first, the wind's

kinetic energy was only transformed into mechanical energy [7] and [8]. The first windmills appeared in Europe at the beginning of the Middle Ages. Charles Brush and his associates created the first system for generating electricity from wind speed 1887 and built it on the Atlantic coast. The turbine had a diameter of 17 m and was fitted with a rotational speed of 144 rad/s. This production is based on a 12 kW DC generator to charge batteries and for the continuous supply of lamps and motors. The oil crisis of 1973 revived interest in these electricity production systems and again relaunched wind research and development worldwide.

I.3 Utilization of wind energy

Wind energy (WE) is experiencing significant expansion in Europe, America, and Asia. The Global WE Council (GWEC) reported that the total installed installed output of WE reached approximately 500 GW in 2017, as shown in Figure I.1. [9].

In 2019, the global installed wind capacity experienced a growth of 19% in comparison to the previous year, 2018. Despite the disruptions caused by the COVID-19 pandemic on supply and construction chains, 21.5 gigawatts (GW) of new installations were completed in the first half of 2020 [10]. In the second half, the number of new installations climbed by a factor of five compared to the first half, resulting in a global installed capacity of 743 GW [9]. This signifies a yearly increase of 59% compared to 2019 and a substantial growth of 77.4% compared to 2018. These numbers demonstrate the comprehensive development of this business and the worldwide dedication to expediting investments in wind energy. Nevertheless, a distinct disparity is evident in local marketplaces across different regions. This difference might be attributed to economic, natural, or geopolitical issues.

The Wind Europe organization predicts that wind energy will have the capacity to meet 35% of the European Union's electricity demand by 2030 [11]. By 2030, the United Nations plans to meet 20% of its electricity requirements through wind power [12]. Asia is the biggest market for wind energy. China aims to achieve a wind energy installation capacity of 200 GW by 2020, 400 GW by 2030, and 1,000 GW by 2050 [13].

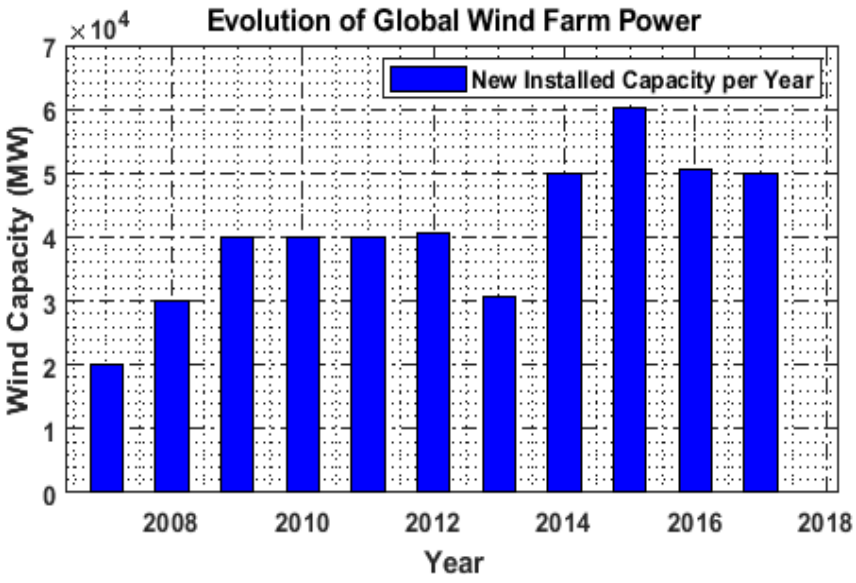

Figure I. 1 *Evolution of global wind fram power*

I.4 Wind energy market: global leaders

The growth of the local wind industry typically mirrors the overall world economic pattern. In 2020, China emerged as the global frontrunner, boasting a total connected capacity of 288.3 GW. The United States is a significant participant in the market, boasting a total capacity of 164.27 GW in 2020. Europe is included in the ranking of the top 5 worldwide wind energy leaders (Table I.1), with a combined capacity of 218.9 GW installed across the continent in 2020. The data presented are the outcome of national plans that have been put into action to encourage the use of wind energy, specifically through the implementation of environmental tax incentives that have been in effect since the 1990s.

Table I. 1 *: Ranking of the Top 5 Global Wind Power Leaders*

Country	Total Installed Capacity (GW)
China	288.3
United States	164.27
Europe	218.9
India	60.04
Canada	13.4

I.4.1 Wind energy in europe

Wind energy accounted for 16.5% of Europe's total electricity demand in 2020, adding 14.36 GW of new installations [9]. In 2020, Germany had Europe's highest wind

energy production, with a total capacity of 62.85 GW. Among the Scandinavian countries, only Sweden is ranked as one of the top producers in terms of renewable energy generation, according to Table I.2 [14]. Sweden has a total installed capacity of 9.8 GW, whereas Denmark has a capacity of around 1.7 GW in 2020.

Table I. 2 *Evolution of Wind Energy Capacity for the Top 5 European Producers.*

Country	2019	2020	Change
Germany	61.4GW	62.85GW	+2.3%
United Kingdom	23.34GW	23.94GW	+2.6%
Spain	25.57GW	25.73GW	+0.6%
France	16.64GW	17.94GW	+7.8%
Sweden	8.8GW	9.8GW	+11.4%

I.4.2 Wind energy in Africa

In Africa, the wind energy sector still needs to be fully developed. As of 2018, the total installed capacity was 5.7 GW, which increased to 6.45 GW in 2019 and 7.27 GW in 2020. Wind energy accounted for 1% of Africa's electricity generation in 2019. Furthermore, the continent's leading producers consist of only three countries: South Africa, which had a total capacity of 2.46 GW in 2020; Egypt, with 1.46 GW; and Kenya, with 338 MW. Tunisia's wind power capacity reached 250 MW in 2019, distributed over three parks in the nation's northern region. The combined output of these parks is 750 GW-hours per year. This figure accounts for merely 3.7% of Tunisia's overall power generation, predicted to be 20.22 TWh per year [15].

Table I. 3 *Top wind energy producers in Africa.*

Country	Total Installed Capacity (GW)
South Africa	2.46
Egypt	1.46
Kenya	0.338
Tunisia	0.25

I.4.3 Wind energy in Algeria

Algeria has a considerable potential for renewable energy that can be technically exploited. Regarding wind energy, Algeria has a 10 MW wind farm in Adrar that was commissioned in June 2014. The electricity generated by this farm is fed into the local grid, and the wind energy penetration rate is estimated to be around 5%.

The total installed wind power capacity in Algeria needs to be more significant. In its new renewable energy program, the Ministry of Energy and Mines has projected to install other wind farms with a total capacity of 1000 MW in the medium term (2015–2020) to reach 5010 MW by 2030.

Figure I.2 shows that the moderate wind regime (2 to 6 m/s) is ideally suited for water pumping, especially in the High Plateaus and the Sahara. The energy potential is enormous, knowing that the Adrar region is in a 6 m/s wind corridor. This is why several wind turbines are installed in Adrar [16].

WE remain one of the most promising sustainable energy solutions to be growth alongside solar energy in Algeria to produce electricity at isolated sites.

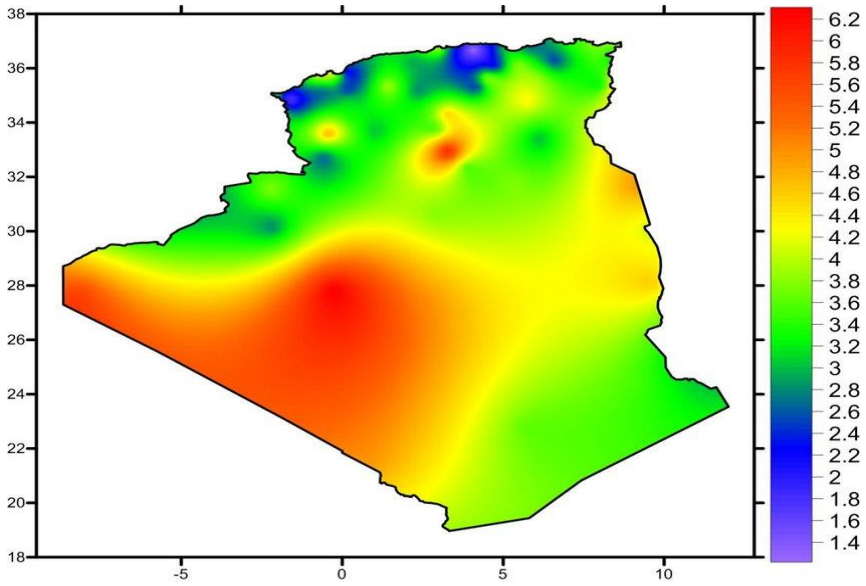

Figure I. 2 *Annual map of average wind speed at 10m above ground level [16].*

I.5 Wind energy market outlook

The global wind energy capacity is 743 GW, installed and operational. The progress must catch up to the estimated 95 TW worldwide wind resource potential projected by the World Wind Energy Association (WWEA) [17]. IRENA's projections indicate that wind capacity will triple by 2030 and expand tenfold by 2050, reaching 5044 GW [17]. These forecasts are derived from the existing market growth rate and are mainly influenced by the tactics implemented by the governments that have ratified the Paris Agreement [18]. The GWEC predicts that the installed capacity of wind energy in Europe will expand by

approximately 15% per year, reaching a total of 322.2 GW by the year 2025 [9]. The "Energy Transition Law for Green Growth" was implemented by the French government in 2015 [19]. One of its goals is to raise the proportion of renewable energy in overall national consumption to 32% by 2030. France's objective with this legislation is to reach a combined wind energy capacity of 40.9 GW linked to the power grid by 2028. Africa The total capacity of WE connected to the power system is projected to reach 14 GW by 2023 [20].

The Tunisian Solar Plan (PST), conducted by the Ministry of Industry, Energy, and Mines and administered by the National Agency for Energy Control, is predicted to increase capacity in Tunisia by 2030. This plan aims to achieve an installed capacity of approximately 3,725 gigawatts (GW) of renewable energy by 2030, with wind power contributing 1.7 GW. By 2050, the United States aims to have 404 GW of installed capacity to fulfill 35% of the nation's electricity requirements [21].

I.6 Advantages and disadvantages of WE

I.6.1 Advantages

The expansion of WE are correlated with the benefits associated with its utilization [22].

- ✓ WE have the primary benefit of being an environmentally friendly power source. Wind energy is a sustainable form of fuel-free energy, emitting no greenhouse emissions and generating no harmful waste. Wind energy plays a role in preserving biodiversity in natural habitats by combating climate change.
- ✓ WE generate electricity without causing air pollution, water pollution (no release into the aquatic environment, no thermal pollution), or soil contamination (no soot or ash).
- ✓ Unlike nuclear energy, wind energy is a non-hazardous form of energy, and it does not generate any radioactive waste.
- ✓ It is a regional energy source that fulfills the energy requirements of the local area. Consequently, the losses incurred by transporting energy over vast distances are reduced. This energy source can invigorate the local economy, particularly in rural regions.
- ✓ When wind farms are erected on agricultural land, just a tiny fraction, approximately 2%, of the land is needed to place wind turbines. The remaining area

is suitable for agricultural use, including livestock farming and other such applications.

- ✓ Wind farms can be destroyed effortlessly and without leaving any discernible evidence.
- ✓ Peak productivity occurs during winter because of the presence of more significant winds. This coincides with the time of year when demand is at its maximum.
- ✓ Wind power provides a reliable source of electricity despite the fluctuating pricing of oil barrels.
- ✓ Wind turbines contribute to local development by generating professional tax revenue. The annual contribution is approximately €10,000 per MW, although this amount may vary depending on the towns involved. Therefore, several rural communities can rejuvenate and do tasks that they were previously indebted for.
- ✓ The price of a wind turbine has significantly decreased since 2011 due to the realized economies of scale in their production [23,24].

I.6.2 Disadvantages

- ✓ This source of energy also has disadvantages that need to be studied so that they do not become a barrier to its development:
- ✓ **Noise**: Noise has been significantly reduced, especially mechanical noise, which has practically disappeared thanks to advances in the multiplier. Aerodynamic noise, on the other hand, is related to the rotor's rotation speed, and this must therefore be limited.
- ✓ **Wind energy is intermittent energy**: The efficiency of a wind turbine in generating power is contingent upon the meteorological conditions, making it challenging to accurately forecast the amount of electricity it will produce over a given period. The turbine rotor will remain stationary if the wind speed is insufficient on a particular day. Consequently, wind energy is intermittently accessible for distribution during periods of high electricity demand.
- ✓ **Visual impact**: Land-based wind turbines tend to disfigure the landscape, but this idea needs to be remembered with the advent of offshore farms.
- ✓ **Impact on birds**: Some studies show that migratory birds adapt to obstacles and can avoid wind farms [25]. Other studies say that wind farms should not be located on bird migration routes to avoid getting caught in the wind turbine blades.

Multiple studies indicate that the quantity of birds that perish as a result of wind turbines is insignificant when compared to the number of birds who die due to other human activities [7].

- ✓ The cost of wind energy compared to conventional energy sources.

I.7 The different classification of WE

The development of the WE sector is closely tied to advancements in wind turbine design and operational technology. This section examines the many classifications of wind turbines and the processes involved in their installation.

I.7.1 Vertical-axis wind turbine (VAWT)

The development of vertical-axis wind turbines marked the initial creation of buildings designed to generate power, which was in contrast to the conventional horizontal-axis windmills. The primary rotor shaft is perpendicular to the wind (although not required in a vertical orientation), whereas the primary components are situated at the turbine's base. This configuration enables the placement of the generator and gearbox near the ground, hence facilitating maintenance and repair.

The vertical design has the benefit of positioning the multiplier and generator at ground level. Nevertheless, the wind turbine is compelled to function with less mighty wind at lower altitudes due to the decelerating impact of the topography. The central vertical axis turbines consist of the Savonius rotor, the conventional Darrieus rotor, and the H-shaped Darrieus (refer to Figure 3).

Figure I. 3 *Vertical-axis Wind Turbines*

I.7.2 Horizontal -axis wind turbine

Windmills served as the inspiration for horizontal-axis wind turbines. They comprise many blades with an aerodynamic shape resembling airplane wings. The purpose of deploying these wings in the wind is not to provide lift for an aircraft but rather to generate a torque that initiates rotation.

A horizontal-axis wind turbine can be categorized as a single-bladed, double-bladed, triple-bladed, or multi-bladed turbine, depending on its number of blades. A wind turbine with only one blade is more cost-effective due to its reduced material usage. Nevertheless, including a counterbalance is essential for the operation of this particular wind turbine design, which has limited its popularity.

Like single-bladed rotors, two-bladed rotors require a tilting rotor mechanism to avoid excessive impact on the wind turbine when a rotor blade moves in front of the tower. Consequently, to address these issues, nearly all wind turbines currently being erected or planned for the near future are of the three-bladed variety. These objects are more stable due to their generally homogenous aerodynamic load and possess the highest power coefficient.

Horizontal-axis wind turbines are more commonly utilized due to their superior aerodynamic efficiency compared to vertical-axis wind turbines. Figure 4 displays illustrations of horizontal wind turbines.

Figure I. 4 *Horizontal -axis Wind Turbines*

I.8 Fixed and variable speed wind turbines

The classification criterion for wind turbines is their operating speed. Under this classification, we distinguish two categories:

I.8.1 Fixed-speed wind turbines:

The electrical generator is connected directly to the power grid in this particular wind turbine design. As a result, the speed of the wind turbine is determined by the frequency of the grid and the number of pole pairs in the machine. There is no need for frequency management, resulting in cost and complexity savings on the grid side. This kind of wind turbine utilizes an asynchronous machine and commonly employs an aerodynamic stall control mechanism to optimize energy extraction [26].

I.8.2 Variable speed wind turbines:

For optimal energy extraction, operating across a broad range of speeds is preferable. The generator's rotational speed must be adjusted to match the wind speed to maximize energy extraction, regardless of the wind profile. This behavior can be accomplished with variable-speed wind turbines. Furthermore, this particular wind turbine design can provide enhanced stability during unpredictable wind conditions by reducing oscillations in the transmission system. Variable-speed wind turbines are better suited for high-power applications due to their more significant dimensions, which result in greater aerodynamic forces. Power electronics interfaces are necessary to connect this particular type of wind turbine and the electrical grid. Static converters are employed. The complexity and cost of the converters are determined mainly by the type of generator used, which can either be synchronous or asynchronous and also by the specific location of the wind turbine.

I.9 Onshore and offshore wind turbines

Selecting a specific geographical location for establishing a wind farm mainly relies on the wind capacity in the area under consideration and the corresponding statistical data. Within this framework, we categorize installations into two distinct types:

I.9.1 Onshore wind turbines:

This particular design of wind turbine is a key contributor to the generation of wind energy, accounting for a significant portion of the global installed capacity of 707 GW in 2020 [9]. In 2019, an additional 86.9 GW were added, further bolstering its prominence. Onshore wind turbines are the earliest type of wind turbine installation, dating back to the introduction of windmills. Their power rating can reach several megawatts. Currently, the largest onshore wind turbine is the Cypress 6 MW wind turbine, which General Electric launched in 2020. It boasts a rotor diameter of 164 meters. This installation type is distinguished by a highly competitive cost per MWh/year in comparison to conventional sources. Consequently, this elucidates the reason behind their current status as the most prevalent form of installation worldwide.

I.9.2 Offshore wind turbines:

The fundamental idea of converting kinetic energy is what largely determines the location of wind farms. As the size of the turbine blades increases, so does the amount of surface area they cover. Consequently, they are able to capture more wind and generate a greater amount of energy. Nevertheless, the amplification of wind turbine dimensions results in substantial noise pollution, rendering them unsuitable for installation in close proximity to urban regions [27]. Consequently, offshore wind turbines have been created as a result. The emergence of offshore wind turbines can be traced back to 1991 in Denmark. Offshore wind turbines have a greater energy output contrast with onshore wind turbines, but they also come with a higher cost per megawatt-hour per year. Presently, offshore wind turbines comprise merely 4% of the total global installed capacity, with highly ambitious potential [28]. Table 4 is provided, which presents a concise overview of the main distinctions between onshore and offshore wind turbines.

Table I. 4 *onshore vs offshore*

Feature	**Onshore Wind Turbines**	**Offshore Wind Turbines**
Location	On land	In the sea
Wind speed	Lower	Higher
Noise pollution	Higher	Lower
Cost	Lower	Higher
Capacity	Smaller	Larger
Yield	Lower	Higher
Number of installations	Higher	Stable
Future prospects	Stable	Growing

I.10 Wind turbines connected to the grid and to an isolated load

Another categorization criterion is closely associated with how the energy generated by the wind turbine is dispersed and utilized. Within this particular framework, we categorize installations into two distinct categories.

I.10.1 Wind turbines connected to an isolated load

In the case of this particular wind turbine, the isolated load typically refers to a rural village, a business, or even a residential complex [29]. Wind turbines were designed to connect to a load not connected to the energy distribution grid to offer a sustainable option in places with a low population not served by the grid. Diesel engines and generators are typically the primary energy sources in these areas. Implementing wind turbines in these regions has effectively mitigated carbon emissions. Nevertheless, a wind turbine connected to a load not connected to a larger power grid often has a low power output, often in the range of a few tens of kilowatts. This limited power output prevents fully utilizing the wind's true potential [29].

I.10.2 Wind turbines connected to the electrical grid

Grid-connected wind turbines accounted for almost 95% of global wind power generation in 2017 [30]. This particular wind turbine design is the prevailing installation method onshore and offshore wind farms. These wind turbines are high-power and operate in a fully connected mode, meaning that all the energy they generate is directly sent into the distribution system. Grid-connected installations allow for extensive wind energy utilization on a broad scale, unlike individual wind turbines operating in isolation. In 2016, wind turbines contributed 6% of the global electricity generated from renewable sources [31].

I.11 Literature review on different types of wind generators

There are two types of wind turbines: fixed-speed (FS) and variable-speed (VS). The FS wind turbines typically employ either a squirrel-cage induction generator or a wound-rotor asynchronous generator, both of which lack a power electronics interface. Conversely, VS wind turbines necessitate a power converter, either partial or full-scale, to regulate the flow of power. In addition, they offer a diverse array of choices for selecting a

generator and its corresponding power converter.

Asynchronous and synchronous machines are the predominant generators in this type of wind turbine. Opting for the appropriate generator is essential to harnessing wind energy across various wind velocities, particularly in low winds where a high-efficiency conversion system is necessary.

The process of choosing an electric alternator for an independent system was examined in [32]. The comparison between induction and synchronous alternator led to the conclusion that the Permanent Magnet (PM) synchronous generator is the most suitable choice for independent operation.

Several articles in [33] have specifically examined induction generators as fully developed machines for independent WE systems. The SCIG has been endorsed by [34] and [35] as a straightforward, sturdy, brushless, and cost-effective generator. Nevertheless, the appeal of using such a generator may diminish when its performance is considered. A study conducted in [36] assessed the losses, output powers, and efficiency of a WECS using a squirrel-cage induction generator, a DFIG, and a PMSG, with wind speed as the variable. Research has demonstrated that the SCIG exhibits the lowest efficiency level, mainly when operating at low rotational speeds.

This paragraph will describe the most commonly utilized generators for stand-alone WECS. The following will be presented:

- Brushless DFIG
- Brushless doubly-fed VRG
- Permanent Magnet Induction Generator **(**PMIG)
- Variable Reluctance Generator (VRG)
- Permanent Magnet Synchronous Generator (PMSG)
- Wound Rotor induction Generator (WRIG)
- Squirrel-Cage Induction Generator (SCIG)
- DFIG

- Wound Rotor Synchronous Generator

I.11.1 Wound rotor induction generator

A starter requires a WECS that utilizes a wind-driven WRIG to minimize the initial electric current surge during the system's start-up phase (figure I.5). Furthermore, the notion necessitates the need for reactive power adjustment. The autonomous WRIG is easily regulated to generate consistent voltages with a fixed amplitude and frequency [37]. Because of the restricted range of speed fluctuation, fixed-speed wind energy systems have relied on employing WRIG for an extended period instead of variable-speed systems.

The stator of the WRIG is directly linked to the electrical grid, while the rotor winding is connected in series with an adjustable resistance. Controlling the energy taken from the rotor of the WRIG allows for the achievement of variable speed operation. Nevertheless, its power will be dispersed or lost in the external resistance. In order to enhance the dynamic speed range, it is necessary to raise the slip, resulting in greater power being taken by the rotor and reduced efficiency of the generator due to the need for more significant resistance.

The main problems with WECS that use WRIG are that they need a starter, can only go at a certain speed, and are less efficient because of power loss in the external resistance. In addition, the WRIG is not a desirable choice for use in isolated places because of the need for frequent maintenance and replacement of the brush-collector system, which can be challenging and costly.

I.11.1.1 Advantages of WRIG:

- ✓ Simple and robust construction
- ✓ Low cost
- ✓ Wide speed range
- ✓ High efficiency

I.11.1.2 Disadvantages of WRIG

- ✓ Need for a starter

- ✓ Reactive power compensation required
- ✓ Limited speed variation range
- ✓ Decreased performance resulting from power dissipation in the external resistance.
- ✓ Brush-collector system requires regular maintenance

I.11.1.3 Applications of WRIG

- ✓ FSWT
- ✓ VSWT (with additional control systems)
- ✓ Electric vehicles
- ✓ Industrial drives

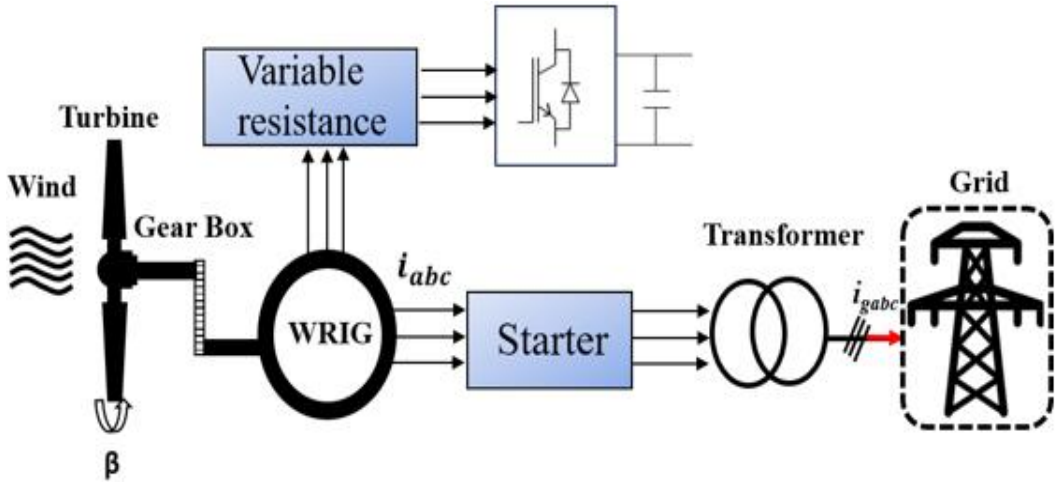

***Figure I. 5** WRIG based Wind Turbines*

I.11.2 Squirrel-cage induction generator (SCIG)

The SCIG is the most compact, cost-effective, and durable among conventional induction generators [38]. SCIG-based wind turbines, depicted in Figure I.6, have garnered attention in numerous research projects focused on developing emulators, power converters, control schemes, self-excitation techniques, and grid connections for stand-alone applications [39]. The maturity of the machine is what drives these projects, which specifically target wind energy applications.

I.11.2.1 Advantages of SCIG

- ✓ Simple and robust construction
- ✓ Low cost
- ✓ High efficiency
- ✓ Wide availability

I.11.2.2 Disadvantages of SCIG

- ✓ Narrow speed variation range
- ✓ Requires a gearbox
- ✓ High mechanical stress at fixed speed
- ✓ Not suitable for direct grid connection

I.11.2.3 Applications of SCIG

- ✓ FSWT
- ✓ VSWT (with additional control systems)
- ✓ Electric vehicles
- ✓ Industrial drives.

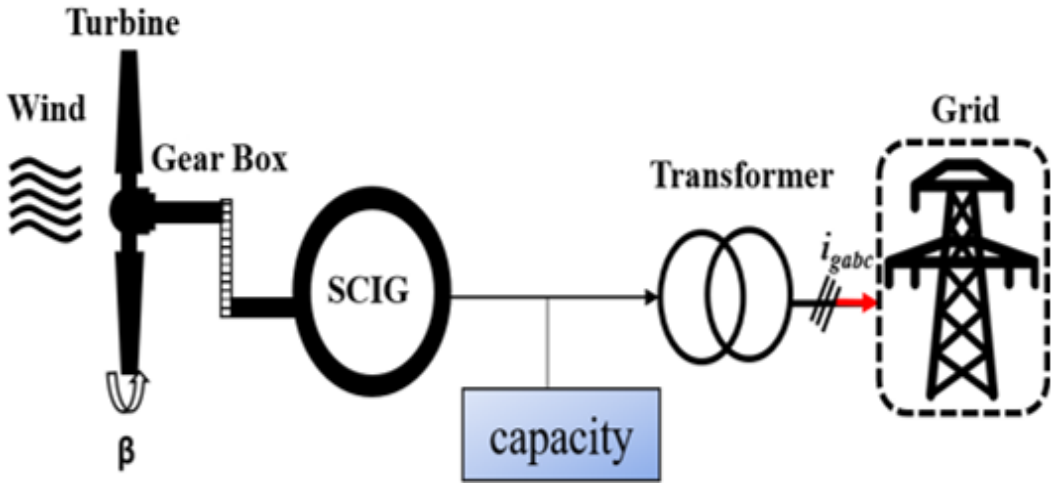

Figure I. 6 *SCIG based Wind Turbines*

I.11.3 Doubly fed induction generator (DFIG)

A DFIG-based WE is constructed by directly linking the stator to the grid and connecting the rotor through a power electronic converter of reduced capacity to the Point of Common Coupling (PCC) (figure I.7). The power flow through the stator is always in

one direction, while the direction of power flow via the rotor varies depending on the generator's working mode. The rotor is supplied with power when the generator runs at a speed lower than synchronous speed. When the generator runs at a speed higher than its synchronous speed, the rotor transfers power. The power converter regulates the frequency of the rotor. This architectural design enables functioning throughout a broad speed range, approximately 30% above and below the synchronous speed.

I.11.3.1 Advantages of DFIG

- ✓ Wide speed range
- ✓ Reduced power converter rating
- ✓ High efficiency
- ✓ Improved power quality

I.11.3.2 Disadvantages of DFIG

- ✓ Requires a gearbox
- ✓ The slip-ring system requires maintenance
- ✓ More complex control systems

I.11.3.3 Applications of DFIG

- ✓ Variable-speed wind turbines
- ✓ Electric vehicles
- ✓ Industrial drives

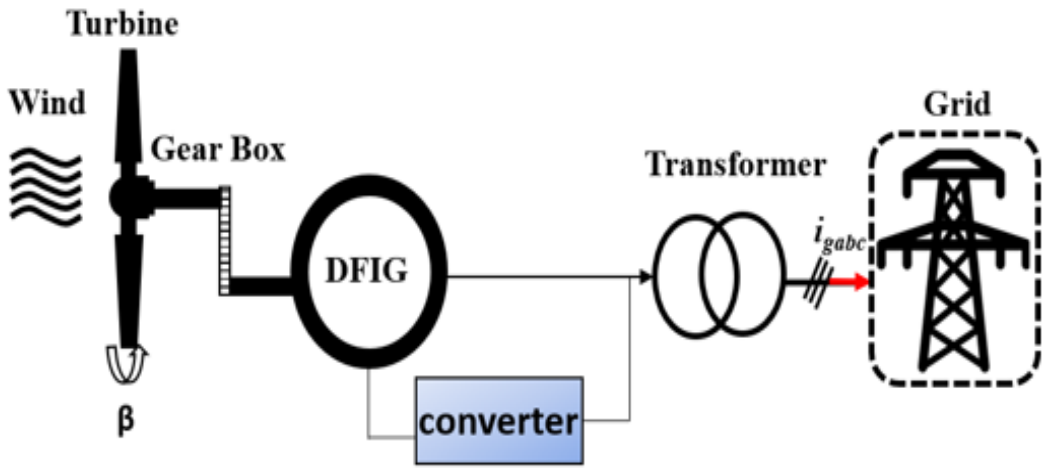

Figure I. 7 *DFIG based wind turbines*

I.11.4 Wound rotor synchronous generator (WRSG)

Stand-alone WECS that utilize a WRSG (as shown in Figure I.8) necessitate DC excitation. Power can be supplied through either an DC outside source using slip rings and brushes or a brushless exciter consisting of a power converter and an auxiliary AC generator. This architectural design was suggested in the publication referenced as [40]. The authors of [40] regard this method as a promising substitute for fulfilling the requirements in situations involving separate loads.

I.11.4.1 Advantages of WRSG

- ✓ Wide speed range
- ✓ High efficiency
- ✓ Good power quality
- ✓ There is no need for a gearbox

I.11.4.2 Disadvantages of WRSG

- ✓ Requires DC excitation
- ✓ The slip-ring system requires maintenance
- ✓ More complex control systems

I.11.4.3 Applications of WRSG

- ✓ Variable-speed wind turbines
- ✓ Hydroelectric generators
- ✓ Industrial drives

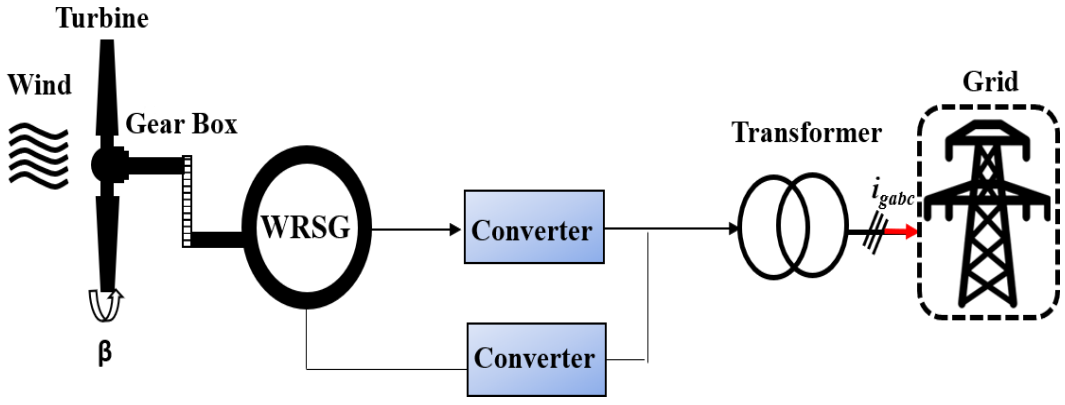

Figure I. 8 WRSG based wind turbines.

I.11.5 Permanent magnet induction generator (PMIG)

The induction generator needs help in voltage control because it relies on a magnetizing current obtained from an excitation source [41]. The induction generator's power factor and efficiency are both reduced by this [42]. Utilizing PMIG can enhance the power factor, voltage regulation, and efficiency [42]. The stator of the PISG is comparable to that of the conventional induction generator, although its rotor design differs. The PMIG comprises two rotor components: a SG rotor and a PM rotor. Due to the partial excitation of the squirrel cage rotor by the permanent magnet rotor, the PMIG-based wind energy system requires less reactive power from an external source. As a result, the capacitance size in a PMIG-based system is smaller than that of a WECS based on WRIG. Furthermore, the PMIG can be operated without the need for a gearbox. There are two conceivable configurations for PMIG-based WECS. The illustrations can be found in Figure I.9.

I.11.5.1 Advantages of PMIG

- ✓ High efficiency
- ✓ High power factor
- ✓ Good voltage regulation
- ✓ Wide speed range
- ✓ No need for a gearbox

I.11.5.2 Disadvantages of PMIG

- ✓ Higher cost than induction generators
- ✓ Complex control system

I.11.5.3 Applications of PMSG

- ✓ Variable-speed wind turbines
- ✓ Electric vehicles

- ✓ Industrial drives

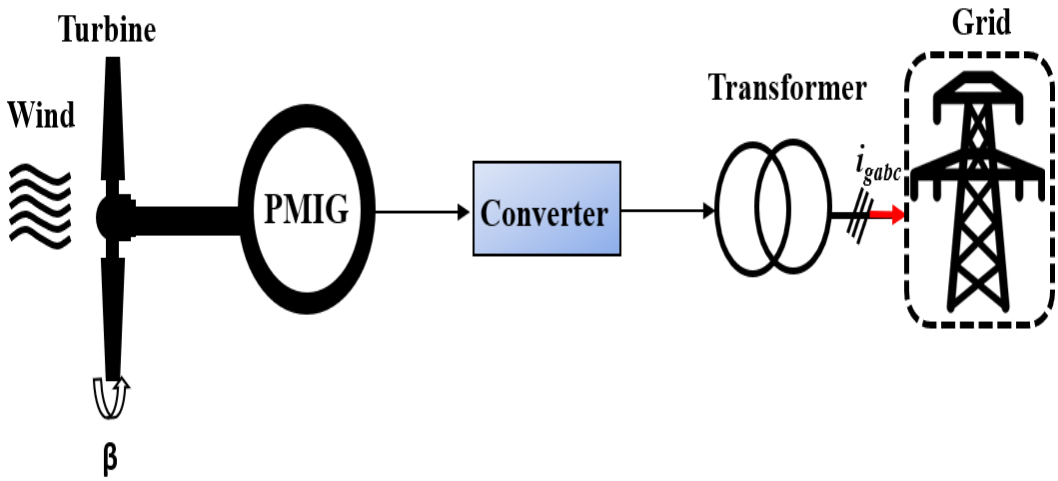

Figure I. 9 *PMIG based wind turbines.*

I.11.6 Variable Reluctance Generator (VRG)

The VRG is a machine that is both structurally simple and sturdy. The stator and rotor are typically constructed from steel sheets. The stator is composed of prominent poles that are surrounded by concentrated windings. The rotor is comprised of salient poles and does not contain windings or permanent magnets [43]. Typically, the machine is powered by a half-bridge converter. The VRG, known for its simplicity, durability, dependability, and affordability, has demonstrated promising capabilities as a direct drive generator in both stand-alone SCEs [44] and grid-connected wind systems [45] (Figure I.10).

I.11.6.1 Advantages of VRG

- ✓ Simple and robust construction
- ✓ Low cost
- ✓ High efficiency
- ✓ Wide speed range
- ✓ No need for rare-earth materials

I.11.6.2 Disadvantages of VRG

- ✓ Complex control system
- ✓ Torque ripple
- ✓ Acoustic noise

I.11.6.3 Applications of VRG

- ✓ Variable-speed wind turbines
- ✓ Electric vehicles
- ✓ Industrial drives

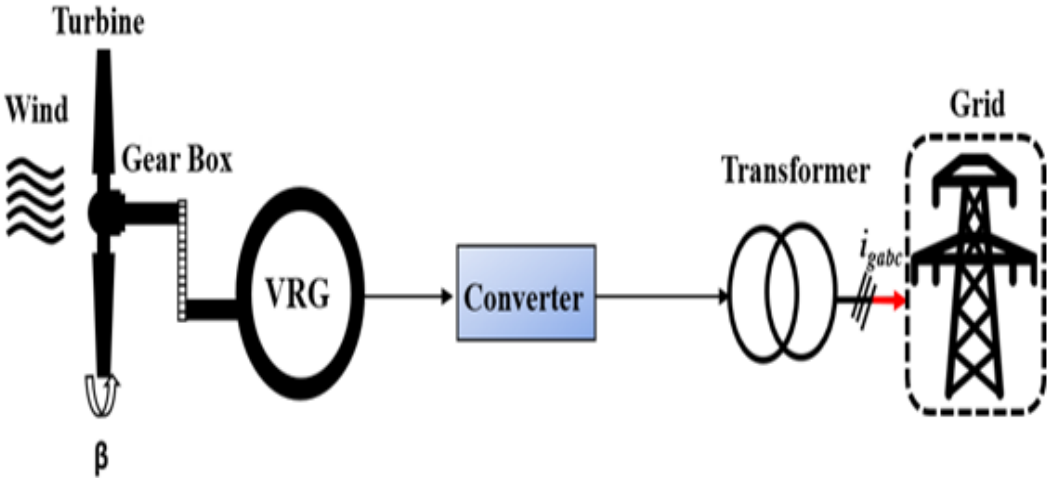

Figure I. 10 *VRG based wind turbines.*

I.11.7 Permanent magnet synchronous generator (PMSG)

A PMSG-based WE, as shown in Figure I.11, eliminates the requirement for a gearbox. Because the PMSG is inherently self-excited, it is possible to utilize a three-phase diode rectifier as the converter on the generator side. A chopper is required to regulate the rotational velocity of the generating shaft. An essential feature of PMSG-based WECS is that a diode rectifier can be utilized without self-excitation capacitors. The wind turbine construction commonly utilizes a diode rectifier and a DC/DC boost converter as a straightforward and economical choice [46]. Permanent magnets in a PMSG eliminate the need to supply magnetizing current to the stator to maintain a steady flux in the air gap. Hence, the stator current solely contributes to the generation of torque. This enables operating with a high-power factor, resulting in increased efficiency.

The PMSG experiences an undesired torque known as cogging torque due to the interaction between the rotor magnets and the stator slots. This torque leads to variations in the speed of the shaft. Particularly at low speeds, the wind turbine's torque can cause vibrations and noise. These effects can have a detrimental impact on the overall performance of the machine, as stated in reference [47]. Furthermore, the PMSG possesses the subsequent drawbacks:

- ✓ The permanent magnets are expensive.
- ✓ Challenges in the manufacturing process.
- ✓ Thermal demagnetization of permanent magnets.

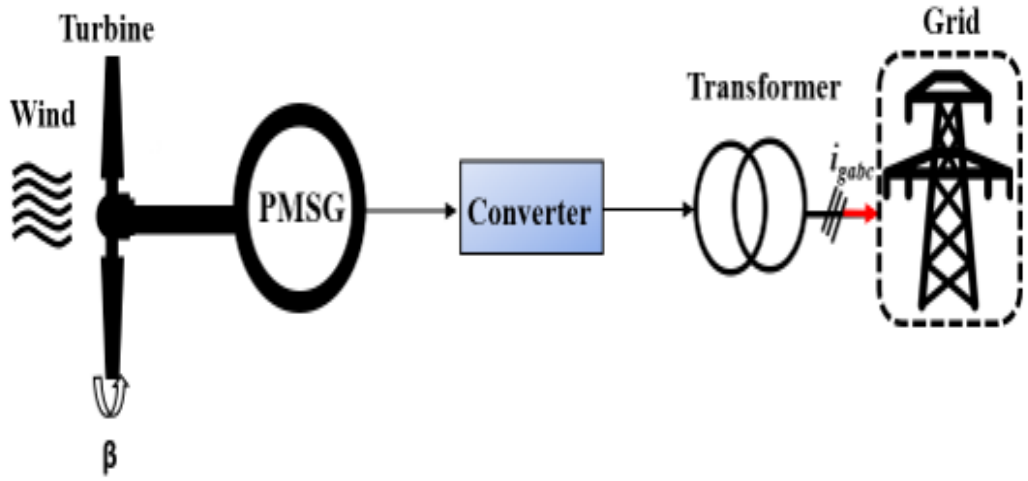

Figure I. 11 *PMSG based wind turbines.*

I.11.8 Hybrid excitation synchronous generator (HESG)

While there is no unanimous agreement on the optimal design for future wind turbines, the prevailing direction is towards synchronous machines. These machines utilize either permanent magnets or wound rotors. Utilizing permanent magnets instead of a rotor winding provides notable benefits, including enhanced efficiency by eliminating rotor copper loss, increased power density, and quicker response due to the low electromechanical time constant. However, the main drawback of this particular machine is that the permanent magnet's primary flow needs to be modifiable. A compelling substitute for traditional synchronous generators is the HESG.

I.11.8.1 State of the art of HESG

The hybrid excitation synchronous machine (HESM) is a prevalent concept seen in numerous studies. Various labels are employed in the literature to classify this particular type of machine:

- ✓ HESM
- ✓ Doubly excited synchronous machines, also known as DESG
- ✓ IESM
- ✓ PMSM equipped with supplementary exciting windings

I.11.8.2 Categorizing HESM

Applying the HE concepts allows for realizing a wide range of machine topology structures. Hence, multiple criteria can be utilized to classify double excitation machines.

This type of electric machine can be put into the same groups as other types using the same classification rules. These include magnetic flux routes in 2D and 3D design, linear and rotational machines, and axial and radial field structures. Because double excitation machines have a unique structure, with HE- flux sources, two criteria seem to work best for classifying them [48]: The initial criterion pertains to the specific location of the excitation sources within the machine: The stator contains two sources, the rotor also contains two sources, and there is a mixed localization.

Mixed localization refers to a configuration with excitation coils or PM in the rotor or stator, with the opposite source of the other component installed to eliminate the need for sliding contacts, the excitation coils are recommended to enter the inner stator [48]. The second method derives from the comparison of electrical circuits, determined by a standard combination of excitation current sources. The topic of discussion is double excitation machines, specifically those arranged in series and parallel configurations [49]. It is important to note that HESMs are utilized in a wide range of field. In [50], the researcher describes the development of HESM linear eddy current brake. This brake has numerous uses, including transmission systems, fast-speed train braking, automotive suspension, and vibration reduction. The authors in [51] described the design of a HESM. Regarding the creation of power from sea waves, Although HESM initially received significant attention in transportation [52,53], academics are growing interested in utilizing these machines for applications of sustainable energy [54,55].

I.11.8.3 Recent literature on HESM

This section presents a comprehensive survey of current works of literature on HESM, focusing on the previous several years. The HE-flux-switching (FS) machine has been extensively researched, with recent studies focusing on various topologies [56]. In FS machines, the magnetic flux demonstrates a two-dimensional characteristic. Notably, the stator accommodates all magnetic field sources, including PM, armature windings, and excitation coils, indicating a passive rotor. This machine suits diverse applications, such as hybrid and electric vehicles [57] and more electric airplanes [58]. Figure I.12 a illustrates a

HE FS structure explored in previous investigations [59]. This setup positions field coils above the PM, creating a magnetic bridge in the stator back iron. On the other hand, figure I.12 b shows a similar HE-FS device with no iron flux bridges and field coils placed below the PM. Researchers have analyzed this configuration in a study [60]. The design depicted in Figure I.13 has been examined in [61]. Figure I.14 depicts a hybrid stimulated topology with two distinct and easily noticeable properties. Both sources of the magnetic excitation field are situated within the stator and operate as FS devices. This topology has been analyzed in a prior investigation [60]. The stator yoke is equipped with PM.

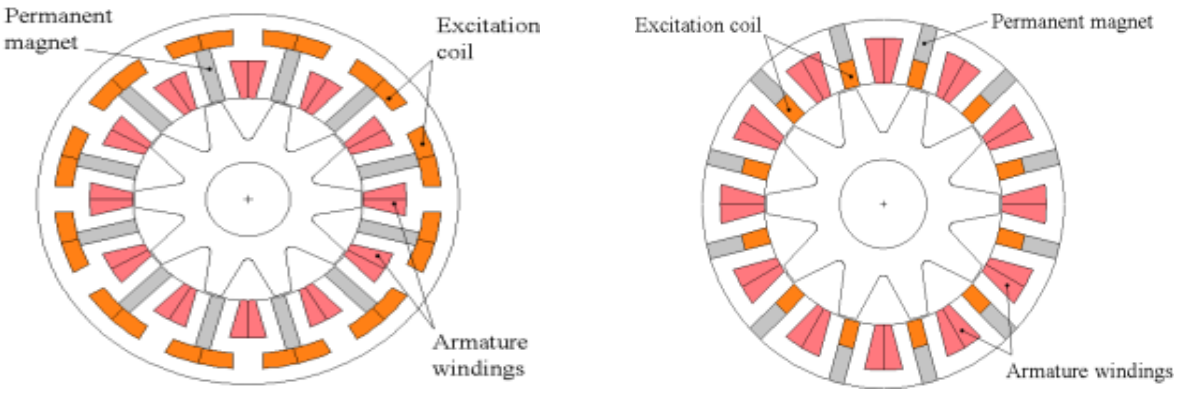

Figure I. 12 *Structures that combine both HE- and FS techniques [60].*

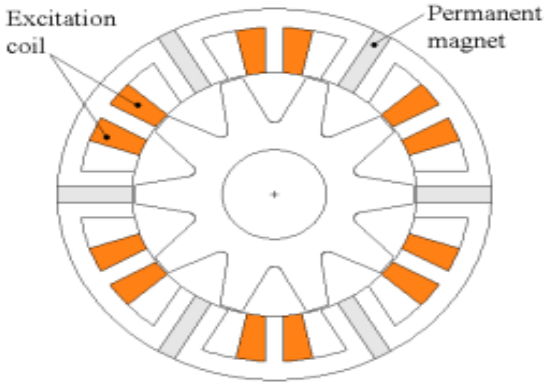

Figure I. 13 *The structure referred to as the E-core HE- flux-switching structure [61].*

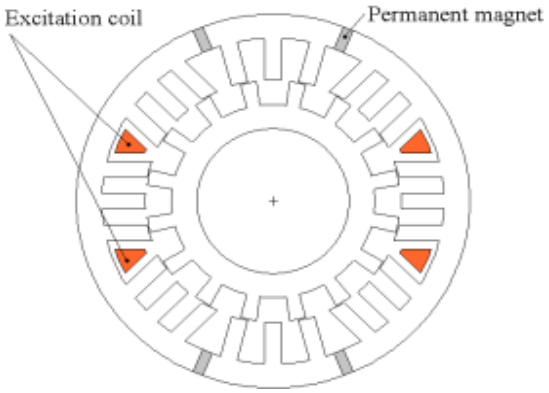

Figure I. 14 *The structure is a hybrid stimulated structure with an inner rotor that has doubly salient characteristics [60].*

Figure I.15 depicts a novel HE-configuration. The sources of the electromagnetic field, such as PM, excitation windings (EW), and armature windings (AW), are situated in the immobile components of the structure. Nevertheless, the AW and EW sources, which include PM and EW, are located in distinct stators. The rotor is entirely non-reactive. This design improves the efficiency of area utilization by overcoming a constraint seen in previous FS machines. Higher current densities are expected to result in magnetic saturation, which in turn enhances torque density [62]. Figure I.16 illustrates a HE-topology recently explored in [63]. In this arrangement, the EW are situated in the stator, avoiding the need for sliding contacts. Furthermore, PM is included into either the stator and rotor.

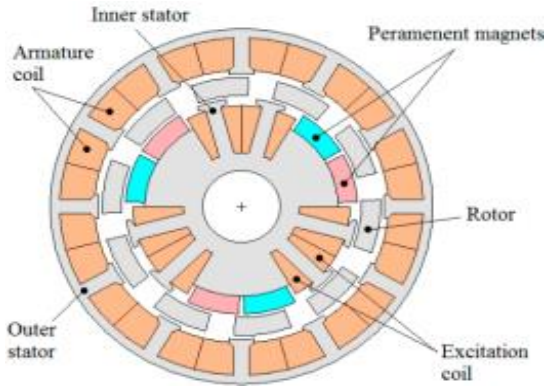

Figure I. 15 *A HE- machine with separate stators.*

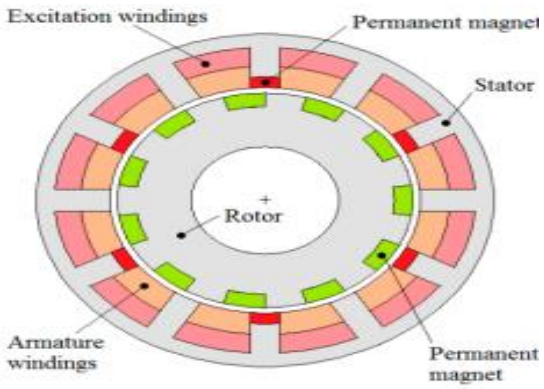

Figure I. 16 *A hybrid excited dual PM [63].*

Figure I.17 displays another innovative hybrid excited structure. This arrangement utilizes the HE principle in an electrical variable transmission. Additional information regarding the functioning [64].

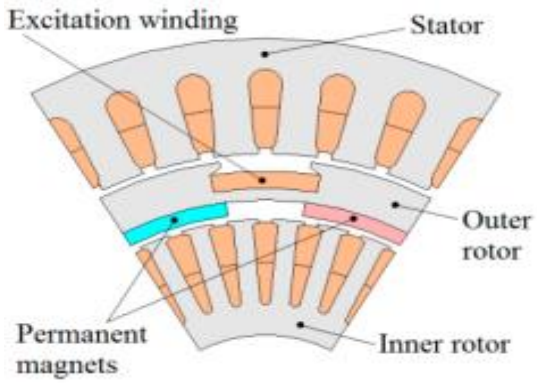

Figure I. 17 *An electrical variable transmission with HE [64].*

The design illustrated in Figure I.18 has been analyzed in reference [62]. Both in this topology and the one depicted in Figure I.13, the magnetic field produced by the PM is linked in a series with the dc EW. The flux-adjusting ability is limited due to the magnets' impermeability. Embedding excitation coils into the rotating component will yield an additional drawback.

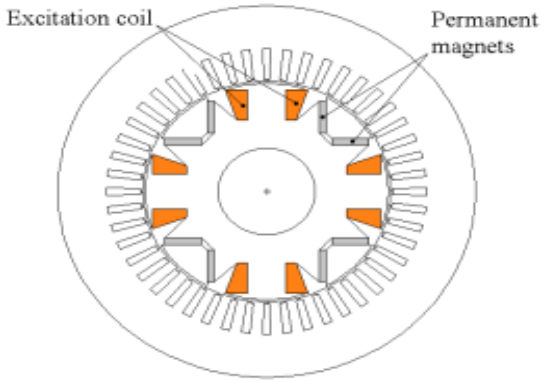

Figure I. 18 *Series HESM [62].*

Additional 2D structures have been examined in previous studies [65]. All previously mentioned structures have a two-dimensional character in terms of magnetic flux. Although the analysis and manufacturing of 3D design are more challenging than 2D structures, research on HESM using 3D structures remains essential. A HE-design is shown in Figure I.19a. It can be thought of as combining two synchronous designs: The design consists of a conventional PM in the center and dual homopolar inductor components at both ends [66]. The fundamental operational specific of this particular HE designs has been previously elucidated in [67]. Many 3D HE structures adhering to this principle have been the subject of recent investigations [61, 68]. Figure 18b depicts a different 3D HE- design, as referenced by sources [69, 70, 71]. The fundamental operational principle of this structure bears resemblance to the structure elucidated in [45]. In the configuration depicted in Figure I.19b, the excitation coils are positioned on a stationary component at one end of the machine. The static component can be positioned either around the rotor's flux collectors, known as radial auxiliary air gaps, or in front of these flux collectors, known as axial auxiliary air gaps. Relocating the excitation windings to this position has the benefit of decreasing the amount of copper used, which reduces the energy loss due to excitation and the overall size and weight of the machine. However, there is a concern that increasing the axial length of the machine may occur, and the chosen solution involves having more air gaps in the route of the DC excitation flux. Multiple HE structures have been documented in patent applications [72]. Although the initial patent applications primarily originated from European countries, Japan, and the USA, there has been a substantial rise in patent applications from China [72].

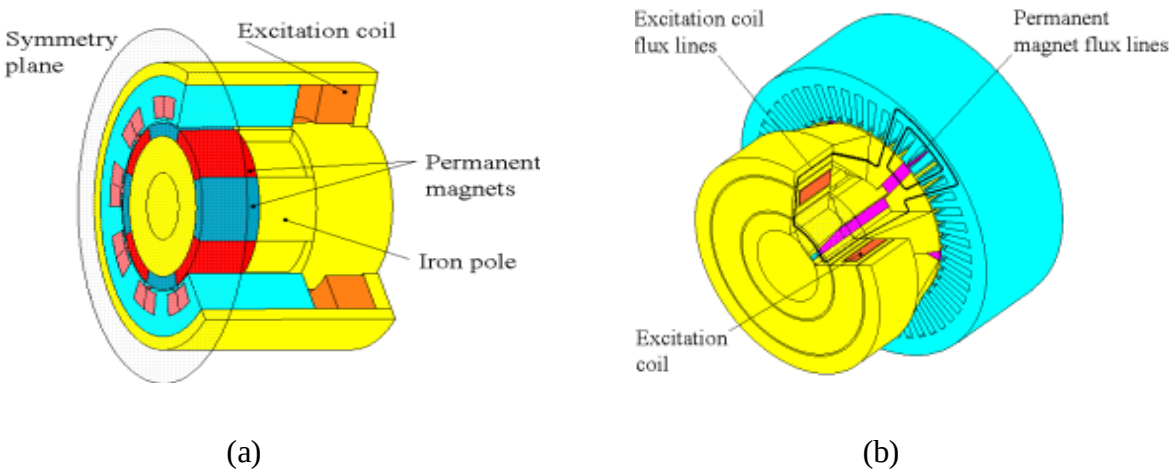

Figure I. 19 *3D parallel HESM [45].*

I.11.8.4 Applications of HESG

Several studies have suggested utilizing HESG as an electrical generator in various applications, including marine [49] [73], small hydroelectric power plants [74], and aeronautics [75]. In [73], finite element analysis (FEA) is used to compare the performance of the HESG to that of the MSAP. For the marine diesel generator in question, it is essential to ensure that the voltage remains within a range of ± 10% of its designated value. Additionally, the short-circuit current must be a minimum of three times the nominal current for at least two seconds. The second requirement is a significant challenge for PMSG. In their study, the authors conducted a performance comparison between a doubly excited synchronous machine and both a wound-field machine and a permanent magnet machine. The study showed that the hydroelectric power plant equipped with a HESG had much greater efficiency when compared to the wound-field MS. The stator copper losses are somewhat elevated (attributable to the length of the HESG stator).

On the other hand, the rotor copper losses are much lower, which shows that the hybrid generator is more efficient than the wound field. The efficiency of the PMSG and HESG is similar when operating at a unity power factor. In terms of powering aircraft, a study [75] showed that the HESG can be used instead of the three-phase synchronous machine that is currently used in most commercial and military aircraft power systems. This is primarily due to the HESG's superior power density, more straightforward design, and smaller physical footprint. Research on integrating a HESG into the wind energy area is ongoing. The team at GREYC in France suggests employing an HESG in this domain by

linking it to the power grid with a three-stage power electronics system (AC/DC/AC converter). It was recently studied at the L2EP lab in France that this generator is better than the salient-pole synchronous generator (SPSG) in terms of mass and energy efficiency for high-power applications, especially in wind generation.

I.12 Conclusion

This chapter has presented the overarching structure of our study endeavor. The initial section emphasized the significance of the wind energy sector. The second section of the study presents a comprehensive analysis of nine different types of wind generators that are now available on the market and have been detailed in the existing literature. Subsequently, it was demonstrated that employing a HESG presented a compelling option compared to current generators due to its adaptable flux control, minimal power consumption for control, and sturdy construction. Next, a comprehensive examination of hybrid excitation machines' technology and a classification based on their series or parallel structure was provided. This generator is described in a state-of-the-art manner, highlighting its various applications.

Chapter II: Principles and Tools for Modeling HESG -based WECS

II.1 Introduction

A wind turbine is a device that harnesses the kinetic energy of the wind and turns it into mechanical energy, subsequently transforming it into electrical energy. Consequently, wind energy production depends on the interaction between the rotor and the wind on one hand and between the rotor and the generator on the other. A good match between the various constituents of the turbine is essential to guaranteeing the efficiency of this conversion and optimizing the energy yield of the WECS.

This chapter presents a model of the wind turbine's aerodynamics. Then, the drive train that ensures the mechanical coupling between the rotor and the generator will be described and analyzed. The electrical system, which includes the generator and its power electronics, will also be modeled while considering the different disturbances, uncertainties, and flaws that can affect how it works, such as the generator's space harmonics and the commutations of the power converters.

Since the purpose of this research is to study the applicability of HESG to the wind energy field, a 2-kW generator was chosen. The different elements of the WECS, presented in Figure 1, will then be described and sized for the case of a 2-kW wind turbine.

II.2 Description of a WECS

The main parts of a WECS are the turbine, the gearbox, and the generator. The choice of the generator and its control remain crucial factors for the system's efficiency and performance. Prior to discussing control concepts, dynamic models, and the equations governing the system presented in Figure 1, it is important to describe and detail the main components of the WECS.

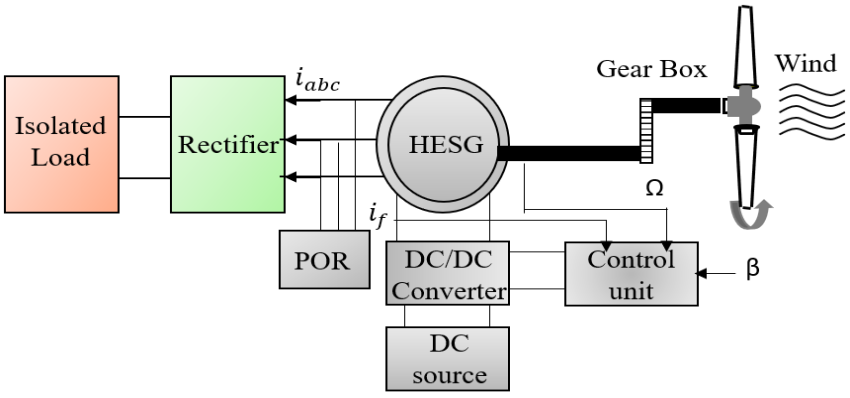

Figure II. 1 *HESG based WECS.*

II.3 Wind turbine model

II.3.1 Aerodynamic modeling of wind turbines

The airflow field around a wind turbine rotor is very complex. Current wind turbine blades have an aerodynamic profile that allows for the optimization of aerodynamic efficiency [76] and the reduction of structural loads [77]. In addition, depending on the wind speed, the blades can be pitched to maximize power extraction at a given wind speed or to limit power production at wind speeds above the rated speed.

Furthermore, the blades undergo elastic deformations and are exposed to wind gusts, turbulence, and other factors. The airflow is turbulent, three-dimensional, and time-varying, which further complicates the problem of modeling the aerodynamic and mechanical aspects. It is important to acquire basic knowledge of energy production without oversimplifying the problem. To this end, it is assumed that the wind turbine extracts energy from the wind "uniformly" over the area swept by the rotor.

II.3.2 Betz's theory

Betz's theory states that a wind turbine can only convert up to 16/27 (or 59%) of the wind's kinetic energy into mechanical energy. The German Albert Betz first formulated the law of Betz in 1929. Let us consider the system in Figure II.2, which represents a stream tube around a horizontal-axis wind turbine [78]. V1 represents the wind speed upstream of the wind turbine, and V2 represents the speed downstream.

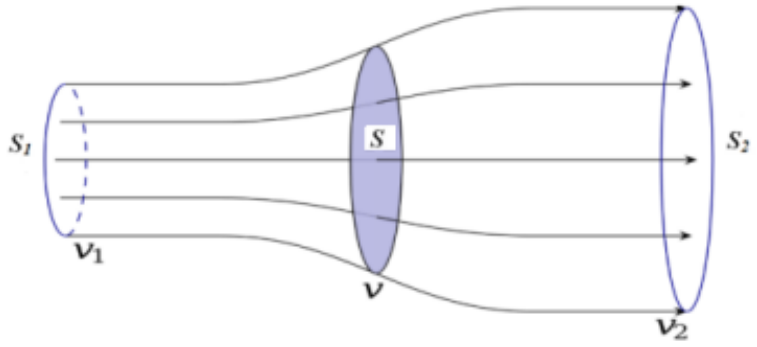

***Figure II. 2** : Wind Displacement*

Presuming that the wind speed across the rotor is the average between the undisturbed wind speed in front of the turbine, V_1, and the wind speed after it passes through the rotor, V_2, or $(V_1 + V_2) / 2$, the mass of air with density ρ moving through the blade surface S per second is:

$$m = \frac{\rho S \left(V_1 + V_2\right)}{2} \qquad (II.1)$$

The extracted power Pm is represented by half the product of mass and the reduction in wind velocity:

$$P_m = \frac{m\left(V_1^2 - V_2^2\right)}{2} \qquad (II.2)$$

Substituting the expression form into the equation for P_m, we get:

$$P_m = \frac{\rho S \left(V_1 + V_2\right)\left(V_1^2 - V_2^2\right)}{4} \qquad (II.3)$$

A theoretically undisturbed wind would cross this same surface S without any decrease in speed, i.e., at speed V1, the corresponding power would then be:

$$P_{mt} = \frac{\rho S V_1^3}{2} \qquad (II.4)$$

With

P: Expressed power (W).

S: Area swept by the blades (m²).

V: Wind velocity (m/s).

ρ: Air density (kg/m³).

II.3.3 Aerodynamic model

The wind turbine converts the kinetic energy of the wind into mechanical energy from the kinetic energy of the air mass particles in motion passing through the section of the active surface S swept by the turbine blades. The mechanical power available on the transmission shaft can be calculated according to the relation [79]:

$$P_t = \frac{1}{2} \cdot C_p(\lambda, \beta) \cdot \rho \cdot \pi \cdot R_p^2 \cdot v_w^3 \qquad (II.5)$$

With: $\lambda = \frac{R.\Omega_t}{v}$

Where:

V: is the upstream wind speed (m/s)

Cp: is the power coefficient of the wind turbine

R: is the radius of the turbine blades (m)

ρ: is the air density (kg/m^3)

The aerodynamic efficiency Cp is a positive coefficient that depends on the upstream wind speed V_w, the number of blades, their radius, their pitch angle β, and the turbine's rotational speed. In practice, values of 0.45 to 0.5 are achieved for the best current wind turbines [80]. There is no exact formula for Cp, but there are empirical formulas, such as the one given in (II.2), where Cp is expressed as a function of the angle β and the specific speed λ defined by (II.6).

$$C_p(\lambda,\beta) = 0.5\left[116(\frac{1}{\lambda_i}) - 0.4\beta - 5\right] exp\left[-21(\frac{1}{\lambda_i})\right] + 0.0068\lambda \qquad (II.6)$$

With: $\frac{1}{\lambda_i} = \frac{1}{\lambda+0.08\beta} - \frac{0.035}{\beta^3+1}$

The characteristics are represented in Figure II.3

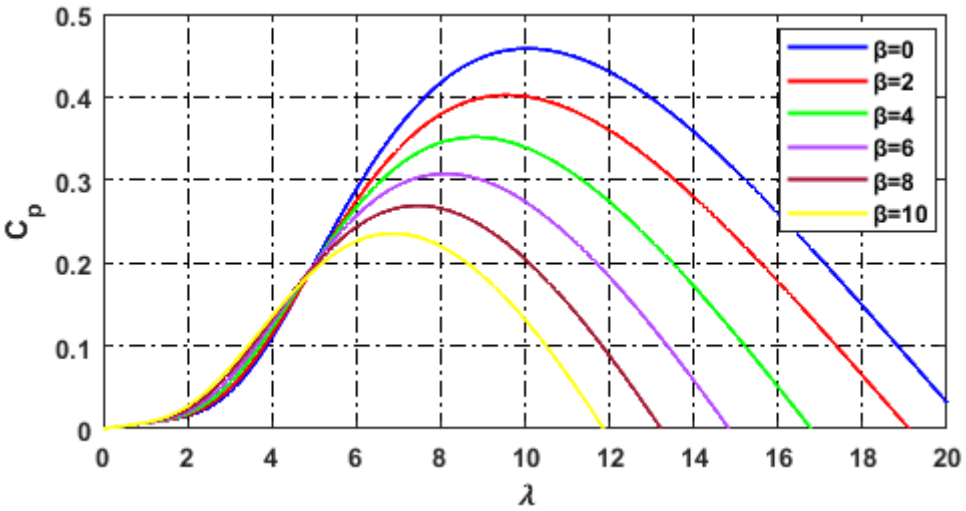

Figure II. 3 *$CP(\lambda.\beta) = f(\lambda)$ for different values of β.*

According to Figure II.3, we conclude that for the wind turbine considered, a maximum aerodynamic efficiency C_{pmax}=0.458 will be obtained for a pitch angle of 0° and an optimal specific speed λ_{opt}=9.24. In the presence of an aerodynamic torque Ct, the multiplier between the WT and the generator transforms the rotational velocity of the turbine Ωt into a higher one of the generator Ωg.

By definition, the wind torque is described by the relation (II.7)

$$T_t = \frac{P_t}{\Omega_t} \tag{II.7}$$

According to (II.5) and (II.7), this torque is defined by (II.8)

$$T_t = \frac{1}{2}\frac{C_p(\lambda,\beta)\cdot\rho\cdot S\cdot v_w^3}{\Omega_t} \tag{II.8}$$

II.3.4 Gearbox model

The gearbox adapts the slow rotational speed of the turbine to the high rotational speed of the generator (see Figure II.4). The following expressions mathematically model this gearbox:

$$\begin{cases} T_g = \dfrac{C_t}{G} \\ \Omega_t = \dfrac{\Omega_g}{G} \end{cases} \tag{II.9}$$

With:

Ω_t and Ω_g: rotational velocity of the WT before and after the gearbox, respectively

Tt: aerodynamic torque of the turbine, Tg: generator torque

G: gearbox gain.

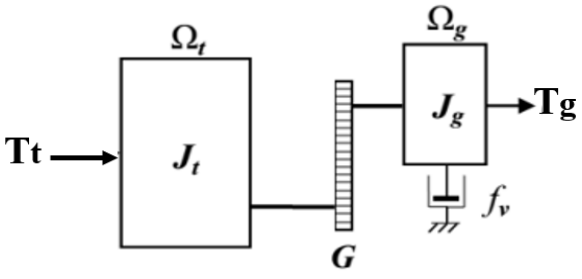

Figure II. 4 *Mechanical model of the turbine.*

By applying the fundamental of mechanics, we can derive the mechanical equation for our wind system in the following way:

$$J\frac{d\Omega_g}{dt} = T_{méc} = T_g - T_{em} - T_f \qquad \text{(II. 10)}$$

The schematic representation of the turbine model corresponding to the previous mathematical equations is illustrated in Figure II.5.

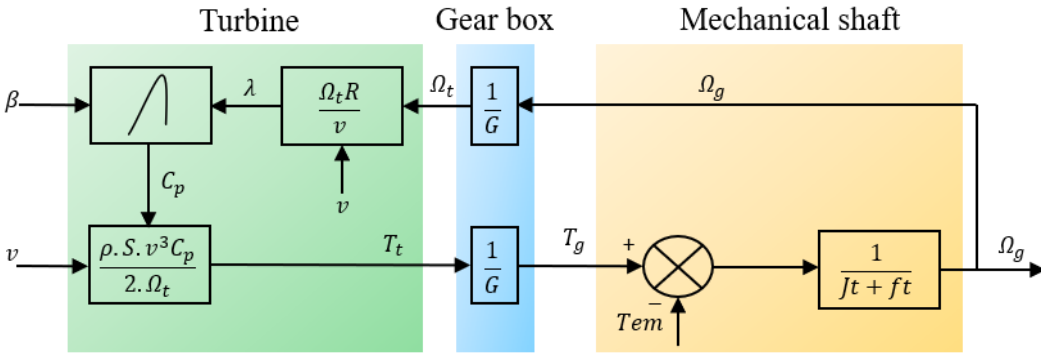

Figure II. 5 *Block diagram of the turbine.*

II.4 Modeling of HESG

II.4.1 Modeling of the electrical part

This section covers the generator, the chopper, the fictitious regulation point, the sensors, the full-bridge diode rectifier PD3 and the load (Figure II.6).

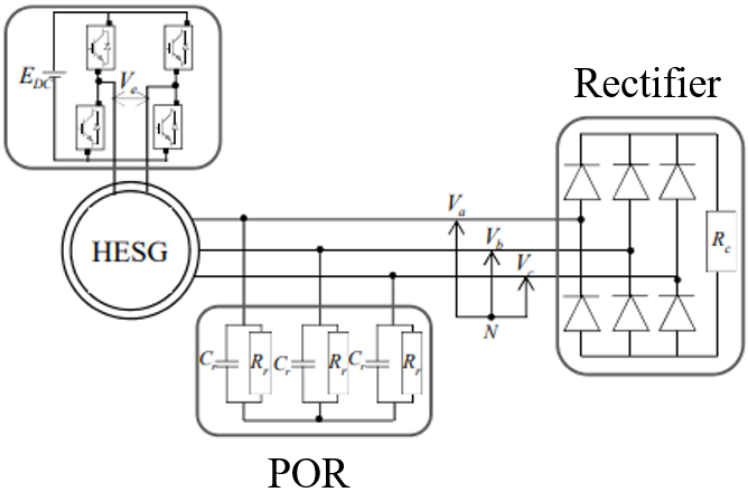

Figure II. 6 *Electrical circuit.*

II.4.2 Dynamic model in the real reference frame (a,b,c)

It is possible to propose a symbolic diagram of the HESG in the form represented in Figure II.7:

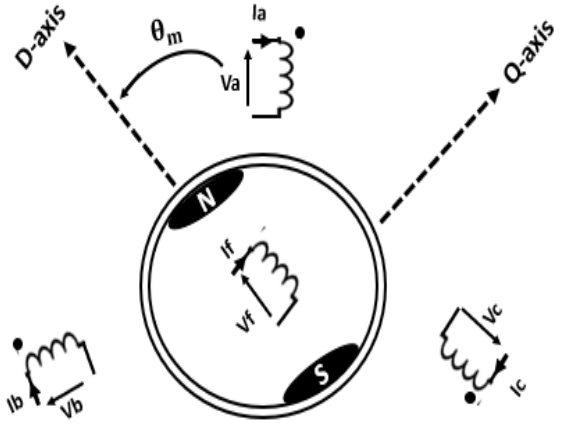

Figure II. 7: *Equivalent diagram of a HESG.*

The machine structure used is a flux-concentrated synchronous type, with excitation coils positioned on the stator and magnets embedded in the rotor. In this hybrid generator, three-phase windings are implemented for the armature, while two ring-shaped coils provide continuous excitation. To address challenges related to slip ring systems, the two halves of the inductor winding are shifted to the stator side and positioned on both sides of the machine between the winding ends and the housing. Furthermore, ferrite APs are placed within the rotor to boost flux density in the air gap according to the flux concentration principle. Due to the 3D nature of the flux path within the machine, the stator (Figure II.8(a)) and rotor (Figure II.8(b)) are constructed using solid and laminated cores. Magnetic collectors (Figure II.8(c)) are incorporated to ensure flux linkage between the stator and rotor magnetic circuits.

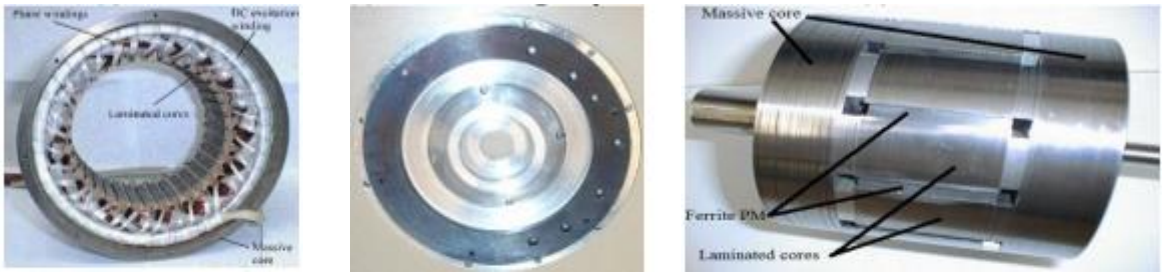

(a) (b) (c)

Figure II. 8 *topology studies.*

The excitation flux collected in the air gap then comes from two sources: a fixed-amplitude flux from the ortho-radial rotor-embedded magnets and another adjustable flux created by the local stator-wound excitation (Figure II.8). Based on this symbolic representation, it is possible to establish a set of equations in the real reference frame (a, b, c).

II.4.2.1 Voltage equations

The equations for the stator voltages are written in the form:

$$[v_s] = [R_s][i_s] + \frac{d}{dt}[\psi_s] \tag{II.10}$$

The rotor voltage is expressed by:

$$v_f = R_f . i_f + \frac{d\psi_f}{dt} \tag{II.11}$$

With:

$[v_s] = [v_a \quad v_b \quad v_c]^T$: Stator voltage vector

$[i_s] = [i_a \quad i_b \quad i_c]^T$: Stator current vector

$[R_s] = \begin{bmatrix} R_s & 0 & 0 \\ 0 & R_s & 0 \\ 0 & 0 & R_s \end{bmatrix}$: Stator resistance matrix

$[\psi_s] = [\psi_a \quad \psi_b \quad \psi_c]^T$: Stator phase flux vector

v_f : Rotor excitation voltage.

i_f : Rotor excitation current.

R_f : Rotor resistance.

ψ_f : Rotor flux.

II.4.2.2 Flux expressions

The stator fluxes are expressed by:

$$[\psi_s] = [L_s][i_s] + [\psi_{pm}] + [L_{sf}].i_f \tag{II.12}$$

With:

$[L_s]$: Stator-Stator Coupling Inductance Matrix**.**

$[L_{sf}]$: Stator-Rotor Coupling Inductance Matrix

$[\psi_{pm}]$: Magnet Flux Defined by:

$$[\psi_{pm}] = \psi_a \begin{bmatrix} \cos(\theta) \\ \cos\left(\theta - \frac{2\pi}{3}\right) \\ \cos\left(\theta + \frac{2\pi}{3}\right) \end{bmatrix} \quad \text{(II.13)}$$

Where ψ_a is the maximum flux of the magnets in a stator winding

It should be noted here that this is a salient-pole machine in order to propose the most general possible modeling. These stator matrix equations must be supplemented by a rotor equation of the form:

$$\psi_f = [L_{fs}][i_s] + L_f . i_f \quad \text{(II.14)}$$

Where L_f denotes the intrinsic inductance of the rotor coil.

The expressions for the inductance matrices $[L_s], [L_{sf}]$ *et* $[L_{fs}]$ are:

$$[L_s] = \begin{bmatrix} l_s & l_{ss} & l_{ss} \\ l_{ss} & l_s & l_{ss} \\ l_{ss} & l_{ss} & l_s \end{bmatrix} \quad \text{(II.15)}$$

$$\left[L_{sf}\right]=\left[L_{fs}\right]^{t}=L_{0}\begin{pmatrix}\cos(\theta)\\ \cos\left(\theta-\frac{2\pi}{3}\right)\\ \cos\left(\theta+\frac{2\pi}{3}\right)\end{pmatrix} \quad \text{(II.16)}$$

Where L_0 is the peak coupling inductance between the inductor coil and an induced stator coil.

II.4.2.3 Dynamic model in the park (d,q) axis framework

The real model (a, b, c) is a system of differential equations with variable coefficients (function of the rotor position θ). To reduce this complexity, we use the Park transformation. The latter makes it possible to obtain equivalent quantities [Xdqo] from the real quantities [Xabc] using the following relationship:

$$\left[X_{dqo}\right]=\left[P(\theta)\right]\left[X_{abc}\right] \quad \text{(II.17)}$$

With [P(θ)] being called the direct transition matrix defined by:

$$\left[P(\theta)\right]=\sqrt{\frac{2}{3}}\begin{pmatrix}\cos(\theta) & \cos\left(\theta-\frac{2\pi}{3}\right) & \cos\left(\theta+\frac{2\pi}{3}\right)\\ -\sin(\theta) & -\sin\left(\theta-\frac{2\pi}{3}\right) & -\sin\left(\theta+\frac{2\pi}{3}\right)\\ \frac{1}{\sqrt{2}} & \frac{1}{\sqrt{2}} & \frac{1}{\sqrt{2}}\end{pmatrix} \quad \text{(II.18)}$$

Note that the rotation angle θ is arbitrary. Additionally, this transformation matrix preserves instantaneous electrical power.

II.4.2.4 Voltage equations

By applying the Park transformation, the voltage equations become:

$$\begin{cases} v_d = R_s i_d + \dfrac{d}{dt}[\psi_d] - p\Omega\psi_q \\ v_q = R_s i_q + \dfrac{d}{dt}[\psi_q] + p\Omega\psi_d \\ v_f = R_f i_f + \dfrac{dv_f}{dt} \end{cases} \quad \text{(II.19)}$$

II.4.2.5 Flux equations

In the same way, the fluxes become:

$$\begin{cases} \psi_d = L_d i_d + L_{sf} i_f \\ \psi_q = L_q i_q - \psi_{pm} \\ \psi_f = L_{sf} i_d + L_f i_f \end{cases} \quad \text{(II.20)}$$

II.4.2.6 Electromagnetic torque

The electromagnetic torque developed by a synchronous machine is written as:

$$T_{em} = p\left(\psi_d . i_q - \psi_q . i_d\right) \quad \text{(II.21)}$$

Therefore, taking into account the flux expressions, we obtain:

$$T_{em} = p\left(L_{sf} . i_q . i_f + \left(L_d - L_q\right) i_d i_q + \psi_{pm} . i_d\right) \quad \text{(II.22)}$$

II.4.2.7 State equations

From the d-axis stator voltage equation and the speed equation, define the variable e_μ as follows:

$$e_\mu = v_d - R_s . i_d + p\Omega L_q i_q = L_d \frac{d}{dt}\left(i_d + \frac{L_{sf}}{L_d} i_f\right) \quad \text{(II.23)}$$

Expressing the magnetizing current as:

$$i_\mu = \left(i_d + \frac{L_{sf}}{L_d} i_f\right) \quad \text{(II.24)}$$

By introducing the ratio: $m = \frac{L_{sf}}{L_d}$, the previous expression (II.25) becomes:

$$\frac{di_\mu}{dt} = \frac{d}{dt}\left(i_d + mi_f\right) = \frac{1}{L_d} e_\mu \tag{II.25}$$

From this representation, it is easy to derive a state-space model. Initially, the input vector u, output vector y , and state vector x are specified as follows:

$$\begin{cases} u = \left(v_d, v_q, v_f, c_r\right)^T \\ y = \left(i_d, i_q, i_f, \Omega\right)^T \\ x = \left(i_\mu, i_q, i_f, \Omega\right)^T \end{cases} \tag{II.26}$$

Therefore, we have:

$$\begin{cases} \frac{di_\mu}{dt} = \frac{1}{L_d}\left(V_d - R_s i_\mu + mR_s i_f + p\Omega\left(L_q i_q - \psi_{pm}\right)\right) \\ \frac{di_q}{dt} = \frac{1}{L_q}\left(V_q - R_s i_q - p\Omega\left(L_d i_\mu\right)\right) \\ \frac{di_f}{dt} = \frac{1}{\sigma L_f}\left(V_f - R_f i_f - me_\mu\right) \\ \frac{d\Omega}{dt} = \frac{1}{J}\left(C_{em} - C_r - f_v\Omega\right) \end{cases} \tag{II.27}$$

With: $\sigma = 1 - \frac{{L_{sf}}^2}{L_f L_d}$ dispersion coefficient.

This enables the system matrices A , B , and C to be represented as:

$$\begin{cases} \boldsymbol{\dot{x} = Ax + B_1.u + B_2.\psi_{pm}} \\ \boldsymbol{y = C.x} \end{cases} \tag{II.28}$$

With:

$$A=\begin{pmatrix} -\frac{R_s}{L_d} & \frac{p\Omega L_q}{L_d} & \frac{mR_s}{L_d} & 0 \\ -\frac{p\Omega L_d}{L_q} & -\frac{R_s}{L_q} & 0 & 0 \\ \frac{mR_s}{\sigma L_f} & -\frac{p\Omega mL_q}{\sigma L_f} & -(\frac{R_f}{\sigma L_f}+\frac{m^2R_s}{\sigma L_f}) & 0 \\ \frac{p\psi_{pm}}{J} & \frac{p(L_{sf}i_f+(L_d-L_q)i_\mu+\psi_{pm})}{J} & \frac{pm(L_d-L_q)i_q}{J} & -\frac{f_v}{J} \end{pmatrix}$$

$$B_1=\begin{pmatrix} -\frac{1}{L_d} & 0 & 0 & 0 \\ 0 & \frac{1}{L_q} & 0 & 0 \\ -\frac{m}{\sigma L_f} & 0 & \frac{1}{\sigma L_f} & 0 \\ 0 & 0 & 0 & -\frac{1}{J} \end{pmatrix}, B_2=\begin{pmatrix} -\frac{p\Omega}{L_q} \\ 0 \\ 0 \\ 0 \end{pmatrix}, C=\begin{pmatrix} 1 & 0 & -m & 0 \\ 0 & 1 & 0 & 0 \\ 0 & 0 & 1 & 0 \\ 0 & 0 & 0 & 1 \end{pmatrix}$$

II.5 Modeling of power converters

A simplified modeling method is usually applied to converters. It consists of using Kirchhoff's laws and considering the perfect switch model. This modeling, which is too simple, does not allow us to obtain the dynamic behavior of the converters directly. Power converters are implemented under Matlab/Simulink to improve this modeling using the behavioral models of power components. The "Simpowersystem" tools are chosen to consider the effects of switching and losses. A DC/DC converter controls the excitation windings, and a PD3 rectifier connects the resistive load to the wind turbine.

II.5.1 DC-DC converter

The HESG we use is parallel. We must be able to increase and decrease the excitation flux ϕ_f. To increase ϕ_f, we must impose a positive, i.e., and to decrease it, i.e., must be negative a four-quadrant current-controlled chopper supplies power to the HESG's excitation system in our application. The chopper's power supply is independent. In this work, two chopper models have been established. The first is a simple model that will be used for the open-loop study of the SCE and for evaluating the effects of switching on the performance of the developed control laws. In this instance, a straightforward gain

designated as G_0 models the chopper [1]. The excitation voltage is given by equation II.29:

$$Vf = (2\gamma - 1)E_{DC} \tag{II.29}$$

Where E_{DC} is the constant voltage source of the cutter and γ is the cyclic ratio of the cutting machine, given by (II.30).

$$\gamma = \frac{1}{2v_p}\left(v_{ec} + v_p\right) \tag{II.30}$$

Where v_{ec} is the control voltage and v_p is the carrier voltage. So, we can write:

$$Vf = \frac{E_{DC}}{v_p} \cdot v_{ec} = G_0 \cdot v_{ec} \tag{II.31}$$

The second model implemented is more realistic and built using the "Simpowersystem" tools of Matlab. The H-bridge chopper (Figure II.7) consists of 4 unidirectional controlled switches Ti (i=1..4), in parallel with four recovery diodes that make the switches bidirectional. It is a flexible and versatile basic configuration. Thanks to its flexibility, different control methods can be used. All practical methods must use an additional switching device on each arm. Depending on the control method of each arm, several pulse width modulation (MLI) control strategies can be used.

In this case, we have chosen the "intersective" or bipolar MLI**:** In this MLI strategy, the diagonal switches of the H-bridge are grouped in pairs. In practice, two complementary signals with a small dead time between them are used. This control strategy is simple and easy to implement. This is why it is used in most applications, even if it is less efficient than others.

A carrier vp(t) (usually triangular) is compared to a modulating vec(t) so that the switching functions leg1,2 f is written as:

$$\begin{cases} f_{\text{leg }1}(t) = f\begin{cases} 1 & if \quad v_{ec}(t) > v_p(t) \\ 0 & if \quad v_{ec}(t) \le v_p(t) \end{cases} \\ f_{\text{leg }1}(t) = \overline{f_{leg2}(t)} \end{cases} \tag{II.32}$$

The excitation voltage is then given by:

$$v_f = \left(f_{leg1} - f_{leg2}\right) \cdot E_{DC} \tag{II.33}$$

II.5.2 Uncontrolled rectifier

Our generator is connected to an isolated charge via a diode adjuster. This device converts the generator's alternate voltage into a continuous voltage, feeding a Rc resistance. The principle of operation is simple: common cathode diodes choose the most positive voltage, and common anode diodes choose the most negative, so two diodes lead at once over each period.

II.6 Sizing of the resistive load

This study assumes that a single resistance, abbreviated as Rc, can represent all individual loads linked to the SCE. In order to determine the appropriate load size, it is necessary to consider the electrical constraints of the generator, namely the maximum current that can be handled by the excitation winding. Yes, the current I_{fmax} is 8 A. Practically, we will restrict this value to 5 A to prevent excessive excitation coil heating.

To prevent damage to the excitation windings at high rotation rates, it is necessary to restrict the load resistance to a maximum of 18 Ω. To take preventive measures, a value of 15 Ω is subsequently established for this load.

II.7 Fictitious regulation point

The fictitious regulation point (denoted POR) is inserted between the generator and the load, as shown in Figure II.2. Indeed, the machine, described by equations from (II.10) to (II.30), is a three-phase AC source. The load is also considered a current source. Therefore, in order to define an appropriate regulation point, the HESG is cascaded with fictitious capacitors and resistors (named Cr and Rr, respectively), as illustrated in Figure II.6. Thus, the inputs will be the load currents and the outputs, the stator voltages of the HESG.

In generator mode, the stator voltages are treated as outputs, while the currents act as inputs to the machine. In this instance, the defined problem needs to be better-conditioned. This regulation point is inserted to solve this problem by having a generator operation (by analogy with the modeling in the motor case).

In the reference frame (a,b,c), the POR is defined by (II.34), where Rcr is an

equivalent resistance given by (II.35). To facilitate the calculation, the load and the diode rectifier are assimilated to a resistance Rc.

$$[I_3] = \frac{[V_3]}{R_c} + C_r \frac{d[V_3]}{dt} \tag{II.34}$$

$$\frac{1}{R_{cr}} = \frac{1}{R_r} + \frac{1}{R_c} \tag{II.35}$$

In the Park frame, the equations that describe the POR are:

$$\begin{cases} -R_{cr}C_r w v_q + R_{cr}C_r \dfrac{dv_d}{dt} + v_d = -R_{cr} i_d \\ R_{cr}C_r w v_d + R_{cr}C_r \dfrac{dv_q}{dt} + v_q = -R_{cr} i_q \end{cases} \tag{II.36}$$

The various elements are computed to reduce the effects on energy consumption and the system's dynamic performance [75]. In the absence of load, each phase corresponds to the RLC circuit illustrated in Figure II.9.

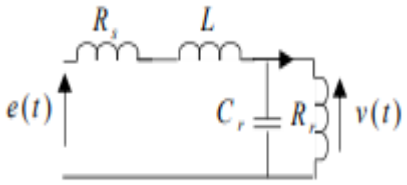

Figure II. 9 *Equivalent scheme of a stator phase.*

The equivalent circuit of a stator phase is then reduced to a resonant RLC circuit described by the 2-order transfer function (II.37). The damping factor of this function is ξ_{RLC} (II.38) and its resonant frequency is ω_{RLC} (II.39) [75]:

$$\frac{v(s)}{e(s)} = \frac{1}{LC_r s^2 + \left(R_s C_r + \frac{L}{R_r}\right) s + 1 + \frac{R_s}{R_r}} \tag{II.37}$$

$$\xi_{RLC} = \frac{R_s C + \frac{L}{R_r}}{2\sqrt{LC_r\left(1 + \frac{R_s}{R_r}\right)}} \tag{II.38}$$

$$w_{RLC} = \sqrt{\frac{1 + \frac{R_s}{R_r}}{LC_r}}\sqrt{1 - 2\xi_{RLC}^2} \tag{II.39}$$

II.8 Conclusion

This chapter presents mechanical and electrical models that reproduce the behavior of our wind energy conversion system (WECS). The principle of aerodynamic conversion is explained, and then the one-mass models of the wind turbine's drive system are described. Although simple, these models are sufficient for analyzing a wind turbine's mechanical behavior. Next, the generator and its power electronics are modeled. Similarly, it was initially proposed that a simple gain model be used for the converters. The behavioral models of the Matlab "Simpowersystem" tool are implemented to evaluate the effect of switching on the wind system. The models presented will be used to synthesize appropriate control laws in the next chapter.

Chapter III: Backstepping Control for MPPT in HESG-Based WECS with Isolated Load

III.1 Introduction

Chapter III: Backstepping Control for MPPT in HESG-Based WECS with Isolated Load

WT are intricate dynamic systems influenced by gravity, stochastic wind problems, and gravity and gyroscopic stresses. As a result, their aerodynamics are nonlinear and unsteady. WT rotors encounter a chaotic wind area, potentially leading to mechanical strain. Therefore, the design of control algorithms for wind turbines must take into account these complexities. These algorithms must capture the most important dynamics of the turbines without being too complex or computationally expensive.

This chapter comprehensively examines a robust control system designed for a self-contained WECS that smoothly integrates a HESG connected to an isolated load during the crucial MPPT phase. The investigation is justified by the growing integration of HESG innovation into WECS systems. This study identifies a notable deficiency in previous studies, which predominantly concentrated on the intricate structure of HESG while neglecting its effectiveness as an operation. The goal is to correct this imbalance. Conventional control systems have restrictions regarding Wide Area Control Systems WECS applications. Specifically, PI controllers face difficulties maintaining power quality and optimizing system performance. In this context, our study has developed a detailed equivalent model of WECS using MATLAB-Simulink. A unique control approach utilizing backstepping control (BSC) is suggested as a solution to current obstacles. This approach enhances the efficiency of WECS control and showcases its expertise in optimizing MPPT.

III.2 Operation of a variable-speed WT

The operation of a WT can be characterized by the changes in useful power on the WT shaft in relation to wind speed variations. From this variation, we can distinguish 4 main operating zones (Figure III.1)

Zone 1: Low Wind Speed Zone

Wind speed is reliable but too weak to spin the turbine. Therefore, both rotation speed and mechanical power are zero.

Zone 2: Variable Speed Zone

Wind speed reaches a minimum level (Vm) to allow the turbine to start. Once started, the turbine operates to capture the maximum available power for ideal operation until the wind reaches the rated velocity (Vn). This rated velocity corresponds to the rated values of mechanical power (Pn) and rotational speed (Ωn).

Zone 3: High Wind Speed Zone

Wind speed exceeds the Vn. Rotation speed and mechanical power are maintained at rated values to protect the turbine (wind turbine/aerogenerator). These limits are achieved by adjusting the turbine blades to reduce efficiency (decrease power output). This adjustment involves increasing the blade pitch angle (β). When wind velocity reaches its Vm a shutdown system activates to prevent any damage to the turbine.

In zone 4: the wind speed is above the maximum speed of 20 m/s and therefore the system must shut down by limiting the transfer of kinetic energy to avoid damage to the turbine.

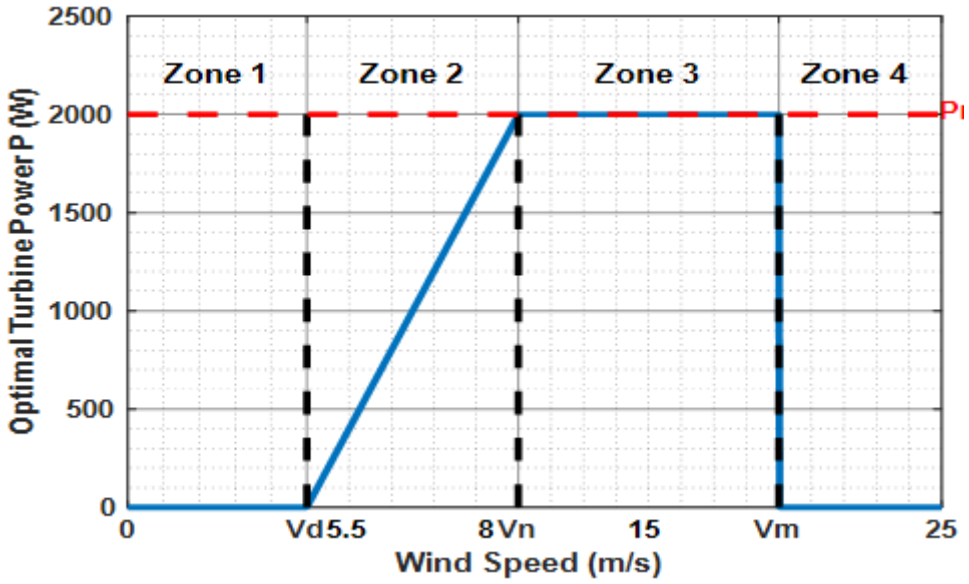

Figure III. 1 *Operating zones of a VSWT.*

III.3 Control of HESG in zone II

The primary objective of control in this zone is to optimize the power harvested from the WT while maintaining safe operation and limiting the mechanical fatigue of the WT. In this paragraph, we define the current and speed controllers that allow for optimizing the extraction of wind energy produced.

Additional control goals encompass altering the operational status of the turbine,

including its initiation and cessation. The control system also provides these functions. To initiate a machine at a variable speed, the mechanical parking brake is released, and the β angle of slope is decreased from the full angle (90°) to a value that permits the aerodynamic torque to accelerate the rotor from a standstill. When the machine is stopped, the blades are quickly flagged, and a mechanical parking brake is activated. In this thesis, we will not deal with these functionalities; we simply assume that for zone I, we have λ=0 and β=0° and for zone IV, β=90° and λ=0.

III.3.1 Current loop

To synthesize the current controller, the following simplifications are made:

Switching and Generator Harmonics Neglected: The effects of commutations and harmonics generated by the turbine's generator are ignored.

Excitation Current Model: The excitation current is modeled according to Figure III.2. This is a multi-input (vec, vd, id, iq) and highly non-linear model. This non-linear behavior is due to the coupling term defined by (III.1) and noted vp.

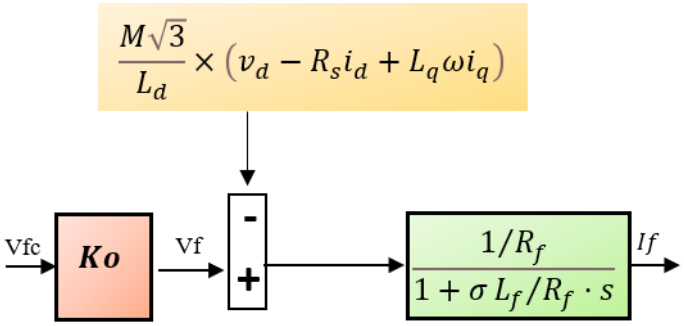

Figure III. 2 *Excitation current model.*

$$v_p = M\sqrt{3}/L_d \times (v_d - R_s i_d + L_q \omega i_q) \quad \text{(III.1)}$$

The term Vp may be regarded as a disturbance concerning the regulation of excited current. A prevalent method involves implementing compensation to negate the coupling (Figure III.3).

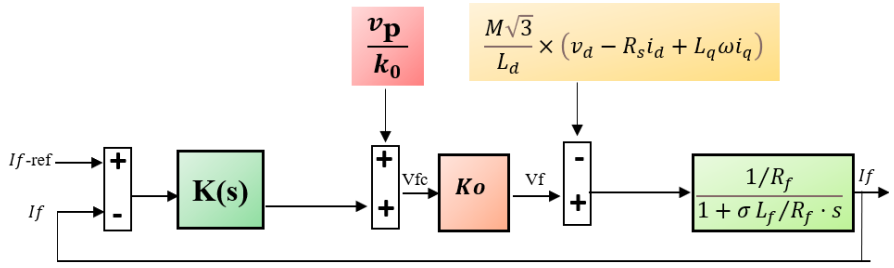

Figure III. 3 *Excitation current model.*

The work carried out in [54] showed that this compensation technique gave good results in the so-called nominal case, where all the parameters of the machine are perfectly known. However, it should be avoided in the case where there are significant uncertainties about the electrical parameters of the hybrid generator. The stability of the system may even be threatened.

This approximation is legitimate and can be verified by simulation. Indeed, the function if=f(v_{fc}) was identified by performing simulations on a Simulink model of the current loop in Figure III.4, for three operating points in the interval [-1V,1V]. In this identification, a simple model of the generator was considered and the effects of commutations were not taken into account (the chopper is modeled by a gain K0, and it is assumed that the generator delivers directly to the load Rc, also modeled by a gain). The generator speed is assumed to be an independent input. Then, the excitation current was analyzed from the perspective of static gain, response time and overshoot for each input value v_{fc}.

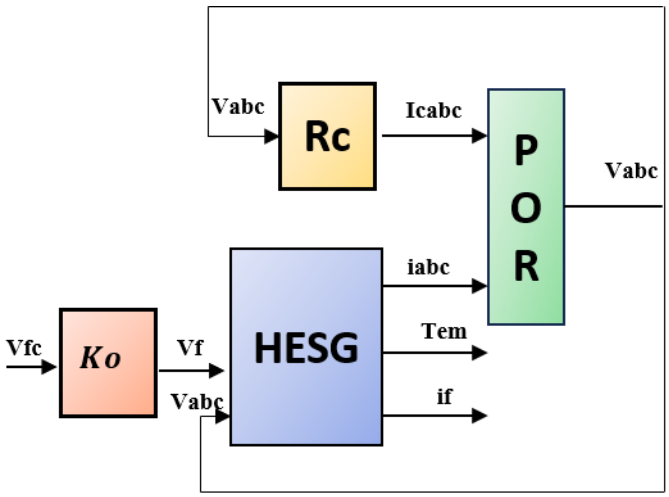

Figure III. 4 *Block diagram of the current loop identification model.*

III.3.2 Speed loop

The HESG is a highly nonlinear machine. Developing accurate nonlinear models is a difficult task, and designing nonlinear controllers for these models is complex, too. Moreover, a controller designed from a linearized wind turbine model around a given wind speed, for example, eight m/s, would work at wind speeds close to 8 m/s but might not work for a speed of 3 m/s. Different methods can approach the problem of the nonlinearity of the SCE. One possible method would be to design a variable gain controller. After linearizing the SCE model for multiple operating points, different linear controllers are designed and intelligently switched between them. Another method is to design a robust linear controller that works throughout the operating range. During this thesis work, BSC controllers were developed. Synthesizing a controller is a whole process; several steps are required to design, implement and test it. This process consists of:

- ✓ We are determining the control objectives.
- ✓ They are developing a streamlined fluid framework based on the controller will be developed.
- ✓ I am applying the specific tools for the synthesis of the chosen controller.
- ✓ I am performing closed-loop dynamic simulations to test the performance of the synthesized controller, first on the simplified model and then on a more complete model.

We start by specifying the specifications that the speed controller must meet. Then, we perform a linearization of the speed loop to have a simplified linear model on which the controller will be calculated.

III.4 The challenges of controlling wind turbines with HESG systems

Wind turbines are complex systems that present significant challenges for control engineers. Their dynamics are inherently nonlinear, meaning simple linear models cannot accurately describe their behavior. Several factors, including the wind's variable speed, the turbine blades' changing pitch angle, and the complex aerodynamic interactions between the blades and the air, cause this nonlinearity.

In addition to the challenges the wind turbine poses, using HESG systems

introduces further complexities. HESG systems are a type of generator that combines the characteristics of induction and synchronous generators. This makes them more efficient than traditional induction generators and more challenging to control.

III.4.1 The limitations of traditional PI controllers

Traditional PI controllers are a common choice for controlling wind turbines. PI controllers are simple and reliable and have been shown to be effective in a wide range of applications. However, PI controllers have several limitations that make them ill-suited for controlling wind turbines with HESG systems.

One of the main limitations of PI controllers is that they are linear controllers. This means that they can only work effectively with linear systems. As discussed above, wind turbines and HESG systems are nonlinear, so PI controllers cannot accurately capture their behavior.

Another limitation of PI controllers is that they could be better at handling time-varying disturbances. Wind speed is a highly variable disturbance, and PI controllers can have difficulty tracking the desired turbine speed in the face of these disturbances.

III.4.2 Corrector backstepping

Wind turbine dynamics are notoriously nonlinear, and the added complexity of HESG systems can push traditional control strategies like PI controllers to their limits. These controllers cannot handle the multitude of challenges that arise during operation [81].

Enter Backstepping Control (BSC), a powerful solution built to tackle these nonlinearities. BSC's inherent strength lies in its ability to refine and continuously optimize control inputs in real time. This ensures that the Wind Conversion System (WCS) consistently operates near its peak efficiency [82].

BSC employs a sophisticated control algorithm to determine the ideal excitation current based on actual turbine speed measurements.
This analytical technique is integrated into an extensive control framework that perpetually monitors and changes the excitation current. By orchestrating this fine-tuning based on real-time turbine dynamics, BSC empowers HESG systems to achieve exceptional

operational efficiency and power transfer within the wind energy conversion process [83, 84].

III.4.3 Benefits of Using BSC for WECS

There are several benefits to using BSC for wind turbine control with HESG systems. These benefits include:

Improved efficiency: BSC controllers can help improve wind turbines' efficiency by ensuring that they operate at their peak power output.

Increased power transfer: BSC controllers can help increase the power transfer from WT to the network by ensuring that they operate at their maximum power point.

Reduced torque oscillations: BSC controllers can help to reduce torque oscillations in wind turbines, which can improve the lifespan of the turbine and reduce wear and tear on the drivetrain.

Improved stability: BSC controllers can help improve the stability of wind turbines, making them less susceptible to disturbances.

Overall, BSC is a powerful and versatile control technique that can address the challenges of controlling wind turbines with HESG systems. BSC controllers can help improve wind turbine efficiency, power transfer, stability, and lifespan.

III.4.4 Mechanical speed control

Step 1 : Establish the error value in the following manner:

$$e(t) = \Omega_g{}^* - \Omega_g \tag{III.2}$$

Step 2: The rate of change of the mistake with regard to time is:

$$\dot{e}(\Omega_t) = \dot{\Omega}_g - \dot{\Omega}_g^* \tag{III.3}$$

Step 3: Select a Lyapunov function.

$$V = \frac{1}{2}e^2 \tag{III.4}$$

Step 4: Calculate the rate of change of the Lyapunov function by the dynamics of the system and its control inputs

$$\dot{V}(e) = e(\Omega_g)\left(\frac{1}{j_t}\left(T_g - T_{em} - f_t\Omega_g\right) - k_1 e(\Omega_g) - \dot{\Omega}_g\right) \tag{III.5}$$

Step 5: Develop the control law with BSC.

$$\dot{\Omega}_g = \frac{1}{J_t}\left(T_g - T_{em} - f_t\Omega_g\right) + k_1 e\left(\Omega_g\right) \quad \text{(III.6)}$$

Step 6: Conducting Stability Analysis

Commencing with the Lyapunov derivative:

$$\dot{V}(e) = e(\Omega_g)\left(\frac{1}{J_t}\left(T_g - T_{em} - f_t\Omega_g\right) - k_1 e\left(\Omega_g\right) - \dot{\Omega}_g\right) \quad \text{(III.7)}$$

Replace the control law with the Lyapunov derivative:

$$V^*(e) = e\left(\Omega_g\right)\begin{pmatrix} \frac{1}{J_t}\left(T_g - T_{em} - f_t\Omega_g\right) - k_1 e - \\ \left(\frac{1}{J_t}\left(T_g - T_{em} - f_t\Omega_g\right) + k_1 e\left(\Omega_g\right)\right) \end{pmatrix} \quad \text{(III.8)}$$

Now, let's reduce the complexity of the expression:

$$V^*(e) = e\left(\Omega_g\right)\begin{pmatrix} \frac{1}{J_t}\left(T_g - T_{em} - f_t\Omega_g\right) - k_1 e\left(\Omega_g\right) - \\ \frac{1}{J_t}\left(T_g - T_{em} - f_t\Omega_g\right) - k_1 e\left(\Omega_g\right) \end{pmatrix} \quad \text{(III.9)}$$

End reduction:

$$\dot{V(e)} = -k_1 e\left(\Omega_g\right)^2 < 0 \quad \text{(III.10)}$$

Integrating the positive control gain k_1 is crucial for enhancing system stability.

A higher value of k_1 strengthens the tabilizing effect of the control rule, hence promoting a more robust stability reaction amidst upheavals.

III.4.5 Speed loop linearization

BSC controllers require that the model of the system to be controlled be linear. The speed loop (Figure III.5) must be linearized for this. Here, Ω is the speed controlled. The reference speed Ω_{ref} is obtained by the MPPT algorithm "optimal speed ratio control" [85]. This algorithm is chosen because the turbine characteristics (C_{pmax}, λ_{opt}) are known. The

optimal rotational speed is a function of the measured wind speed as in (III.11).

$$\Omega^{*}=\frac{\lambda_{op}\cdot v_{w}}{R_{p}} \qquad \text{(III.11)}$$

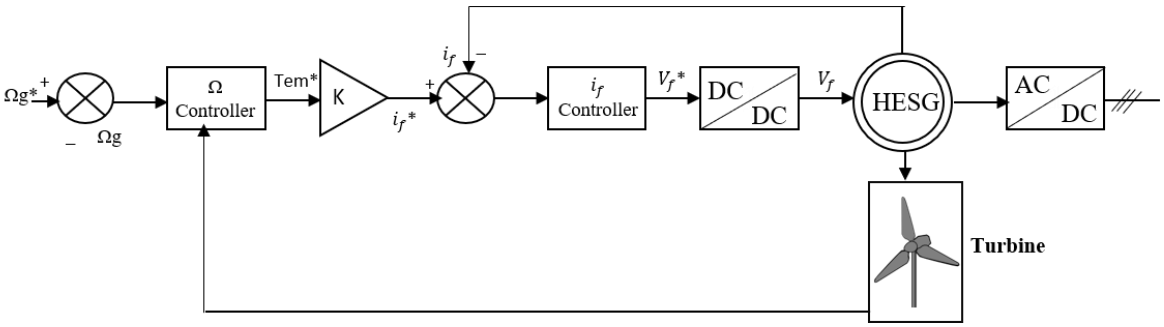

Figure III. 5 *MPPT with excitation field*

III.4.6 Excitation current control

Step 1: The error's dynamics may be described by the the following formula:

$$e(t)=I_{f}^{*}-I_{f} \qquad \text{(III.12)}$$

Step 2: Upon incorporating error dynamics, we derive the following:

$$\dot{e}(t)=\dot{I}_{f}^{*}-\dot{I}_{f} \qquad \text{(III.13)}$$

Step 3: Select a Lyapunov function:

$$V=\frac{1}{2}e^{2} \qquad \text{(III.14)}$$

Step 4: Taking the derivative of V with respect to time results in $\dot{V}=e\dot{e}$, Substituting this expression with the error dynamics gives.

$$V\dot{(e)}=e(I_{f})(\frac{1}{\sigma L_{f}}\left(V_{f}-R_{f}i_{f}-me_{\mu}\right)-k_{1}e\left(I_{f}\right)-\dot{I}_{f}) \qquad \text{(III.15)}$$

Step 5: Currently, a control law u is formulated as

$$\dot{I}_{f}=\frac{1}{\sigma L_{f}}\left(V_{f}-R_{f}i_{f}-me_{\mu}\right) \qquad \text{(III.16)}$$

Step 6: Analysis of stability

Commencing with the Lyapunov derivative:

$$V\dot{(e)}=e(I_{f})(\frac{1}{\sigma L_{f}}\left(V_{f}-R_{f}i_{f}-me_{\mu}\right)-k_{1}e\left(I_{f}\right)-\frac{1}{\sigma L_{f}}\left(V_{f}-R_{f}i_{f}-me_{\mu}\right)) \qquad \text{(III.17)}$$

final streamline:

$$\dot{V(e)} = -k_1 e\left(I_f\right)^2 < 0 \qquad \text{(III.18)}$$

The system in question will demonstrate stability when a positive stable, indicated by k_1

An identification process obtains the linearized model: simulations are performed on the complete Simulink model of the SCE (Figure III.6), where commutations, space harmonics and transmission shaft flexibilities are taken into account for four operating points distributed in zone II.

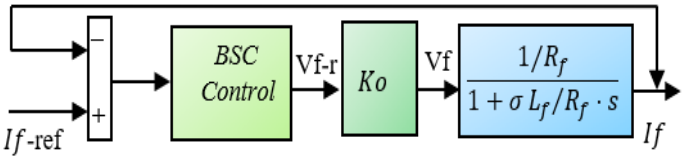

Figure III. 6 *model of excitation current.*

III.5 Mechanical adjustment of the wind turbine in zone III

Wind energy is certainly a free energy source, but unfortunately, wind profiles are difficult to predict. Beyond a certain wind speed, the control objectives change: the torque is no longer controlled to maximize the power extracted from the wind, but the power is regulated to its nominal value to reduce the stresses on the WT structure.

To set the power extracted from the WT to a constant value, a mechanism is required that modifies the turbine's operation according to the wind. Experimentally, the value of Cp can be modified by changing the pitch angle. When the wind speed changes, the blades change their inclination and therefore their lift. This reduces the aerodynamic torque and allows power generation to be regulated. This is the role of pitch control, which only works in zone III. In this zone, the turbine and generator rotation speeds must be kept constant, knowing that a small variation in pitch can cause the output power to vary considerably.

To model the pitch angle adjustment system, it can be divided into four subsystems: mechanical, electrical, aerodynamic and control system, and the interactions between the four must be taken into account [86].

III.5.1 Generation of the reference angle

The reference angle βref applied to the blade orientation system is the sum of a pitch angle obtained by power adjustment and another calculated in steady state [87]. It is customary to use experimental characteristics to obtain information about the reference angle βref. Since the characteristics of our wind turbine (Cpopt, λopt) are known, it is possible to define the optimal values of the pitch angle in steady state.

The calculation of the optimal pitch angle in steady state is done as follows:

- ✓ **Determine the optimal tip-velocity ratio (λopt):** The optimal tip-velocity ratio is the tip-vlelocity ratio that maximizes the power output of the WT at a given wind speed. This value can be obtained from experimental data or from a WT model.
- ✓ **Calculate the specific velocity (λi):** The specific velocity is the ratio of the WT rotation speed to the square root of the wind power. It is a dimensionless quantity that is used to characterize the performance of WT.
- ✓ **Set the specific velocity to the optimal value:** In order to maintain the turbine rotation speed at Ω_{tnom}, the specific speed must be set to the optimal value (λ_{opt}). This can be done by adjusting the pitch angle of the blades.
- ✓ **Calculate the optimal pitch angle (βopt):** The optimal pitch angle is the pitch angle that corresponds to the optimal tip-velocity ratio and the specific speed. This value can be obtained from a table of experimental data or from a wind turbine model.

III.5.2 Power Adjustment

The reference angle is given either by the servo-control of the turbine rotation speed to the nominal speed or by the regulation of the measured power to the nominal power. In this work, the latter method has been chosen. It is illustrated by Figure III.7. This requires the estimation of the mechanical power of the turbine from the operating conditions (λ, β) [88]. One solution is to identify the dynamics of the wind turbine system in order to define a function of Pt=f(βref).

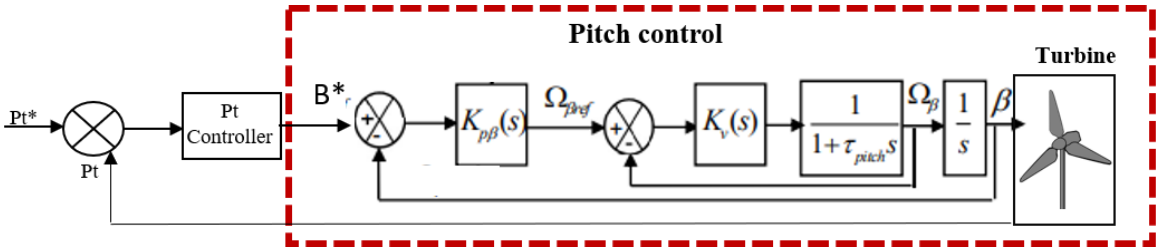

Figure III. 7 *pitch control*

III.6. Simulation results

III.6.1 Performance study through simulation

Initial testing of the corrector is carried out on a simplified model of the generator: neither harmonics nor commutations are considered. In this case, the generator delivers directly to a 3ph- resistive load Rc = 15 Ω. The load is modelled by a gain. The chopper is also modelled by a gain K_0. Simulation results show that, regardless of the current value, a 5% rise time of 0.01s is obtained with almost zero overshoot (Figure III.7). The response time is therefore fully in line with the setting made to dimension the current loop. Figure III.7 demonstrates the BSC's robustness against harmonic effects. When the PI method is inverted, a significant overshoot indicates that the BSC outperforms the PI control.

III.6.2 Zone II:

In test 2, a systematic method is used, beginning with a regulated wind with four discrete stages (as shown in Figure.III.9) and shifting to a nonlinear system in zone 2, which is meant to rigorously analyses the methods adaptation to rapid wind variations. The principal emphasis of this investigation is on important performance measures, including settling time and overshoot. Moreover, Figure.III.10 offers a perceptive perspective on the rotating speeds of the generator, which are affected by a wind profile with distinct steps. The definitive findings unequivocally confirm the superior efficiency of the BSC, effectively reducing static error to almost negligible levels and guaranteeing well-controlled oscillations under all operating conditions, with a maximum overshoot well below the acceptable limit of 5%. In contrast, the PI controller shows a higher overshoot of 20%, indicating its relatively reduced reliability. Both controllers have constant resting times across all speed settings, indicating remarkable performance. Within the steady-state domain, the BSC provides a little improvement in accuracy, resulting in minimal variations in the extraction of wind energy, as depicted in Figure III.11.

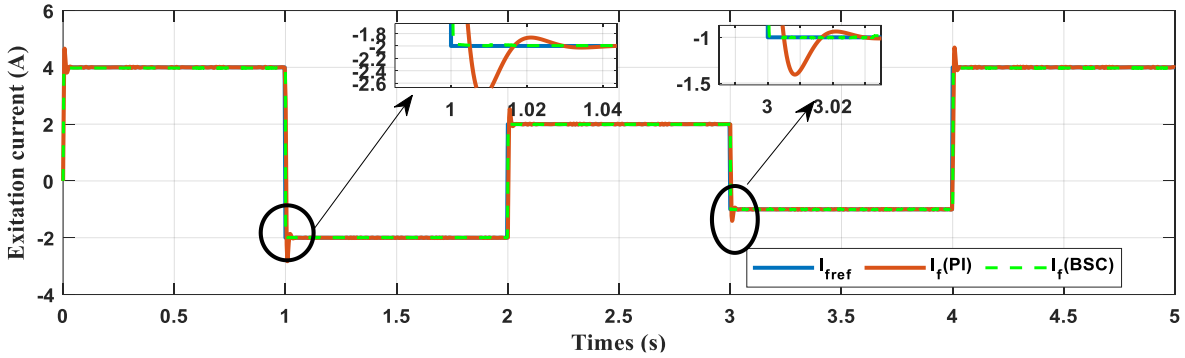

Figure III. 8 *: Evaluation of the existing controller's Robustness.*

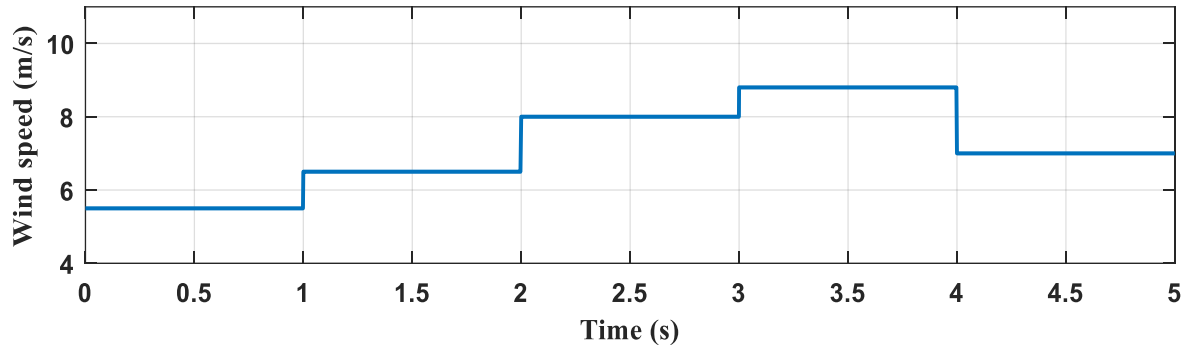

Figure III. 9 *: Wind velocity [m/s] (step in zone II)*

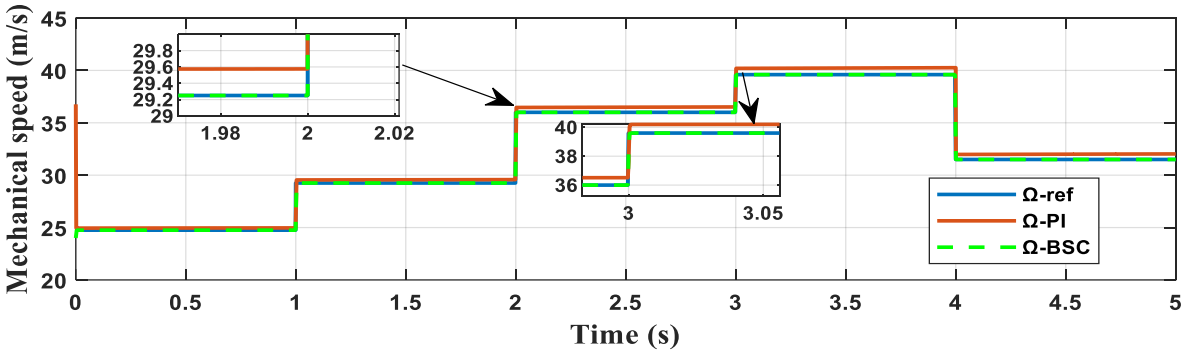

Figure III. 10 *Mechanical velocity (step in zone II)*

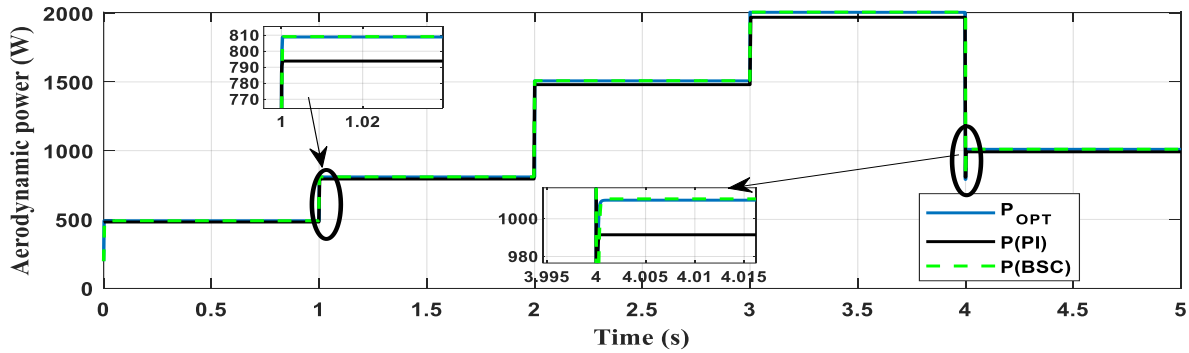

Figure III. 11 *Aerodynamic energy (W) (step in zone II)*

The first tests conducted in zone 2 do not sufficiently certify the controllers, as they fail to accurately simulate genuine meteorological wind conditions. In order to tackle this issue, the system goes through further evaluation utilizing a stochastic wind profile, as illustrated in Figure.III.12. The simulations, depicted in Figure.III.13 and 14, illustrate that both controllers effectively achieve reference tracking and efficiently handle the full-bridge rectifier and DC/DC converter. Furthermore, they demonstrate a strong ability to withstand variations in harmonic currents in the generator. The BSC method outperforms the typical PI controller in accurately following the optimal rotational speed, as demonstrated by the minimal power variation shown in Figure 15. The outcomes highlight the capability of the BSC controller to improve the efficiency of wind power harvesting, providing practical advantages for deployment.

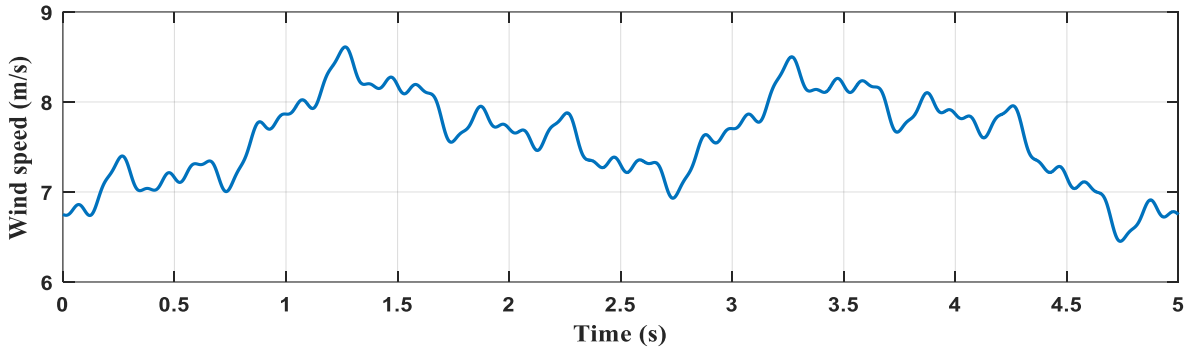

Figure III. 12 *Wind velocity [m/s] (stochastic in zone II)*

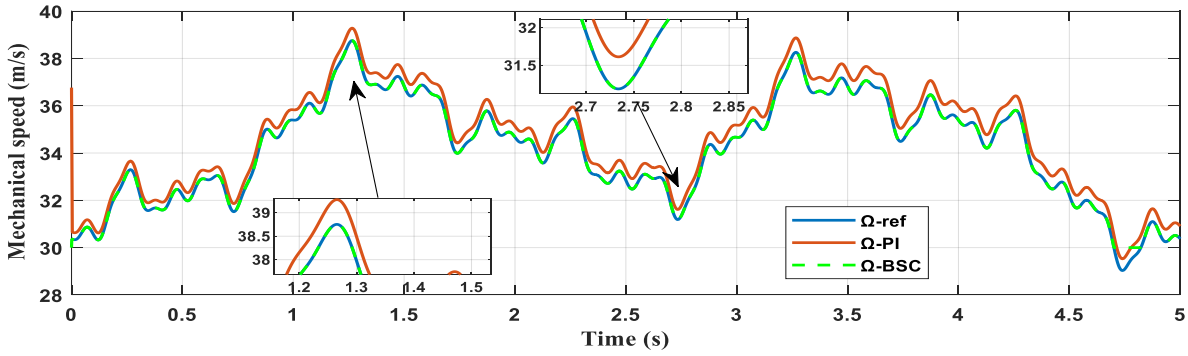

Figure III. 13 *Mechanical velocity (stochastic in zone II)*

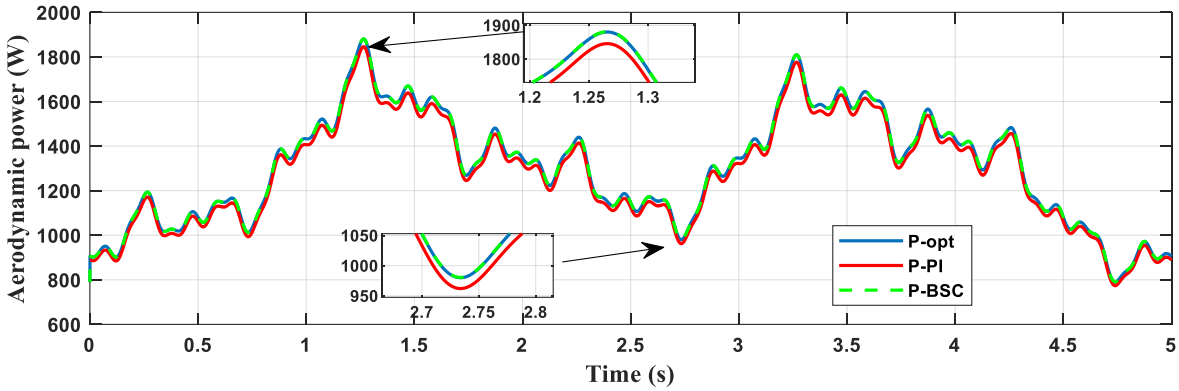

Figure III. 14 *Aerodynamic energy (W) (stochastic in zone II)*

III.6.3 Zone III:

By replicating the test in Zone III, the investigation is expanded to assess the transient stability that is naturally present in the drive train dynamics of the wind energy system. Zone III is marked by increased mechanical strain, which necessitates the need to maintain a continuous rotational speed for stability. Figures III.15 and 16 depict the wind profile and velocity response, respectively. The implementation of the BSC controller leads to a substantial decrease in velocity variations, demonstrating its better closed-loop performance. Figure III.17 illustrates the relationship between turbine output and wind velocity shifts, with distinct peaks observed, especially in the hard step wind profile. The lack of these peaks in a stochastic wind profile demonstrates that although turbulence is possible in real conditions, it seldom approaches the extremes caused by these abrupt changes.

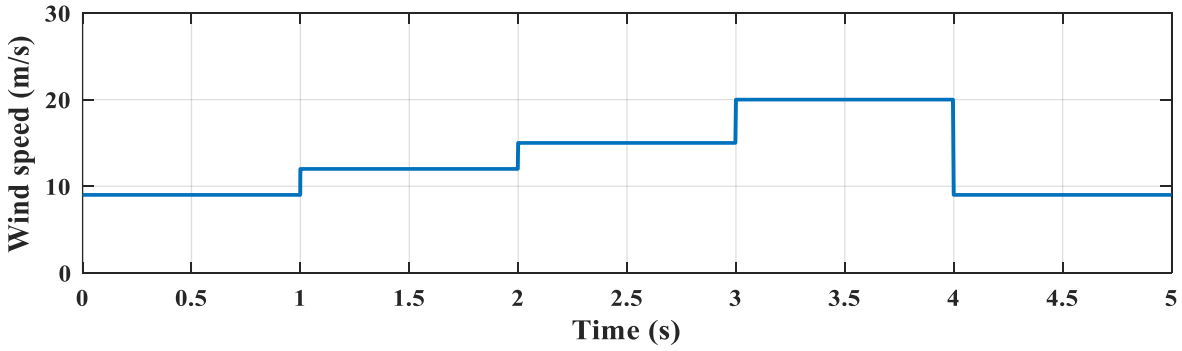

Figure III. 15 *Wind velocity [m/s] (step in zone III)*

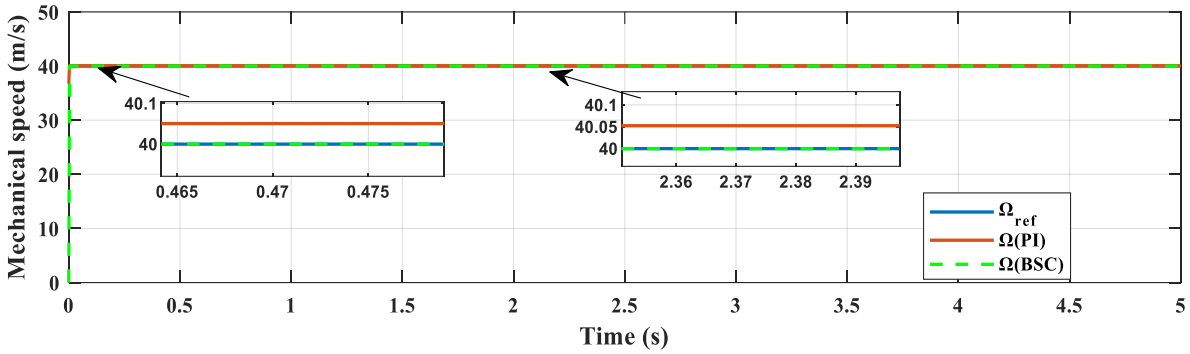

Figure III. 16 *Mechanical velocity (step in zone III)*

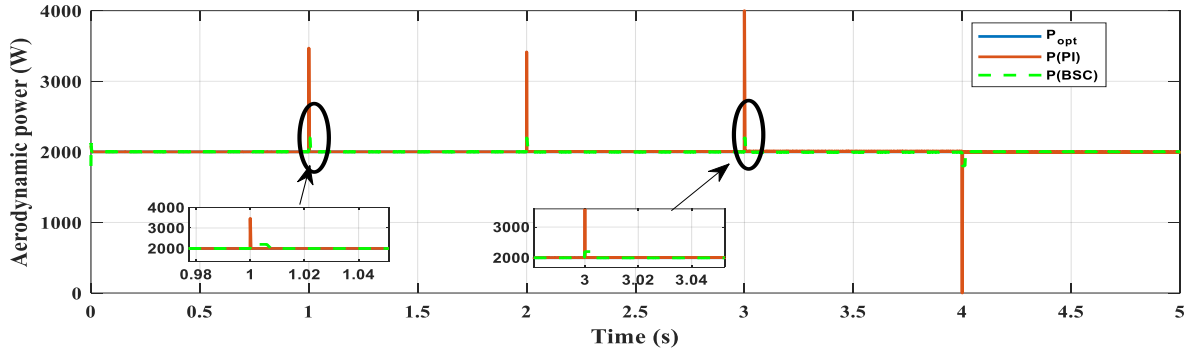

Figure III. 17 *Aerodynamic energy (W) (step in zone III)*

In Zone III, the effectiveness of the BSC controller in reducing mechanical vibrations and minimizing oscillation was seen, as demonstrated by the stochastic wind profile depicted in Figure.III.18 and Figure.III.19. These figures demonstrate that the rotational velocity shows more efficiently damped oscillations compared to other approaches being considered. Furthermore, Figure.III.20 illustrates the turbine's peak power capacity, which amounts to 2 kw. BSC shines compared to PI control. BSC can automatically adjust to the wind's constantly changing nature. It excels at handling sudden wind speed variations because it can deal with non-linear behavior effectively. BSC is also very resistant to outside influences and tracks power output precisely. This translates to lower errors when the system reaches a steady state, less oscillation, and a peak power overshoot that stays below the acceptable limit of 5%. While PI control can be useful in some situations, it allows for a 20% larger overshoot, indicating it's less stable during wind changes. Overall, BSC outperforms PI control when it comes to managing the complexities of a wind turbine's drivetrain and achieves high accuracy during stable operation.

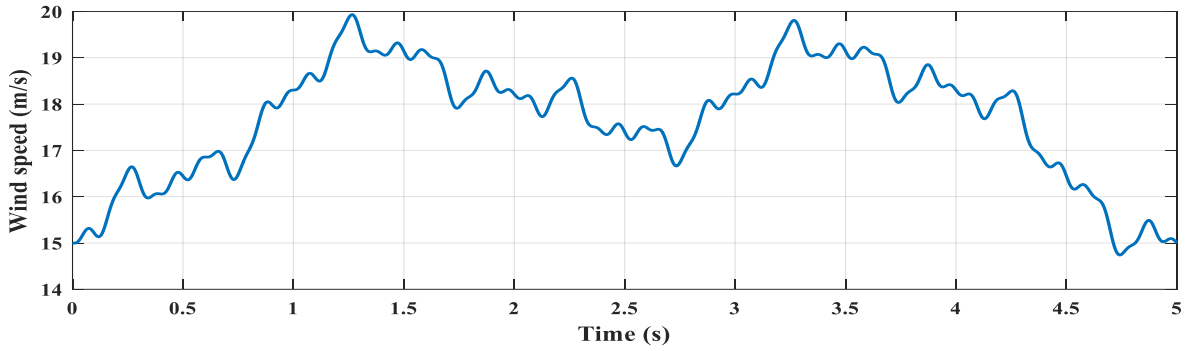

Figure III. 18 *Wind Velocity [m/s] (stochastic in zone III)*

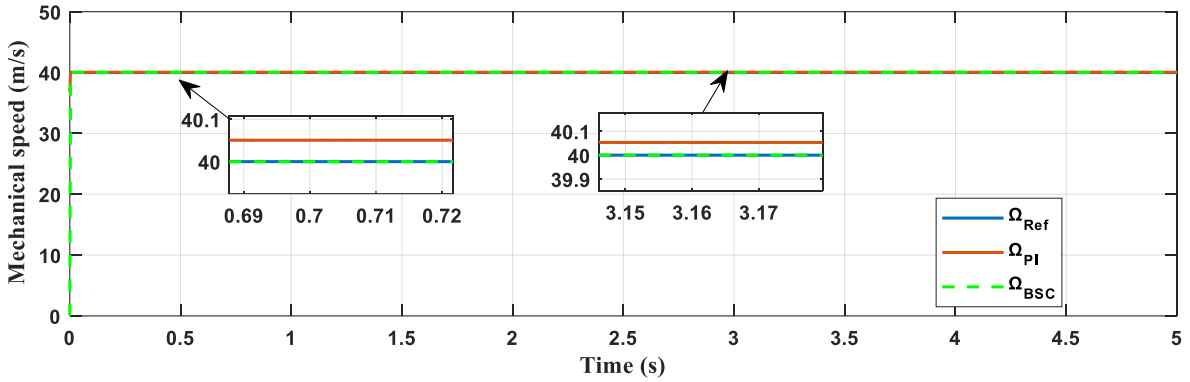

Figure III. 19 *Mechanical velocity (stochastic in zone III)*

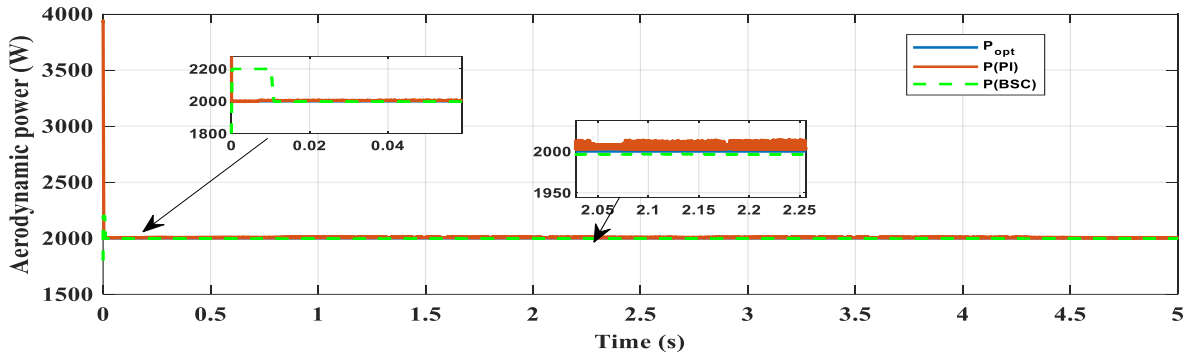

Figure III. 20 *: Aerodynamic energy (W) (stochastic in zone III).*

III.7 Conclusion

In this chapter, we have detailed the control strategy for the HESG-based WECS. We began with an open-loop study of our system to evaluate the controlled variables as a function of the system inputs. This evaluation aims to ensure that each optimal point can be reached in closed loop without exceeding the electrical and mechanical limits of the WTS.

Next, two control strategies for the rotation speed of a hybrid generator are developed. Finally, a pitch controller is implemented for power limitation in zone III. The simulation findings confirm that the implementation of a BSC in WECS improves productivity, stability, and reliability. These advancements signify a significant enhancement in the efficacy of wind power systems to achieve heightened durability and efficiency.

The following chapter focuses on the issue of connecting our 1.5 MW WECS to the electrical grid.

Chapter IV: Advanced Super-Twisting Control for Grid-Connected HESG-Based WECS

IV.1 Introduction

The integration of wind energy into the electrical grid presents a range of challenges for various stakeholders, from power producers to transmission and distribution system operators, and ultimately to consumers. To effectively integrate wind energy, it is necessary to address these challenges in several areas:

- Challenges in Market Transformation: Engaging all participants to maintain equilibrium between production and demand [89].
- Power Grid Planning and Management: Optimizing current systems, with strategic expansion and strengthening where needed.
- Connecting Wind Energy to the Grid: Control strategies, power quality, and wind turbine capabilities.

This chapter focuses on developing the control laws necessary to establish this connection. After validating the applicability of the hybrid generator in isolated mode, the goal is to connect the WP wind turbine based on a double-excited generator to the electrical grid. For this purpose, a medium-voltage (MV) grid is implemented in Matlab/Simulink. The structure of the studied grid is first modeled. The connection device is presented in the park reference frame. This simplified representation facilitates the development of control laws. Then, a more "realistic" architecture of an MV grid and its connection device will be implemented using Matlab's "Simpowersystem" tools. The second part of this chapter is dedicated to the synthesis of appropriate controllers to ensure the reliability of this connection. The last part will be devoted to simulation results.

IV.2 Modeling of the grid side converter

This section focuses on modeling the electrical configuration that enables the wind energy conversion system to connect to the grid. Figure IV.1 illustrates the fundamental arrangement, with a DC bus linking the rectifier and inverter. The inverter governs the DC bus voltage and manages the transfer of active and reactive power between the turbine and the grid. Before entering the grid, the current flows through an RL filter. A phase-locked loop (PLL) is employed to provide real-time measurements of grid-side voltage and frequency.

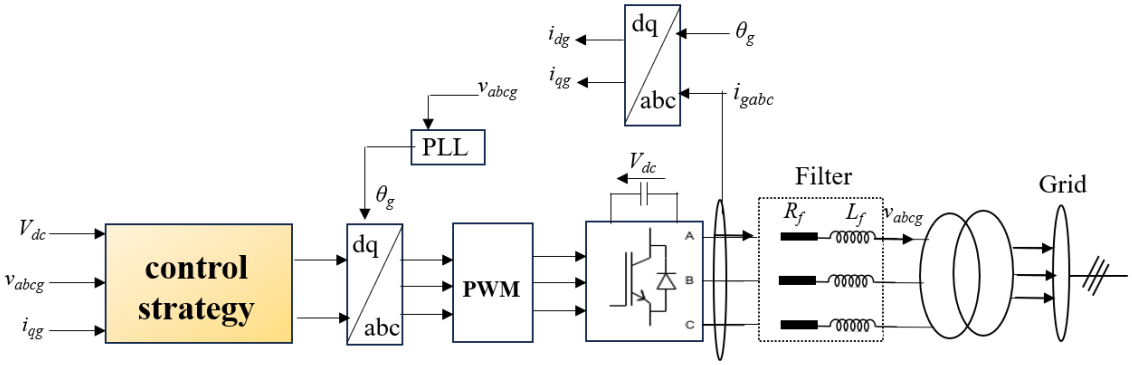

Figure IV. 1 *control of the grid side converter*

IV.3 Modeling of the DC Bus:

The HESG-side rectifier and the grid-side inverter are linked via a DC bus (Figure IV.2). This bus facilitates power transfer from two separate sources with disparate frequencies by separating the fixed grid frequency from the variable frequency of the generator.

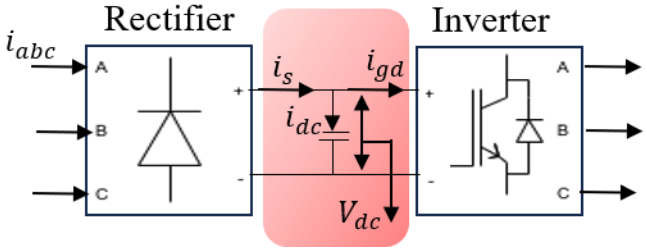

Figure IV. 2 *Back-to-Back Converter with Intermediary DC Bus.*

The mathematical model of the continuous bus can be expressed by (IV.1)

$$V_{DC}(t) = \frac{1}{\Delta T}\int_{t_0}^{t_0+\Delta T} \frac{1}{C} i_{DC}(t) + V_{DC}(t_0) \qquad \text{(IV.1)}$$

Where $V_{DC}(t0)$ is the starting voltage reading across the capacitor.

The capacitor current is determined by the difference between the two modulated currents:

$$i_{DC}(t) = i_s(t) - i_{gd}(t) \qquad \text{(IV.2)}$$

The transfer function of the DC bus is given by (IV.3), and its block diagram is shown in Figure IV.3.

$$\frac{V_{DC}(s)}{i_{DC}(s)} = \frac{1}{C \cdot s} = \frac{\tau_c}{s} \qquad \text{(IV.3)}$$

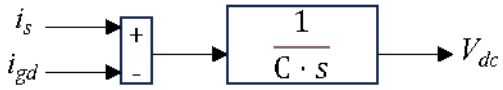

Figure IV. 3 *Block Diagram of the DC Bus model*

To send a current into the grid, the VDC voltage must satisfy the following condition [90]:

$$V_{DC} \geq \sqrt{6} \cdot V_g \tag{IV.4}$$

In this context, Vg denotes the voltage present on the filter side. Since the effective voltage at the primary of the connection transformer is 690 V (as indicated in Table VI.1), the nominal voltage of the DC bus is configured to be 1800 V.

$$V_{DC} \geq \sqrt{6} \cdot 690 \tag{IV.5}$$

Table IV. 1 *Grid Connection Parameters [169]*

Parameter	Value
R_g	0.00095Ω
L_g	0.000303H
V1	690V
V2	25KV
C	0.01F
V_{dc}	1800V

IV.4 Model of the electrical grid:

To examine the performance of our WECS, we propose the electrical network configuration depicted in Figure IV.4. The infinite HTB grid is represented by a three-phase RLE-type source with a short-circuit power of Scc = 1,300MVA. The nominal voltage of the HT network U_{source} is specified as 120 kV, with zero phase shift between the source's voltage and current. The rest of the network consists of:

- A step-down transformer rated at 120 kV/25 kV with a nominal power of 47 MVA, referred to as "Transformer (2)" in Figure IV.4.
- Two three-phase loads, one with a capacity of 2.6 MW and the other with a capacity of 1.5 MW.
- The WP turbine is linked to the network through a 690 V/25 kV transformer, designated as "Transformer (1)" in Figure IV.4.

All the elements outlined above are represented through the "Simpowersystem" blocks in Matlab, as shown in Figure IV.5. Here, the block labeled "wind turbine" depicts the model of the 1.5 MW WT interfaced with the hybrid generator and its power converters, specifically the chopper for control and the rectifier for connection to the DC bus.

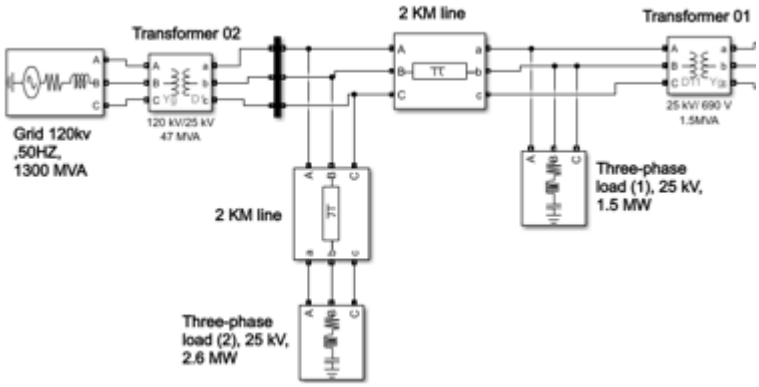

Figure IV. 4 *grid model*

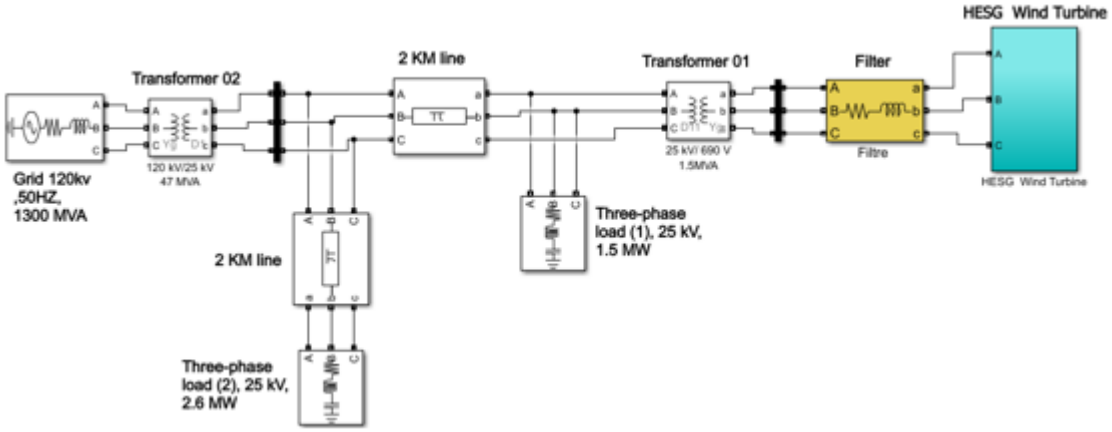

Figure IV. 5 *Grid Integration of HESG-Based WECS implemented in Matlab/Simulink.*

IV.5 Grid-side converter control

Once the system modeling is complete, the next step is to control the inverter and the DC bus. The aim is to keep the DC bus voltage stable, transfer all active power generated by the wind turbine to the grid, and eliminate reactive power transfer to reach a unity power factor. The control block diagram is illustrated in Figure IV.6.

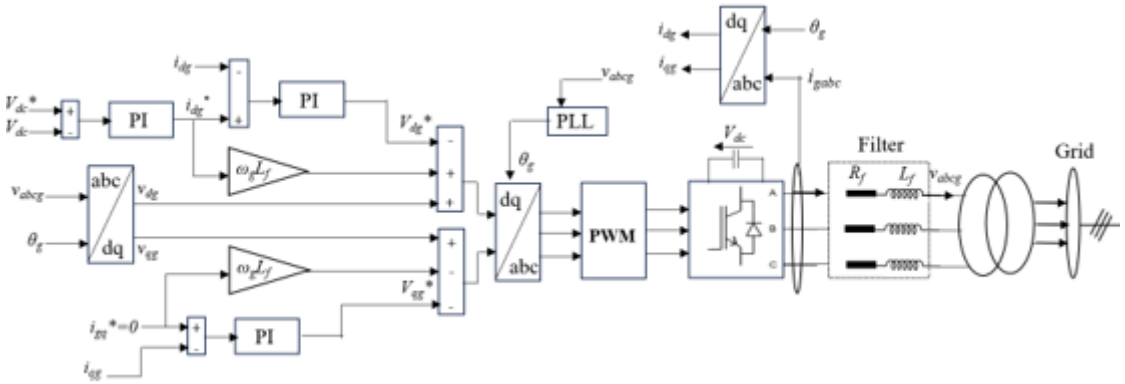

Figure IV. 6 *Grid-side converter control loop.*

This control is executed by two interdependent loops. The inner loops focus on regulating the filter currents, whereas the outer loops are designed to regulate the DC bus voltage and reactive power.

IV.5.1 DC bus voltage control

The DC bus is regulated by a PI controller denoted $C_{DC}(s)$ [91, 92] which generates the reference current id-ref at its output (Figure IV.7). The reaction time for the outer DC bus control loop is generally set to a few milliseconds [93]. This duration should be at least ten times longer than the inner loop managing the filter currents and must also exceed the calculation period for 50 Hz frequency components (10 ms). A reaction time of 15 ms is considered sufficient for this loop [90]. The time constant of the DC bus controller is equivalent to C_{DC}.

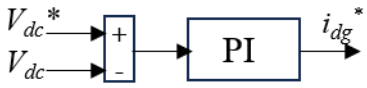

Figure IV. 7 *DC Bus Control Block Scheme.*

The quadrature component of the current is utilizing to regulate reactive power, and the direct component is utilizing to regulate the DC bus voltage. The direct current id-ref comes from the DC bus controller $C_{DC}(s)$ (Figure IV.7). The quadrature reference current is maintained at zero. This enables the elimination of reactive power, achieving a unity power factor. In the Park reference frame, the power injected into the grid can be articulated as (IV.6) [94]:

$$\begin{cases} P_g = v_{gd} i_{gd} - v_{gq} i_{gq} \\ Q_g = v_{gq} i_{gd} + v_{dg} i_{gd} \end{cases} \quad \text{(IV.6)}$$

The paragraph explains that the synchronization of the park reference frame with grid

voltages leads to a zero quadrature component of the grid voltage in the Park reference frame. This observation, along with equation (IV.7), enables further deductions or calculations related to the behavior of grid-connected systems in the park reference frame.

$$\begin{cases} i_{dg}^{*} = \dfrac{P_g^{*}}{V_g} \\ i_{qg}^{*} = -\dfrac{Q_g^{*}}{V_g} \end{cases} \tag{IV.7}$$

IV.6 Proposed ASTC design

The TOSMC is a recently developed strategy that is a viable alternative to the conventional SMC technique. This technique is non-linear. The primary benefits of this approach, in contrast to various alternative methods like backstepping control, are its simplicity and straightforward implementation. The ASTC approach is a contemporary technology that aims to substitute the previous approach and enhance the effectiveness and longevity of systems [95, 96]. The ASTC method uses a sliding surface (SS) [97], which is a mathematical function that measures the difference between the current state of the system and the desired reference state [98 ,99]. The goal is to reduce this SS to zero [100,101], and thus provide accurate reference signal tracking has been achieved. Equation (IV.8) depicts the comprehensive framework of the STC [102].

$$x(t) = x_1(t) + x_2(t) + x_3(t) \tag{IV.9}$$

With

$$\begin{cases} x_1(t) = a_1 \cdot \mathrm{Sign}(S) \\ x_2(t) = a_2 \cdot \int \mathrm{Sign}(S)dt \\ x_3(t) = a_3 \cdot \sqrt{|S|} \cdot \mathrm{Sign}(S) \end{cases} \tag{IV.10}$$

Equation (IV.11) provides the expression that precisely characterizes the output of the STC .

$$x(t) = a_1 \cdot \mathrm{Sign}(S) + a_2 \cdot \int \mathrm{Sign}(S)dt + a_3 \cdot \sqrt{|S|} \cdot \mathrm{Sign}(S) \tag{IV.11}$$

The control input, denoted as $x(t)$, and the SS, denoted as S, are defined. Additionally, a_1, a_2, and a_3 represent the controller gains.

This algorithm uses a discrete function (sign function) that defined as following:

$$\text{sgn}(S)=\begin{cases}\dfrac{S}{|S|}=\begin{cases}1 & \text{if S}>0\\ -1 & \text{if S}<0\end{cases}\\ 0 \quad \text{if S}=0\end{cases} \tag{IV.12}$$

A simple approach is to add a term ‘b’ to its denominator to address the sign function's discontinuity. The resulting smoother function is given below:

$$smooth(S)=\frac{S}{|S|+b} \tag{IV.13}$$

The constant "b" regulates the degree of smoothness that this function exhibits. When the value of b is too small, the function represented by smooth (S) approaches the standard sign function. If the value of b tends towards infinity, the equation for the evolution of S only significantly impacts a narrow range of values close to 0. Therefore, the function tanh is highly responsive to the argument b. Hence, it is imperative to select the value of b meticulously. We aim to mitigate or ignore the influence of b while maintaining the accuracy of the aforementioned smooth approximation. To gain a more comprehensive comprehension, the suggested controller's control law is designed as follows, based on equation IV.10 and by changing the "sign" function with the proposed "smooth" function:

$$\begin{cases}x_1(t)=a_1\cdot \text{smooth}(S)\\ x_2(t)=a_2\cdot \int smooth\ (S)dt\\ x_3(t)=a_3\cdot \sqrt{|S|\cdot \text{smooth}(S)}\end{cases} \tag{IV.14}$$

Equation (23) provides the expression that precisely characterizes the output of the suggested ASTC.

$$x(t)=a_1\cdot \text{smooth}(S)+a_2\cdot \int \text{smooth}\ (\text{S})\text{dt}+a_3\cdot \sqrt{|S|}\cdot \text{smooth}(S) \tag{IV.15}$$

Figure IV.8 shows the simplify concept and operating principles of the proposed ASTC method.

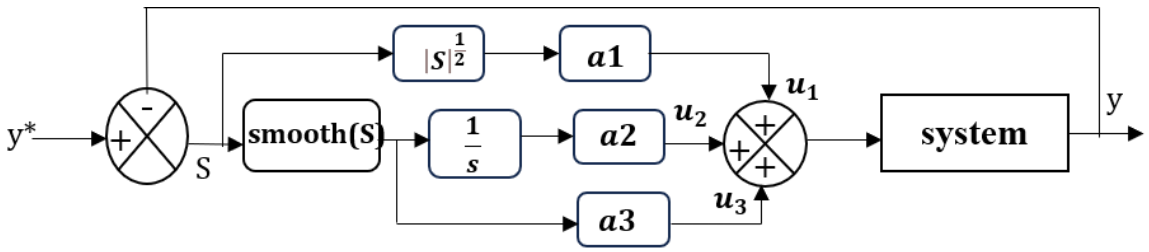

Figure IV. 8 *Proposed ATSC Desing.*

To implement the technique devised in the preceding section, three SS are used and defined as follows:

$$\begin{cases} s_{V_{dc}} = V_{dc}^{*} - V_{dc} \\ s_{idg} = i_{dg}^{*} - i_{dg} \\ s_{iqg} = i_{qg}^{*} - i_{qg} \end{cases} \quad \text{(IV.16)}$$

The SS specified in Equation (IV.16) are employed as ASTC law inputs. As a result, the dc bus voltage and dq current is regulated by regulators, which in turn affect the dq voltage, as illustrated in (IV.17)

$$\begin{cases} i_d^* = a_1 \cdot \text{sign}(S_{V_{dc}}) + a_2 \cdot \int \text{sign}(S_{V_{dc}})dt + a_3 \cdot \sqrt{|S_{V_{dc}}|} \cdot \text{sign}(S_{V_{dc}}) \\ V_q^* = a_1 \cdot \text{sign}\left(S_{i_q}\right) + a_2 \cdot \int \text{sign}\left(S_{i_q}\right) dt + a_3 \cdot \sqrt{|S_{i_q}|} \cdot \text{sign}\left(S_{i_q}\right) \\ V_d^* = a_1 \cdot \text{sign}(S_{i_d}) + a_2 \cdot \int \text{sign}(S_{i_d})dt + a_3 \cdot \sqrt{|S_{i_d}|} \cdot \text{sign}(S_{i_d}) \end{cases} \quad \text{(IV.17)}$$

The control strategy of the HESG-based WECS follows a cascade structure, as seen in Fig. IV.9

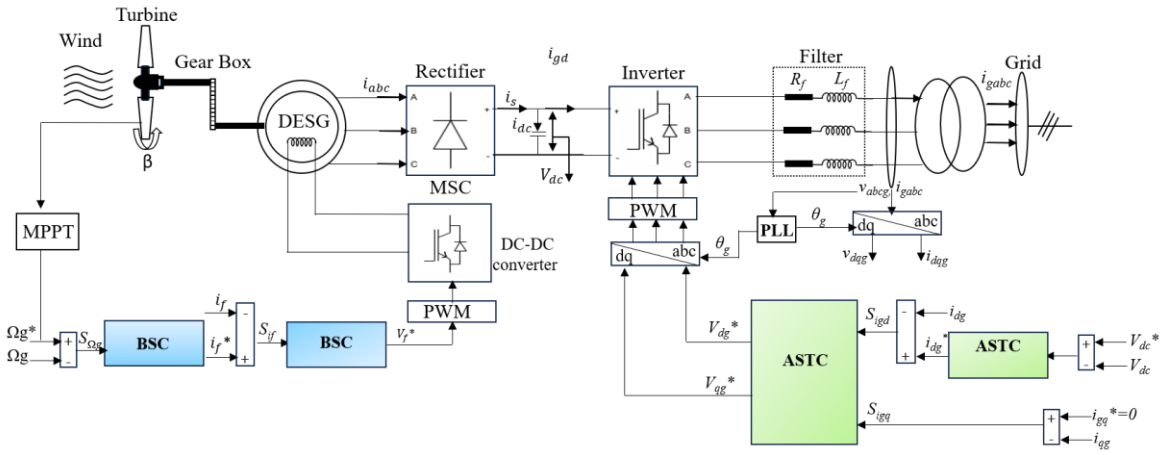

Figure IV. 9 *HESG-based WECS.*

IV.7 Simulation results

The performance of the controller is assessed in zones 2 and 3 using MATLAB/Simulink software and compared to conventional control methods. Five numerical simulation tests were performed to assess the efficacy of the control techniques described in this study and to showcase the functioning of the HESG-based WECS (Figure IV.9) in different scenarios. The simulation's parameters are specified in the appendix. The numerical simulations employed a reactive power reference of Qg* = 0 and a reference voltage of Vdc = 1800V for the DC bus.

IV.7.1 First test

The present study will assess the effectiveness of the proposed ASTC control method in Zone 2 when subjected to step wind speed conditions, in comparison to the STC and PI control methods. The comparison evaluates various parameters, including reference tracking, total harmonic distortion (THD) of electrical current, fluctuations in active and reactive power, and response speed. The velocity profile of the step wind utilized in this test is shown in Figure IV.10. Figure IV.11 depicts the operational efficiency of a WECS employing three different control techniques: STC, PI controls, and the innovative ASTC.
Figure IV.12 illustrates the connection between the variations in the wind profile and the mechanical speed produced by MPPT. The MPPT-BSC outperforms the MPPT-PI in minimizing fluctuations in speed, lowering the time it takes to reach a stable state, minimizing the inaccuracy in the steady-state, and preventing overshooting. The proposed BSC exhibits a markedly reduced overshoot of 0.1%, in contrast to the PI, which have overshoot values of 0.60%, respectively. With respect to settling time, the BSC exhibits an initial settling time of 10 ms, whereas the PI achieves settling in 40 ms, Moreover, variations in the rotor's velocity are observed when the wind speed changes, guaranteeing that it stays near the desired value above the set wind speed. Upon analyzing the speed curves in relation to the reference, it is evident that both the PI controller (with a steady-state error of 3.6%) display variations. However, the BSC implementation effectively reduces this level of error to 0.43%, as seen in Table 2

Table IV. 2 *Overshoot and response time of the mechanical speed*

Controller	Overshoot ratio (%)	Response time (ms)	Steady-state error (%)
PI	0.60	40	3.6
BSC	0.1	10	0.43

Figure IV.12 illustrates the current that stimulates the HESG. The results indicate that the BSC performs better than the PI, with a setting time of under 10 ms. whereas the response PI controller is 40 milliseconds. Furthermore, the BSC exhibits stronger reference tracking capabilities, surpassing the PI. Figure IV.13 demonstrates the effective management of the DC-link voltage control when a sudden gust of wind occurs. The new ASTC demonstrates significant advantages in its control mechanism when compared to other regulators such as PI and STC. The main focus was on the duration it takes for anything to be set, the monitoring of references, and the degree of exceeding the target. The ASTC shows a deviation of 0.15% from the nominal voltage value. A response time of approximately 10 ms is sufficient for the DC voltage to reach a stable condition at the desired value. The presence of an efficient tracking system is clearly observed in stable conditions, since it demonstrates a low static error rate. Contrary to the STC, it demonstrates a response time of 30 milliseconds with an overrun of 0.3%. Conversely, the PI controller demonstrates a response time of 40 milliseconds, accompanied by an overrun of 0.55 percent. The result is displayed in Table 3.

Table IV. 3 *Overshoot and response time of the DC-link voltage*

Controller	Overshoot ratio (%)	Response time (ms)
PI	0.55	40
STC	0.3	30
ASTC	0.15	10

In addition, it is noted that the active and reactive powers (Pg and Qg) nearly conform to the references for all control methods (Figure IV.14 and 15). The active power is mostly associated with the wind speed seen in Figure IV.10, and its magnitude increases as the wind speed rises. The reactive power (Qg) in Figure IV.15 remains constant as changes in wind speed have no effect on it. The recommended control strategy prioritizes the dynamic response and aims to reduce ripples. It is implemented before the PI and STC controls. Active power generation entails the direct insertion of electrical current into the grid, guaranteeing that the current waveform adheres to the network code standards for frequency and quality as depicted in Figure IV.16. Figure IV.17 and j show the THD of grid current for two controllers: one using the STC approach with a THD of 3.24%, and the other using the ASTC method with a THD of 1.68%. THD experienced a reduction of around 48.14% when utilizing ASTC in comparison to STC. The THD value produced by ASTC is lower than the THD value provided by STC. Furthermore, the power efficiency of the HESG-based WECS rose to 97.3% with the integration of ASTC. According to Table

4, this outperforms typical STC and PI controllers, which achieve efficiencies of 91.8% and 89.2%, respectively.

Table IV. 4 *Injected current THD and power efficiency*

Controller	Injected current THD (%)	power efficiency (%)
PI	-	82.2
STC	3.24	91.8
ASTC	1.68	97.3

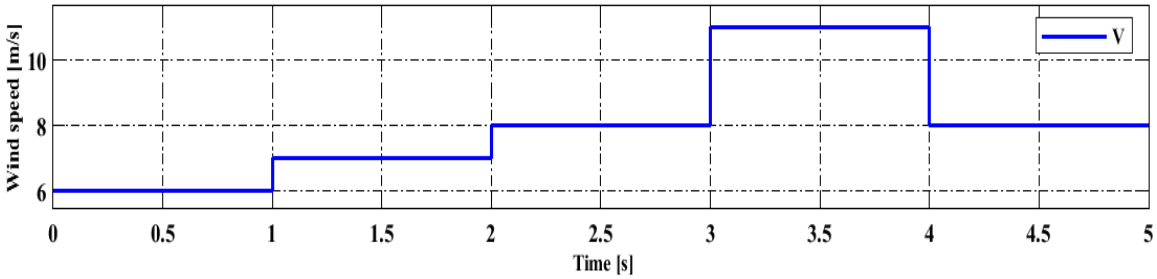

Figure IV. 10 *step wind [m/s] (zone 2)*

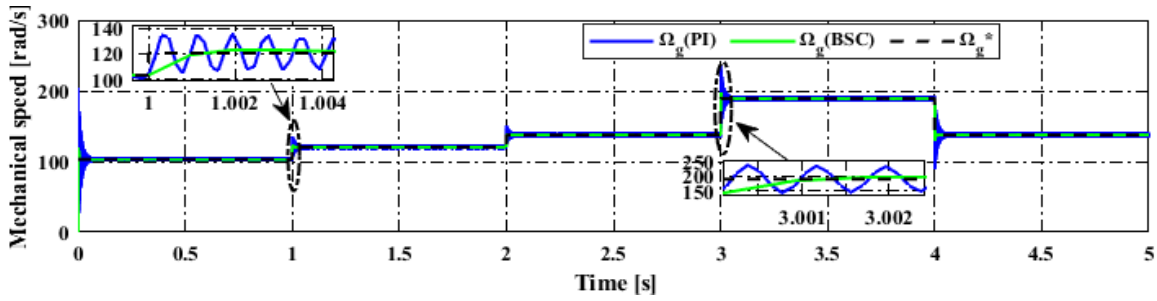

Figure IV. 11 *mechanical velocity [rad/s] (zone 2)*

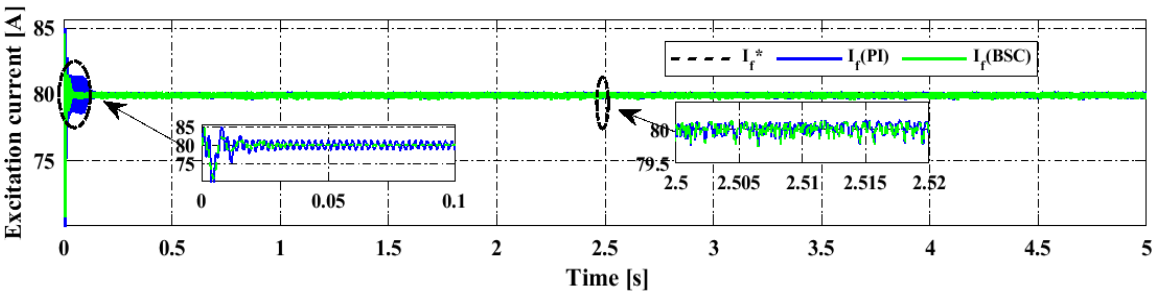

Figure IV. 12 *Excitation current [A] (zone 2)*

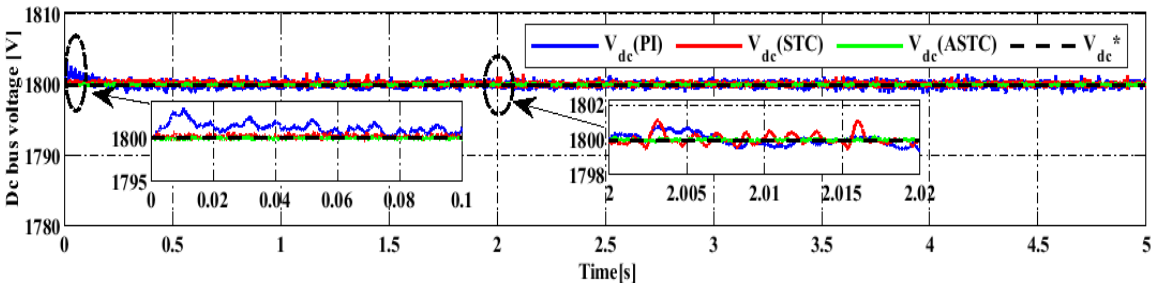

Figure IV. 13 *Dc bus voltage [V]*

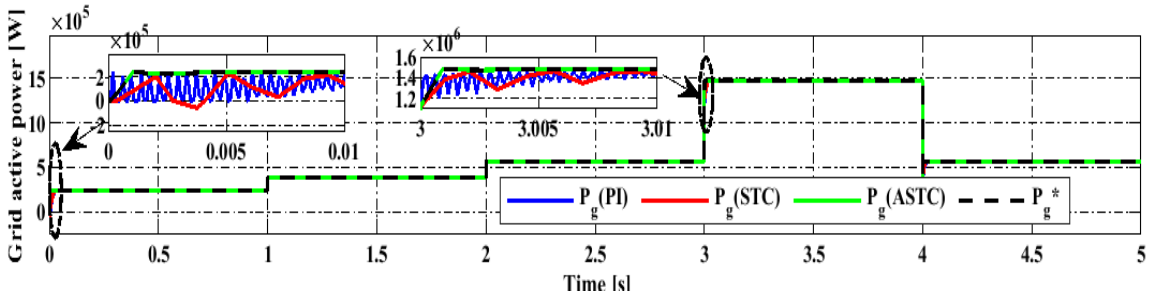

Figure IV. 14 *Active power [W]*

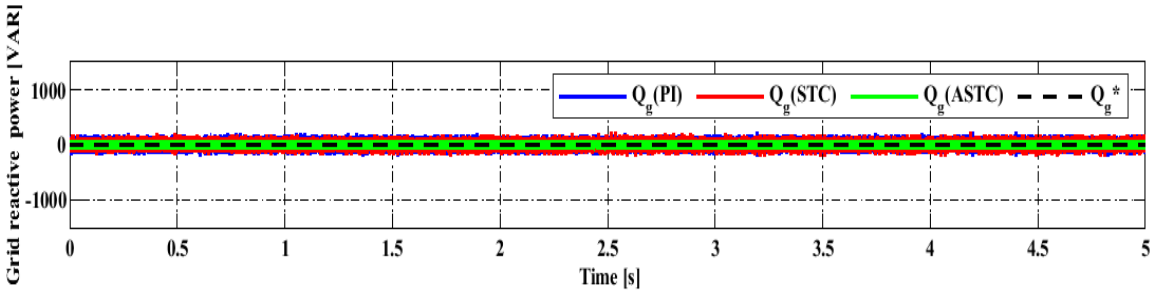

Figure IV. 15 *Reactive power [VAR]*

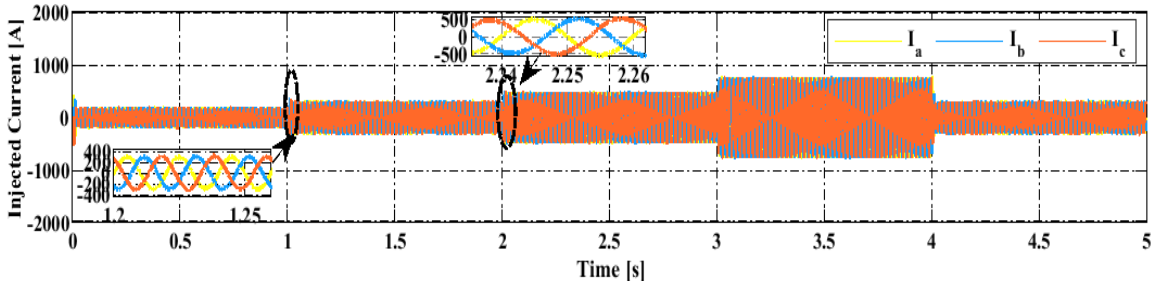

Figure IV. 16 *grid current [A] (zone 2)*

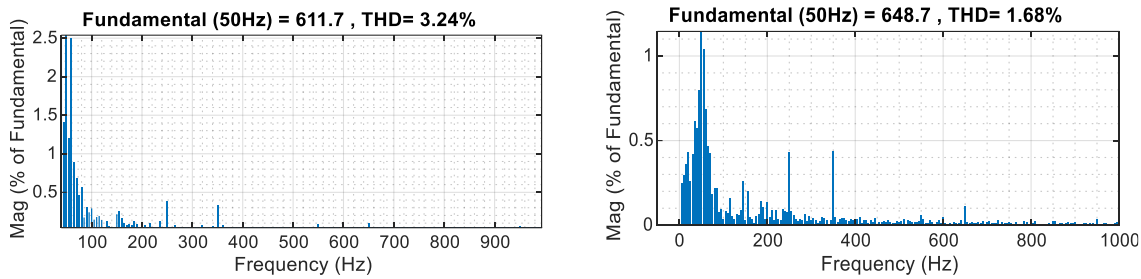

Figure IV. 17 *THD comparisons between STC and ASTC (step wind)*

IV.7.2 Second test:

This test will evaluate the effectiveness of the BSC in zone 3, featuring pitch control, under varying wind speeds. A comparative study is conducted to assess the performance of BSC in comparison PI control methodologies. The comparison assesses different characteristics, such as reference tracking, active and reactive power fluctuations, and settling time. Zone 3 demonstrates a significantly higher level of mechanical stress. Therefore, it is crucial to maintain a constant rotating speed of 188.5 rad/s without any variations. The simulation

produced outcomes for the three variables being manipulated. Figure IV.18 illustrates the sequential stages of the wind profile. Figure IV.19 displays the operating performance of a WECS employing three different control methods: PI control, and the innovative BSC with pitch control in zone 3. Figure 11a illustrates the velocity response. The BSC outperforms the PI in reducing speed fluctuations, achieving faster stabilization, lowering steady-state error, overshooting, and improving tracking accuracy. Our observations indicate that BSC demonstrates greater tracking performance in comparison to PI. The suggested BSC has a significantly lower overshoot of 0.15% in comparison to the PI, which display overshoot values of 0.40% and 0.60% respectively. In terms of settling time, the BSC has an initial settling time of 10 ms, , the PI controller requires 40 ms. Upon examining the speed curves of the reference, it is clear that the PI controller (with a steady-state error of 3.6%) exhibit discrepancies. Nevertheless, the BSC implementation significantly decreases this inaccuracy to 0.23%, as indicated in Table 5.

Table IV. 5 *Overshoot and response time of the mechanical speed*

Controller	Overshoot ratio (%)	Response time (ms)	Steady-state error (%)
PI	0.60	40	3.6
BSC	0.15	10	0.23

Figure IV.20 demonstrates the consistent stability of the DC-bus voltage control, even in the presence of a sudden change in wind speed in Zone 3, with the implementation of pitch control. The ASTC shows a deviation of 0.1% beyond the recommended voltage value. A response time of around 5 ms is sufficient for a DC voltage to achieve a stable state at the desired value. Contrary to the STC and PI, it demonstrates a response time of 30 ms and an overshoot of 0.33%, and a response time of 40 ms and an overshoot of 0.54%, respectively. The outcome is presented in Table 6.

Table IV. 6 *Overshoot and response time of the DC-link voltage*

Controller	Overshoot ratio (%)	Response time (ms)
PI	0.54	40
STC	0.33	30
ASTC	0.11	5

Figure IV.21 depicts the active power, which exhibits peaks when there are fluctuations in wind velocity. The presence of these peaks is solely attributed to the extremely intense wind profile illustrated in Figure IV.18. Turbulence can happen, but its impact is milder compared to the consequences caused by sudden changes. The peaks acquired using ASTC

demonstrate a lesser magnitude compared to those obtained using STC and PI. The Qg in Figure IV.22 remains constant as changes in wind speed have no effect on it. Active power generation involves the direct injection of electric current into the grid to ensure that the current waveform fulfills the frequency and quality standards established in the network code Figure IV.23.

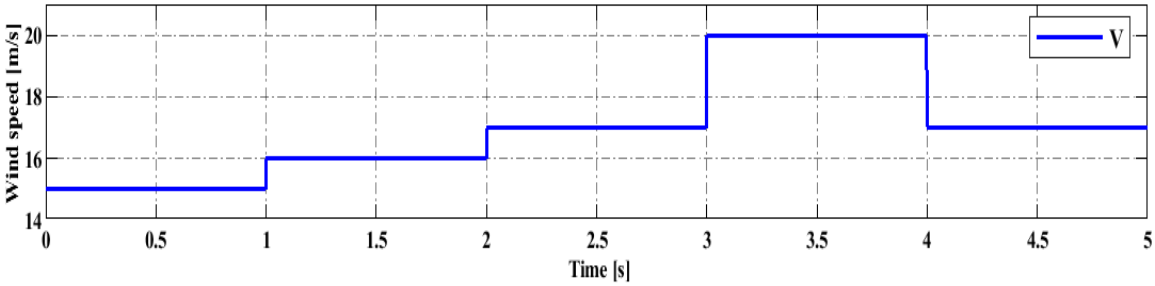

Figure IV. 18 *step wind [m/s] (zone 3)*

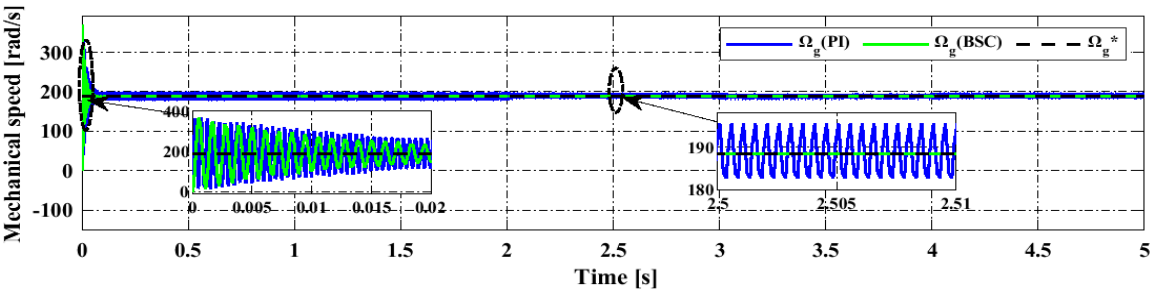

Figure IV. 19 *mechanical velocity [rad/s] (zone 3)*

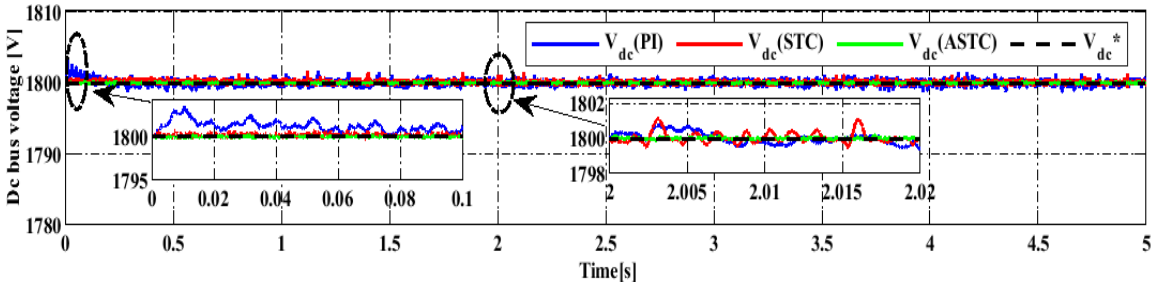

Figure IV. 20 *Dc bus voltage [V]*

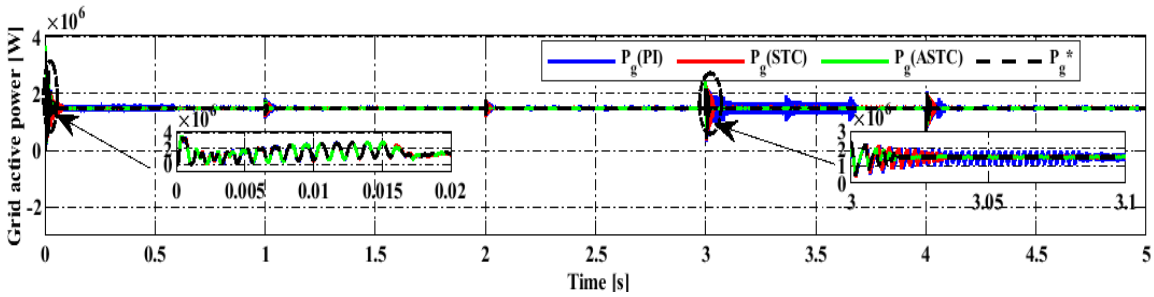

Figure IV. 21 *Active power [W]*

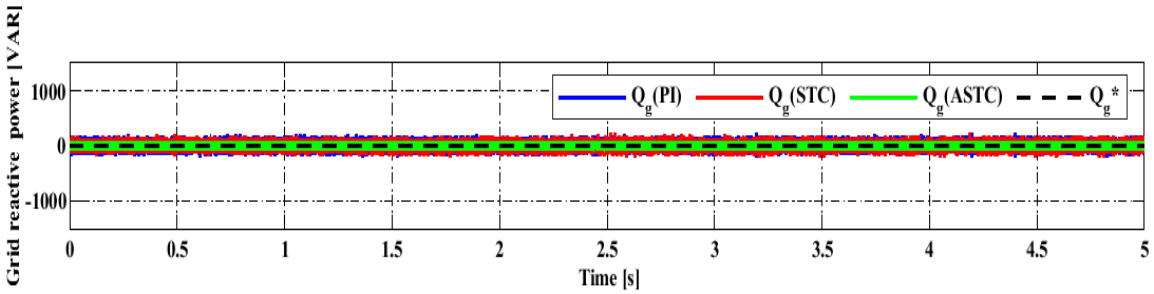

Figure IV. 22 *Reactive power [VAR]*

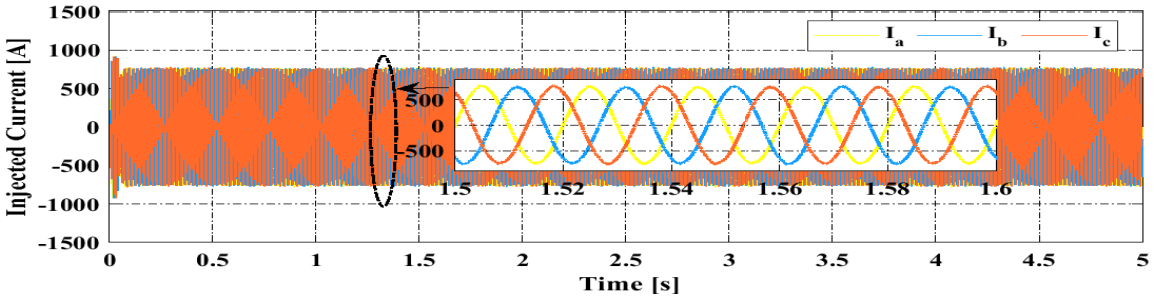

Figure IV. 23 *grid current [A](zone 3)*

IV.7.3 Third test

The previous test is insufficient for validating the controllers. In a meteorological context, they do not accurately represent real wind conditions. Therefore, for the second test, we employed a random wind profile from Figure IV.24 in zone 2. Similar to the initial test, Figure IV.25 demonstrates the correlation between the mechanical speed, obtained by MPPT techniques, and the wind profile. The MPPT-BSC outperforms the MPPT-PI in terms of speed fluctuations, settling time, steady-state error, and overshoot. The suggested BSC has a significantly lower overshoot of 0.1% compared to the existing PI controllers, which have overshoot values of 0.35% and 0.53% respectively. Regarding settling time, the BSC has an initial settling time of 5 ms, the PI controller requires 40 ms. Upon comparing the speed curves to the reference, it is evident that both the PI controller (with a steady-state error of 3.6%). However, the BSC implementation decreases the steady-state error to 0.33%, as indicated in Table 7.

Table IV. 7 *: Overshoot and response time of the mechanical speed*

Controller	**Overshoot ratio (%)**	**Response time (ms)**	**Steady-state error (%)**
PI	0.53	40	3.6
BSC	0.1	5	0.33

Figure IV.26 illustrates the excitation current of HESG, highlighting the superior performance of BSC compared to PI in terms of a setting time of less than 10 ms. The inverse of the typical STC displays a reaction time of 30 milliseconds, but the PI shows a reaction time of 40 milliseconds. Furthermore, the BSC exhibits exceptional reference tracking abilities, surpassing the PI. The results suggest that the regulation of the DC-link voltage is efficiently managed when there is a random wind, as depicted in Figure IV.27. The ASTC demonstrates a deviation of 0.1% above the nominal voltage value. A response time of approximately 5 ms is sufficient for the DC voltage to achieve a stable condition at the desired value. Contrary to the STC, it has a response time of 30 ms and an overshoot of 0.33%. The PI controller exhibits a response time of 40 ms and a 0.54% overshoot simultaneously. The outcome is presented in Table 8.

Table IV. 8 *Overshoot and response time of the DC-link voltage*

Controller	Overshoot ratio (%)	Response time (ms)
PI	0.54	40
STC	0.33	30
ASTC	0.11	5

In Figure IV.28, the active power is primarily linked to the wind speed, and its magnitude escalates with higher wind speeds. The Qg in Figure IV.29 remains constant as variations in wind speed do not impact it. Active power generation involves the direct injection of electric current into the grid to ensure that the current waveform matches the frequency and quality standards established in the network code Figure IV.30. The relatively small amount of reactive power in comparison to active power leads to a greater power factor, as depicted in Figure IV.31. Figure IV.32 depicts the THD of grid current for two controllers. The first controller utilizes the STC methodology and exhibits a THD of 2.37%. On the other hand, the second controller employs the innovative ASTC method and demonstrates a THD of 0.7%. The THD was reduced by approximately 70% when using the ASTC compared to the STC. In addition, the use of ASTC led to a substantial improvement in the power efficiency of the HESG-based WECS, achieving an outstanding 98.5%. Based on the data shown in Table 7, this particular controller outperforms both the standard STC and PI controllers, achieving efficiencies of 91.8% and 89.2% respectively.

Table IV. 9 Injected current THD and power efficiency

Controller	Injected current THD (%)	power efficiency (%)
PI	-	82.2
STA	3.24	91.8
ASTC	1.68	98.5

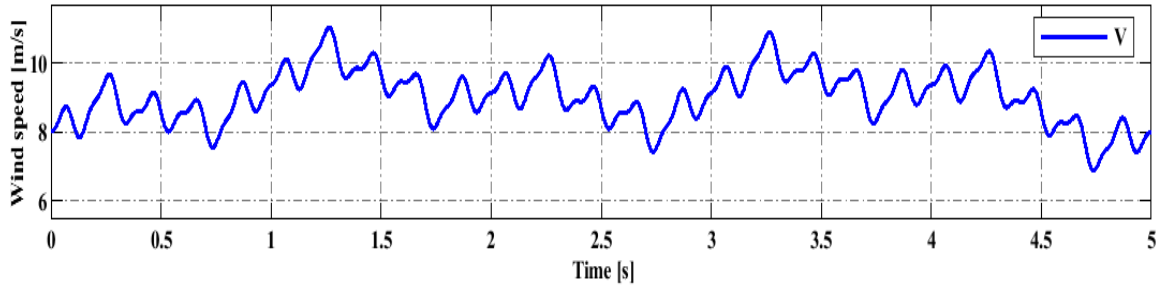

Figure IV. 24 *stochastic wind [m/s] (zone 2)*

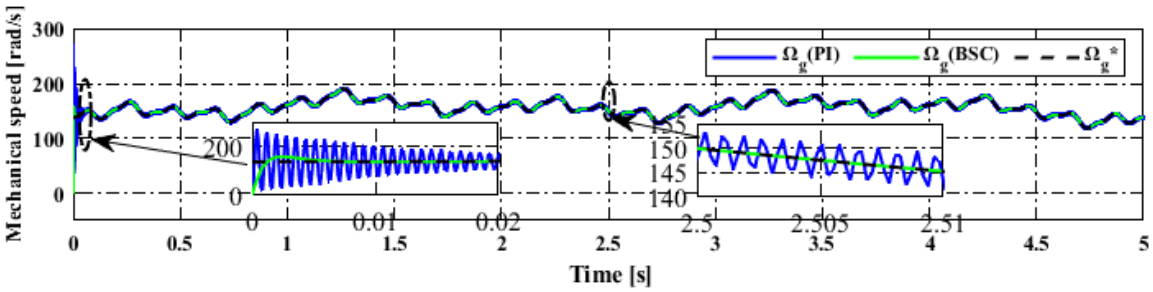

Figure IV. 25 *mechanical speed.*

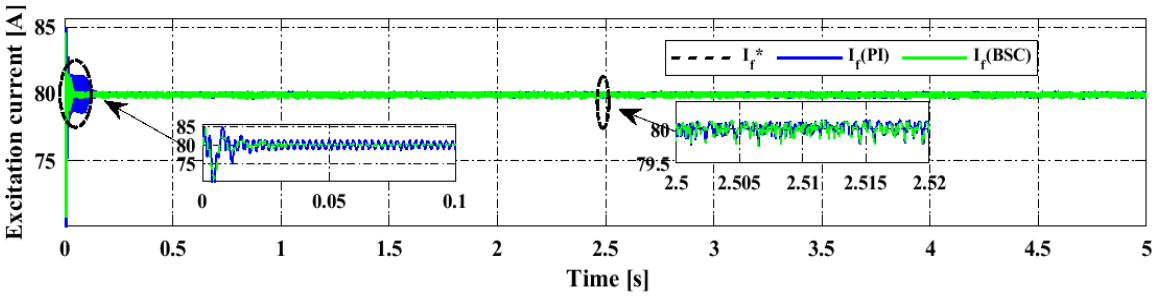

Figure IV. 26 *Excitation current [A] (zone 2)*

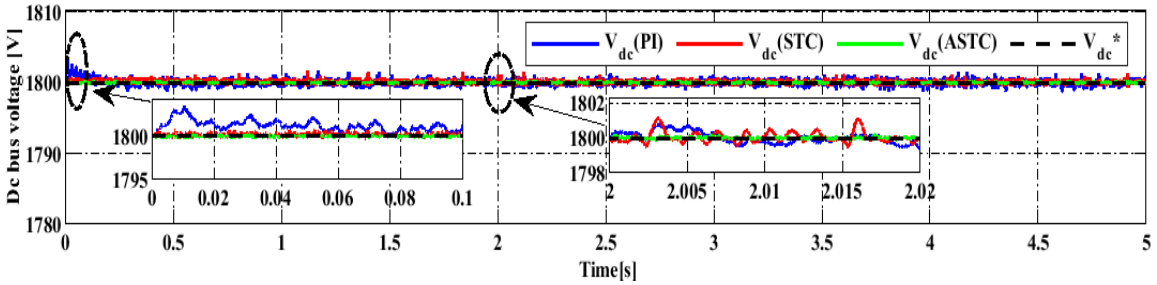

Figure IV. 27 *Dc bus voltage [V]*

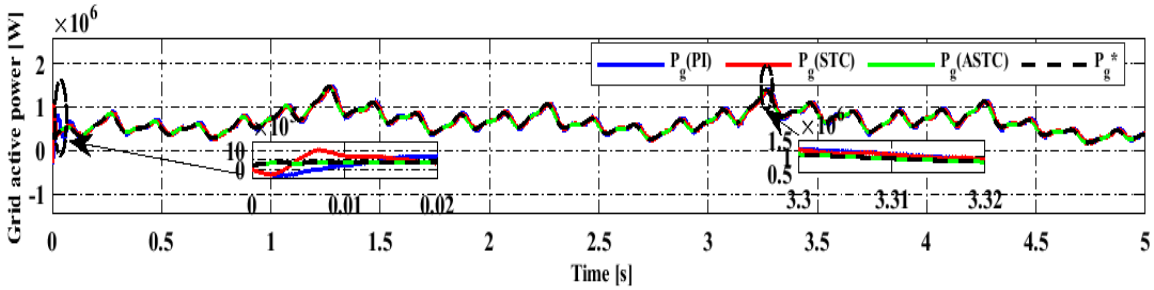

Figure IV. 28 *Active power [W]*

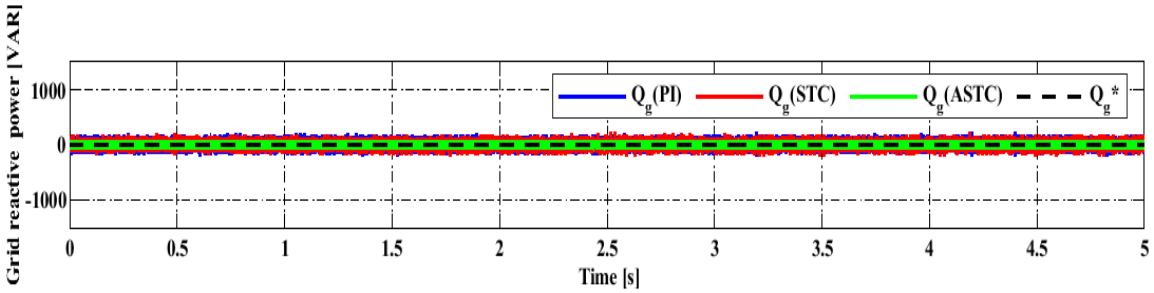

Figure IV. 29 *Reactive power [VAR]*

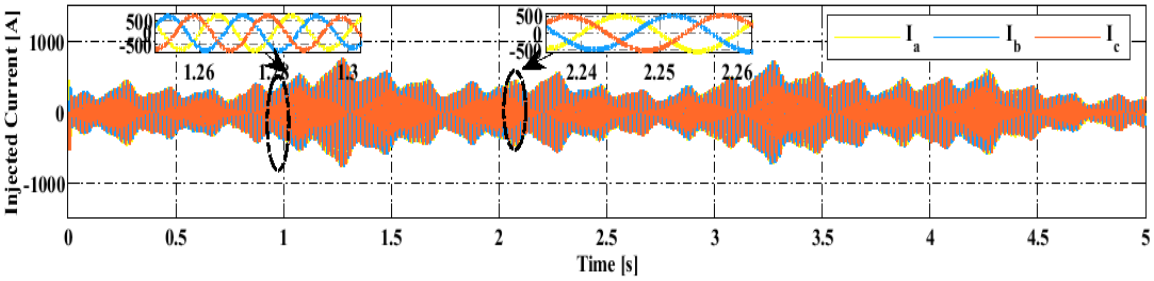

Figure IV. 30 *grid current [A](zone 2)*

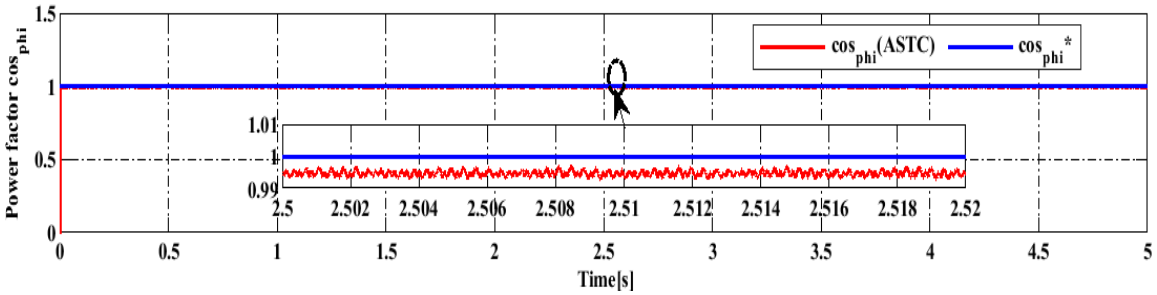

Figure IV. 31 *power factor*

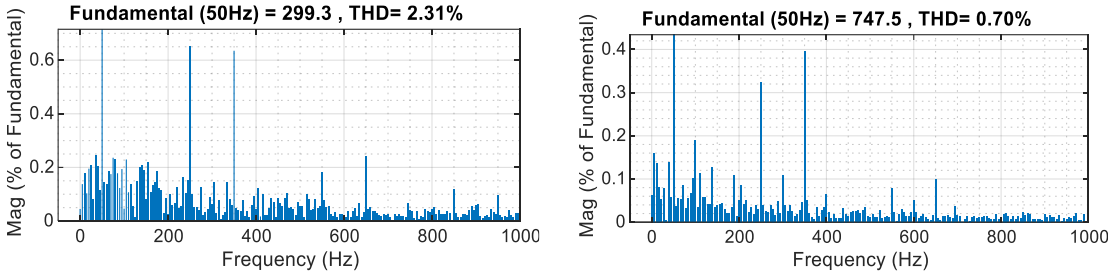

Figure IV. 32 *THD comparisons between STC and ASTC (stochastic wind)*

IV.7.4 Fourth test

The previous test should be more thorough in order to validate the controllers. In a meteorological scenario, they do not accurately represent the current wind conditions. We utilized a stochastic wind profile from Figure IV.33 in zone 3, with pitch control, for this test. Figure IV.33 illustrates the randomness of the wind profile. Figure IV.34 depicts the velocity response in the fourth test. The BSC surpasses the PI in terms of speed variations, settling time, steady-state inaccuracy, overshoot, and tracking. Our findings indicate that BSC demonstrates superior tracking performance compared to PI. The proposed BSC has a notably reduced overshoot of 0.15%, in contrast to the conventional PI controllers, which display overshoot values of 0.40% and 0.60% respectively. The BSC has an initial settling time of 10 milliseconds, upon analyzing the speed curves of the reference, it is evident that both the PI controller (with a steady-state error of 3.6%) and the Table 10 demonstrates the successful reduction of steady-state error to a mere 0.23% by the adoption of BSC. The findings demonstrate that the regulation of the DC-link voltage control is effectively managed when dealing with a random wind in zone 3, utilizing pitch control. This is visually depicted in Figure IV.35. The findings are displayed in Table 11

Table IV. 10 *Overshoot and response time of the mechanical speed*

Controller	Overshoot ratio (%)	Response time (ms)	Steady-state error (%)
PI	0.60	40	3.6
ASTC	0.15	10	0.23

Table IV. 11 *Overshoot and response time of the DC-link voltage*

Controller	Overshoot ratio (%)	Response time (ms)
PI	0.54	40
STC	0.33	30
ASTC	0.11	5

The ASTC controller demonstrates exceptional effectiveness in attenuating mechanical vibration, as evidenced by the diminished oscillatory behavior illustrated in Figure IV.36. Figure IV.37 depicts the active power. The power output is limited to 1.5 MW for wind speeds ranging from 11 m/s to 20 m/s. The Qg in Figure IV.37 remains constant as variations in wind speed do not impact it. Active power generation involves the direct injection of electric current into the grid to ensure that the current waveform fulfills the frequency and quality standards outlined in the network code Figure IV.38.

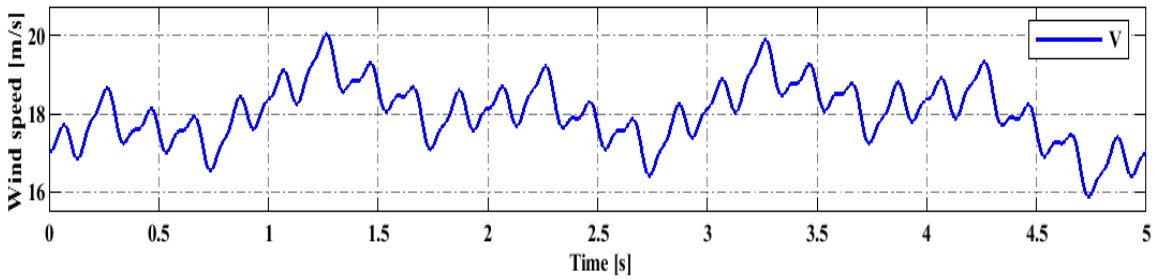

Figure IV. 33 *stochastic wind [m/s] (zone 3).*

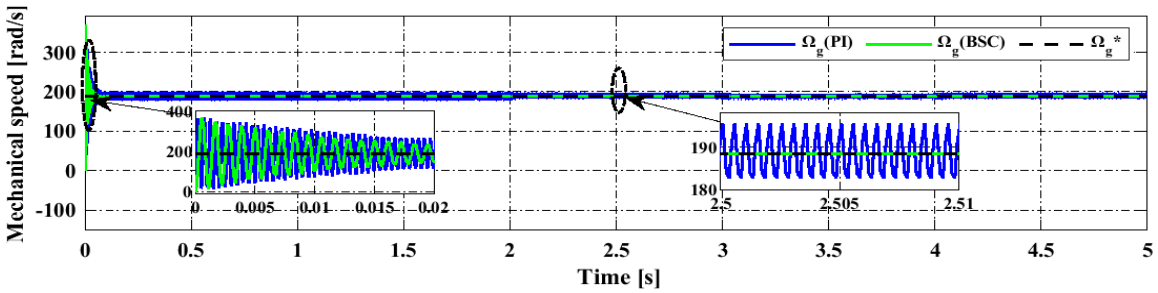

Figure IV. 34 *mechanical velocity [rad/s] (zone 3)*

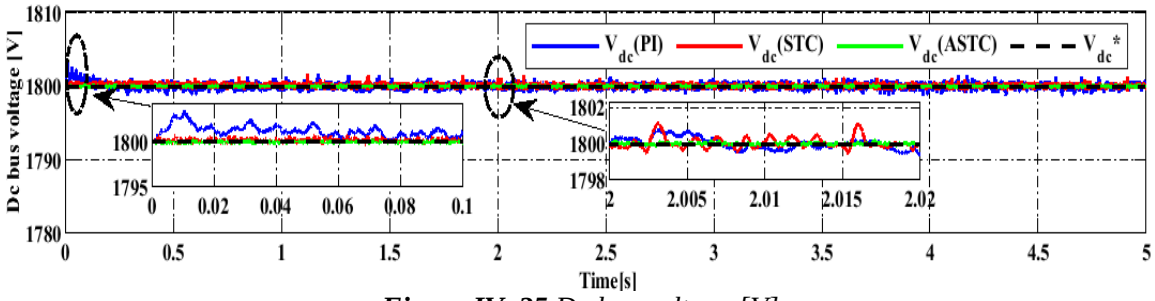

Figure IV. 35 *Dc bus voltage [V]*

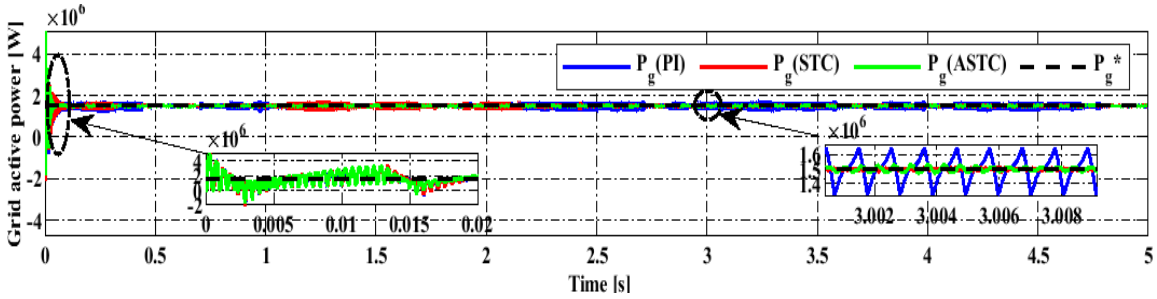

Figure IV. 36 *Active power [W]*

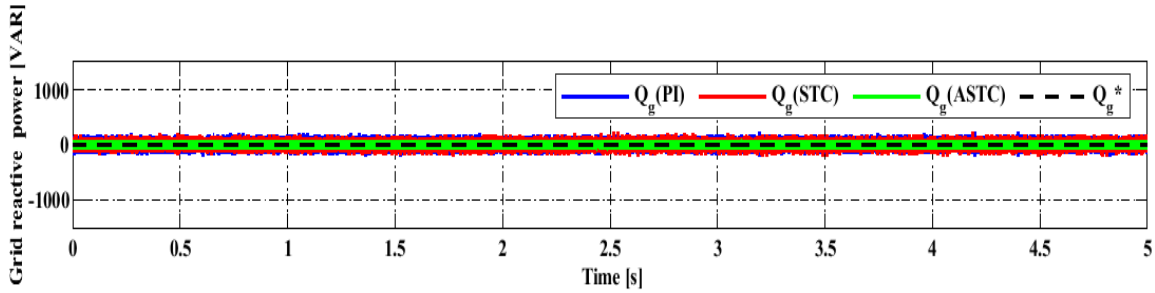

Figure IV. 37 *Reactive power [VAR].*

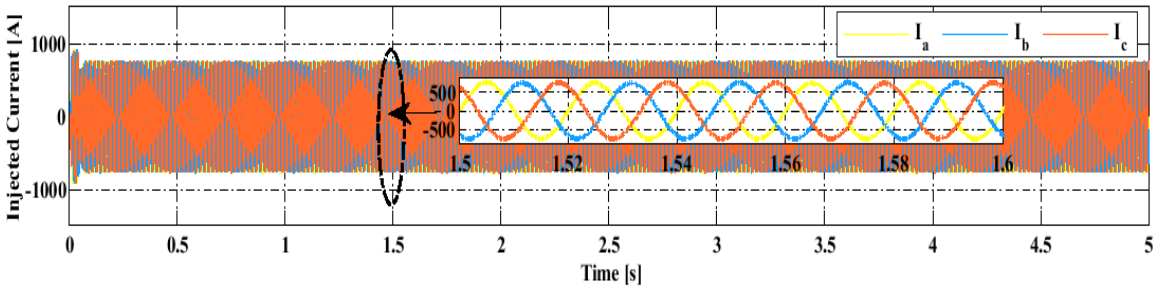

Figure IV. 38 *grid current [A] (zone 3).*

IV.7.5 Five tests (for robustness)

The present test assesses the robustness of the suggested ASTC in comparison to traditional approaches such as PI controllers and STC. To achieve this, deliberate modifications have been made to the machine's settings, as shown below:

The HESG stator resistance value, Rs, has increased by 50% from its initial nominal value.

The inductances, Ld and Lq, have decreased by 50% from their initial nominal values.

The HESG was compelled to function by a 50% augmentation in the overall inertia of the system.

Figure IV.39 depicts an error in generator speed tracking at step-wind speeds. The error in generator speed tracking is smaller with ASTC indicating that the suggested ASTC control is more robust and performs well than STC and PI. Figure IV.40 presents the primary results of the robustness test, specifically the generator speed error (expressed as a percentage) while using the stochastic wind profile. The graphic illustrates that the PI controller displays the largest level of generator speed inaccuracy compared to the other two controllers. Conversely, the proposed ASTC controller exhibits the smallest amount of inaccuracy.

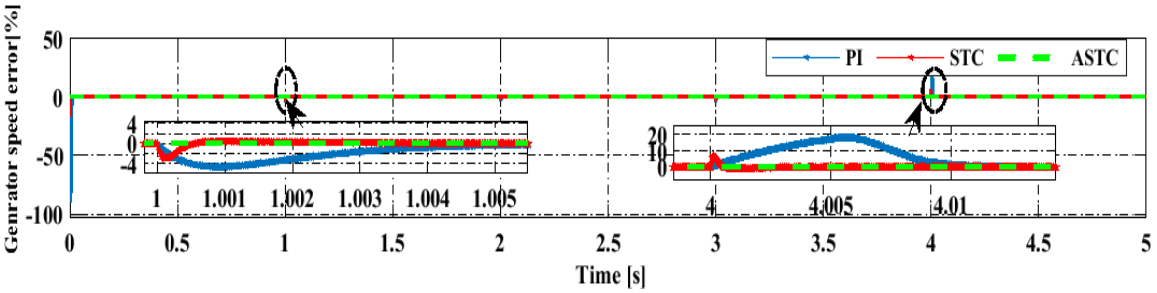

Figure IV. 39 *robustness under step wind*

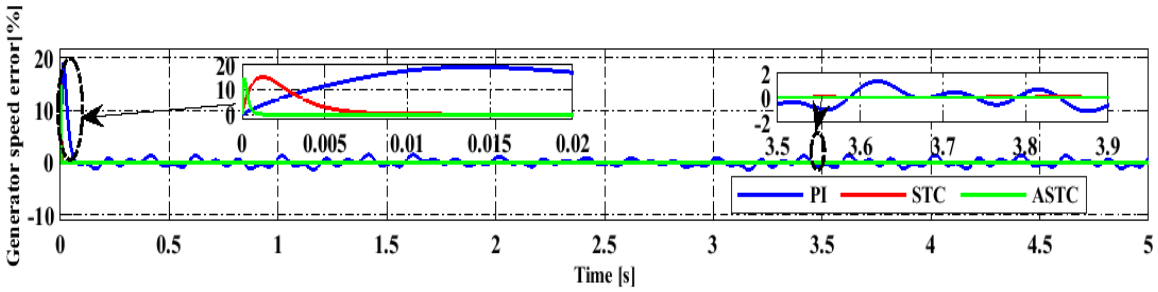

Figure IV. 40 *robustness under stochastic wind.*

IV.8 Conclusion

This chapter focuses on the modeling and control of the grid connection of a wind turbine (WP) based on a HESG. The "behavioral" models of SimPowerSystem are used for modeling the electrical network. A robust control technique is employed in the control scheme to mitigate the significant system nonlinearities resulting from the wind turbine's aerodynamics and the generator's harmonics. The new ASTC is implemented across the entire system, enhancing performance monitoring and robustness compared to conventional STC and PI controllers. Simulation results demonstrate the turbine's strong performance and validate the efficiency of the designed controllers. Reactive power delivered to the grid is zero, while all active power produced is successfully transferred to the grid. Additionally, results confirm that the wind turbine's performance is unaffected during grid disturbances, maintaining stable operation and consistent power delivery. This highlights the system's reliability and robustness in handling grid fluctuations without compromising power quality or efficiency.

General Conclusion

This thesis has undertaken an in-depth study on the implementation and control of Hybrid Excitation Synchronous Generators (HESG) in Wind Energy Conversion Systems (WECS). The primary goal was to explore the potential of HESG in improving the efficiency, reliability, and overall performance of wind turbines, while addressing the inherent challenges of wind energy generation, such as variability and intermittency. The research presented in this thesis is organized into four main chapters, each addressing critical aspects of the problem. This general conclusion provides a comprehensive synthesis of the research findings, highlights the key contributions, discusses the broader implications, identifies limitations, and suggests future research directions.

The global energy landscape is rapidly shifting towards sustainable and renewable energy sources, with wind energy emerging as one of the most promising options due to its abundance and cost-effectiveness. However, the inherent variability of wind poses significant challenges for conventional generator technologies, such as Permanent Magnet Synchronous Generators (PMSG) and Doubly-Fed Induction Generators (DFIG), which struggle to maintain efficiency and stability under fluctuating wind conditions. The need for more robust and adaptable solutions has driven the exploration of advanced generator technologies like HESG, which offer dynamic control over magnetic flux and can potentially improve the performance of WECS across a broader range of operating conditions.

This thesis was motivated by the potential of HESG to overcome the limitations of traditional generators. It aimed to develop and validate advanced control strategies specifically tailored to the unique characteristics of HESG-based WECS. The research was structured around four core chapters, each building on the findings of the previous one to address the overall research objectives.

The first chapter provided a comprehensive review of the evolution and current state of wind turbine technologies. It traced the historical development of wind energy, highlighted the leading global markets, and discussed the advantages and disadvantages of various wind turbine generator technologies. The chapter emphasized the limitations of conventional generators in terms of efficiency, reliability, and control under variable wind conditions. It introduced HESG as a promising alternative, noting its capability to dynamically control magnetic flux and adapt to changing wind conditions. The chapter set the stage for the subsequent research by clearly defining the motivations, objectives, and

scope of the study.

Chapter 2 focused on the development of a comprehensive model of the WECS incorporating HESG. A detailed dynamic model of the HESG was presented, including the modeling of the electrical part in both the real reference frame (a,b,c) and the Park (d,q) reference frame. This model was integrated with the aerodynamic and mechanical models of the wind turbine to form a complete representation of the WECS. The modeling work provided a solid foundation for analyzing the performance of the WECS under various operating conditions and for testing the proposed control strategies. The validation of the model against theoretical predictions confirmed its suitability for simulating the complex interactions within the WECS, paving the way for the control design and analysis in Chapter 3.

Chapter 3 presented the core of the research: the design and implementation of control strategies for HESG-based WECS. The chapter focused on two primary control strategies: the Backstepping Control (BSC) and the Proportional-Integral (PI) control. Backstepping Control (BSC): The BSC strategy was developed for the speed control loop of the wind turbine, providing a structured approach to handle the nonlinear dynamics of the system. The BSC controller was designed to ensure optimal speed tracking under varying wind conditions, with a particular focus on minimizing mechanical stress and improving energy capture efficiency. The controller was rigorously tested through simulations, demonstrating its effectiveness in maintaining stable operation and enhancing the overall performance of the WECS. Proportional-Integral (PI) Control: The PI control strategy was implemented as a baseline for comparison with the BSC controller. While the PI controller is widely used in industrial applications due to its simplicity and ease of implementation, it was shown to be less effective than the BSC in handling the nonlinear and dynamic nature of the WECS. The comparative analysis highlighted the limitations of the PI controller in terms of speed regulation and robustness to disturbances, underscoring the need for more advanced control strategies like BSC. The results of the simulations showed that the BSC controller outperformed the PI controller in several key metrics, including speed regulation, energy capture efficiency, and robustness to parametric variations. This chapter provided a comprehensive evaluation of the control strategies, offering valuable insights into their strengths and weaknesses.

Chapter 4 addressed the critical issue of integrating HESG-based WECS into

electrical grids. A detailed analysis of the grid integration challenges was conducted, focusing on synchronization, voltage regulation, and reactive power management. An Advanced Super-Twisting Control (ASTC) strategy was proposed to manage the interaction between the WECS and the grid, ensuring stable and reliable operation. The chapter also explored the development of a realistic simulation platform for a 1.5 MW WECS, incorporating high-frequency electrical phenomena and flexible mechanical couplings. The simulation results validated the effectiveness of the proposed control strategies in managing grid disturbances and maintaining power quality, paving the way for future research into large-scale integration of HESG-based wind turbine.

The research presented in this thesis makes several significant contributions to the field of wind energy technology. These contributions are discussed in detail below, highlighting their impact on the development of more efficient and reliable wind energy systems.One of the primary contributions of this thesis is the development and validation of innovative control strategies tailored to the unique characteristics of HESG. The Backstepping Control (BSC) and Advanced Super-Twisting Control (ASTC) methods represent a substantial advancement in the control of WECS. The BSC approach offers a systematic method for handling the nonlinear dynamics of wind turbines, ensuring optimal speed regulation and reducing mechanical stress. The ASTC strategy, on the other hand, provides robust control of active and reactive power, enhancing the stability and efficiency of grid-connected WECS. The performance of these controllers was rigorously tested through simulations, demonstrating their effectiveness in a wide range of operating conditions. The development of a comprehensive model of WECS incorporating HESG is another key contribution of this thesis. The model includes detailed representations of the aerodynamic, mechanical, and electrical subsystems, providing a robust platform for analyzing the performance of the system under various operating conditions. This model serves as a valuable tool for researchers and engineers working on the design and optimization of advanced WECS, enabling them to evaluate the impact of different control strategies and system configurations.

The research contributes to the understanding of how HESG-based WECS can be effectively integrated into electrical grids, addressing key challenges such as synchronization, voltage regulation, and reactive power management. The proposed ASTC strategy offers a practical solution for managing the interaction between WECS and the grid, ensuring stable and reliable operation under a wide range of conditions. The

successful implementation of these control strategies in a simulated environment highlights their potential for real-world applications, paving the way for further research and development in this area. The development of a realistic simulation framework for large-scale WECS is a significant contribution to the field. This framework incorporates high-frequency electrical phenomena and flexible mechanical couplings, providing a comprehensive tool for analyzing the performance of WECS in complex grid environments. The simulation results demonstrate the effectiveness of the proposed control strategies in managing grid disturbances and maintaining power quality, supporting the design and optimization of large-scale wind energy systems. The findings of this thesis have significant implications for the development and deployment of wind energy technology:

- Enhanced Efficiency and Reliability: The integration of HESG in WECS, combined with the proposed control strategies, can lead to significant improvements in the efficiency and reliability of wind turbines. This has the potential to lower the cost of wind energy and increase its competitiveness relative to conventional energy sources.
- Reduced Mechanical Stress and Maintenance Costs: The advanced control strategies developed in this thesis help to reduce mechanical stress on turbine components, which can lead to lower maintenance costs and longer operational lifetimes for wind turbines. This is particularly important for large-scale wind farms where maintenance costs can be a significant factor.
- Scalability and Adaptability: The research demonstrates that HESG-based WECS can be effectively scaled to larger systems, making them suitable for a wide range of applications, from small isolated installations to large wind farms connected to the grid. The adaptability of the proposed control strategies to different operating conditions and grid requirements further enhances their applicability.

The findings of this thesis open up several avenues for future research:

- Experimental Validation: Future work should focus on the experimental validation of the proposed control strategies using a physical test bench. This would provide valuable insights into the practical challenges and limitations of implementing these strategies in real-world wind turbines.
- Development of Intelligent Control Algorithms: The use of artificial intelligence and machine learning techniques for the control of HESG-based WECS represents

a promising area for future research. These techniques could be used to develop adaptive and fault-tolerant control strategies that can respond dynamically to changing operating conditions and grid requirements.

- Optimization of HESG Design: Future research could focus on optimizing the design of HESG for specific applications, such as offshore wind farms or isolated power systems. This could involve the development of new materials and manufacturing techniques to improve the performance and reduce the cost of HESG-based WECS.
- Exploration of Multilevel Inverters: The use of multilevel inverters in HESG-based WECS could improve power quality and reduce harmonic distortion. Future research should explore the potential of these technologies to enhance the performance of WECS and their integration with the grid.

In conclusion, this thesis has made significant contributions to the development and control of HESG-based Wind Energy Conversion Systems. The findings provide a solid foundation for future research and development in this area, supporting the continued advancement of wind energy technology as a key component of sustainable energy systems. The innovative control strategies and modeling tools developed in this thesis offer practical solutions for enhancing the efficiency, reliability, and scalability of wind energy systems, contributing to the global transition towards cleaner and more sustainable energy sources.

References

References:

[1] A. Mseddi, *Modélisation et commande d'un générateur éolien à double excitation isolé en vue de l'amélioration de son rendement et de la diminution de la fatigue mécanique*, PhD thesis, Université de Cergy Pontoise; École nationale d'ingénieurs de Sfax, Tunisia, 2019. [Online]. Available: https://theses.hal.science/tel-02888660.

[2] J. K. Kaldellis and D. Zafirakis, "The wind energy (r)evolution: A short review of a long history," *Renewable Energy*, vol. 36, no. 7, pp. 1887–1901, Jul. 2011, doi: https://doi.org/10.1016/j.renene.2011.01.002.

[3] H. Gallas, *Contribution à la Commande d'un Générateur de type Synchrone à Double Excitation dans le cas d'une Application Éolienne et Comparaison avec d'autres Architectures*, PhD thesis, CY Cergy Paris Université; École Nationale d'Ingénieurs de Sfax, 2021. [Online]. Available: https://theses.hal.science/tel-03433652.

[4] A. Ammar, *Modélisation et Optimisation d'un Générateur Synchrone à Double Excitation de Forte Puissance*, PhD thesis, Ecole Centrale de Lille, France, 2013. [Online]. Available: https://theses.hal.science/tel-00907699.

[5] R. Haas, C. Panzer, G. Resch, M. Ragwitz, G. Reece, and A. Held, "A historical review of promotion strategies for electricity from renewable energy sources in EU countries," *Renewable and Sustainable Energy Reviews*, vol. 15, no. 2, pp. 1003–1034, Feb. 2011, doi: https://doi.org/10.1016/j.rser.2010.11.015.

[6] H. Moradi and G. Vossoughi, "Robust control of the variable speed wind turbines in the presence of uncertainties: A comparison between H∞ and PID controllers," *Energy*, vol. 90, pp. 1508–1521, Oct. 2015, doi: https://doi.org/10.1016/j.energy.2015.06.100.

[7] G. S. Kaloi, J. Wang, and M. H. Baloch, "Active and reactive power control of the doubly fed induction generator based on wind energy conversion system," *Energy Reports*, vol. 2, pp. 194–200, 2016, doi: https://doi.org/10.1016/j.egyr.2016.08.001.

[8] International Energy Agency, "Global Energy Review 2020 – Analysis," *IEA*, Apr. 2020. [Online]. Available: https://www.iea.org/reports/global-energy-review-2020.

[9] Global Wind Energy Council, “Global wind report 2019 and 2020,” *Global Wind Energy Council*. [Online]. Available: https://gwec.net/.

[10] S. Roga, S. Bardhan, Y. Kumar, and S. K. Dubey, “Recent technology and challenges of wind energy generation: A review,” *Sustainable Energy Technologies and Assessments*, vol. 52, Part C, 2022, Art. no. 102239, doi: https://doi.org/10.1016/j.seta.2022.102239.

[11] Q. Hassan *et al.*, “Mapping Europe renewable energy landscape: Insights into solar, wind, hydro, and green hydrogen production,” *Technology in Society*, vol. 77, 2024, Art. no. 102535, doi: https://doi.org/10.1016/j.techsoc.2024.102535.

[12] Wind Energy Technologies Office, “20% Wind Energy by 2030: Increasing Wind Energy’s Contribution to U.S. Electricity Supply,” *Energy.gov*, 2017. [Online]. Available: https://www.energy.gov/eere/wind/20-wind-energy-2030-increasing-wind-energys-contribution-us-electricity-supply.

[13] IEA, “World Energy Outlook 2023 – Analysis,” *IEA*, Oct. 24, 2023. [Online]. Available: https://www.iea.org/reports/world-energy-outlook-2023?ref=aretenews.com&language=fr (accessed Mar. 28, 2024).

[14] M. Tiss, “Quelle stratégie énergétique de la Tunisie à l’horizon 2030 ?,” *Leconomiste Maghrebin*, Jan. 19, 2017. [Online]. Available: https://www.leconomistemaghrebin.com/2017/01/19/strategie-energetique-tunisie-horizon-2030/ (accessed Mar. 28, 2024).

[15] Agence Nationale de la Maitrise de l’Energie (ANME), *ANME*. [Online]. Available: https://www.anme.tn/.

[16] H. Abderrezek and K. Gasmi, “Les énergies renouvelables, un pilier de développement de l’agriculture algérienne - Cas de l’énergie éolienne,” *Journal of Renewable Energies*, vol. 19, no. 3, pp. 497–508, Oct. 2023, doi: https://doi.org/10.54966/jreen.v19i3.587.

[17] “Future of wind,” *Irena.org*, Oct. 2019. [Online]. Available: https://www.irena.org/publications/2019/Oct/Future-of-wind.

[18] C. A. Horowitz, “Paris Agreement,” *International Legal Materials*, vol. 55, no. 4, pp. 740–755, Aug. 2016, doi: https://doi.org/10.1017/s0020782900004253.

[19] “LOI n° 2015-992 du 17 août 2015 relative à la transition énergétique pour la croissance verte (1) - Légifrance,” *Gouv.fr*, 2015. [Online]. Available: https://www.legifrance.gouv.fr/loda/id/JORFTEXT000031044385/2021-01-10/.

[20] “Africa Wind Energy Handbook,” *Global Wind Energy Council*. [Online]. Available: https://gwec.net/africa-wind-energy-handbook/ (accessed Oct. 28, 2023).

[21] “E4 Country Profile: Energy Efficiency in Mexico – Analysis,” *IEA*, 2021. [Online]. Available: https://www.iea.org/articles/e4-country-profile-energy-efficiency-in-mexico.

[22] H. Camblong, “Minimisation of the wind perturbations impact on the generation of electricity by variable speed wind turbines,” *pastel.hal.science*, 2003. [Online]. Available: https://pastel.hal.science/pastel-00000679 (accessed Mar. 28, 2024).

[23] Bourillon, “Wind energy — Clean power for generations,” *Renewable Energy*, vol. 16, no. 1–4, pp. 948–953, Jan. 1999, doi: https://doi.org/10.1016/s0960-1481(98)00338-3.

[24] European Wind Energy Association and European Commission. Directorate-General For Energy, *Wind energy: the facts*. Luxembourg: Office For Official Publications Of The European Communities, 1999.

[25] “The World Wind Energy Association,” *Wwindea.org*, Sep. 02, 2019. [Online]. Available: https://wwindea.org/.

[26] C. Jauch, A. D. Hansen, P. Sørensen, and F. Blaabjerg, “Simulation Model of an Active-Stall Fixed-Speed Wind Turbine Controller,” *Wind Engineering*, vol. 28, no. 2, pp. 177–195, Mar. 2004, doi: https://doi.org/10.1260/0309524041211341.

[27] M. Nissenbaum, J. Aramini, and C. Hanning, “Effects of industrial wind turbine noise on sleep and health,” *Noise and Health*, vol. 14, no. 60, p. 237, 2012, doi: https://doi.org/10.4103/1463-1741.102961.

[28] G. Failla and F. Arena, “New perspectives in offshore wind energy,” *Philosophical Transactions of the Royal Society A: Mathematical, Physical and Engineering Sciences*, vol. 373, no. 2035, p. 20140228, Feb. 2015, doi: https://doi.org/10.1098/rsta.2014.0228.

[29] S. Goel and R. Sharma, “Performance evaluation of stand-alone, grid-connected, and hybrid renewable energy systems for rural application: A comparative review,” *Renewable and Sustainable Energy Reviews*, vol. 78, pp. 1378–1389, Oct. 2017, doi: https://doi.org/10.1016/j.rser.2017.05.200.

[30] “Global Energy & CO2 Status Report 2017 – Analysis,” *IEA*. [Online]. Available: https://www.iea.org/reports/global-energy-co2-status-report-2017.

[31] IRENA, “International Renewable Energy Agency (IRENA),” *Irena.org*, 2023. [Online]. Available: https://www.irena.org/.

[32] A. Bouharchouche, E. M. Berkouk, and T. Ghennam, “Control and energy management of a grid-connected hybrid energy system PV-wind with battery energy storage for residential applications,” *2013 Eighth International Conference and Exhibition on Ecological Vehicles and Renewable Energies (EVER)*, Mar. 2013, doi: https://doi.org/10.1109/ever.2013.6521525.

[33] M. K. Singh, S. P. Singh, B. Singh, A. K. Pandey, R. Dixit, and N. Mittal, “Stand alone power generation by 3φ asynchronous generator: A comprehensive survey,” *International Conference on Power, Control and Embedded Systems*, Dec. 2012, doi: https://doi.org/10.1109/icpces.2012.6508085.

[34] R. C. Bansal, “Three-Phase Self-Excited Induction Generators: An Overview,” *IEEE Transactions on Energy Conversion*, vol. 20, no. 2, pp. 292–299, Jun. 2005, doi: https://doi.org/10.1109/tec.2004.842395.

[35] R. C. Bansal, T. S. Bhatti, and D. P. Kothari, “Bibliography on the application of induction generators in nonconventional energy systems,” *IEEE Transactions on Energy Conversion*, vol. 18, no. 3, pp. 433–439, Sep. 2003, doi: https://doi.org/10.1109/TEC.2003.815856.

[36] J. Tamura, “Calculation Method of Losses and Efficiency of Wind Generators,” *Green Energy and Technology*, pp. 25–51, Jan. 2012, doi: https://doi.org/10.1007/978-1-4471-2201-2_2.

[37] Y. Amirat, M. Benbouzid, B. Bensaker, and R. Wamkeue, “The State of the Art of Generators for Wind Energy Conversion Systems,” *Semantic Scholar*, 2007.

[38] S. Hazra and P. S. Sensarma, “Self-excitation and control of an induction

generator in a stand-alone wind energy conversion system," *IET Renewable Power Generation*, vol. 4, no. 4, p. 383, 2010, doi: https://doi.org/10.1049/iet-rpg.2008.0102.

[39] G. K. Kasal and B. Singh, "Voltage and Frequency Controllers for an Asynchronous Generator-Based Isolated Wind Energy Conversion System," *IEEE Transactions on Energy Conversion*, vol. 26, no. 2, pp. 402–416, Jun. 2011, doi: https://doi.org/10.1109/tec.2010.2102029.

[40] S. Sharma and B. Singh, "Variable speed stand-alone wind energy conversion system using synchronous generator," *International Conference on Power, Control and Embedded Systems (ICPES)*, Dec. 2011, doi: https://doi.org/10.1109/icpes.2011.6156617.

[41] T. Zhou and B. Francois, "Energy Management and Power Control of a Hybrid Active Wind Generator for Distributed Power Generation and Grid Integration," *IEEE Transactions on Industrial Electronics*, vol. 58, no. 1, pp. 95–104, Jan. 2011, doi: https://doi.org/10.1109/tie.2010.2046580.

[42] T. Fukami, K. Nakagawa, Y. Kanamaru, and T. Miyamoto, "A Technique for the Steady-State Analysis of a Grid-Connected Permanent-Magnet Induction Generator," *IEEE Transactions on Energy Conversion*, vol. 19, no. 2, pp. 318–324, Jun. 2004, doi: https://doi.org/10.1109/tec.2004.827009.

[43] A. Ivanov and I. Kalanchin, "Application of maximum power point tracker method in wind energy conversion system based on the switched reluctance generator," *2017 International Multi-Conference on Engineering, Computer and Information Sciences (SIBIRCON)*, Sep. 2017, doi: https://doi.org/10.1109/sibircon.2017.8109930.

[44] R. Karthikeyan, K. Vijayakumar, R. Arumugam, and V. Kamaraj, "Design and analysis of a switched reluctance generator for rural electrification in standalone wind energy conversion system," *International Conference on Power and Water Systems (ICPWS)*, Jan. 2009, doi: https://doi.org/10.1109/icpws.2009.5442717.

[45] G. P. Viajante *et al.*, "Study and Dynamic Performance Analysis of a Switched Reluctance Generator 8/6 for Wind Energy Application," *IEEE International Conference on Environment and Electrical Engineering (EEEIC)*, Jun. 2018, doi: https://doi.org/10.1109/eeeic.2018.8493726.

[46] F. Blaabjerg, M. Liserre, and K. Ma, “Power Electronics Converters for Wind Turbine Systems,” *IEEE Transactions on Industry Applications*, vol. 48, no. 2, pp. 708–719, Mar. 2012, doi: https://doi.org/10.1109/tia.2011.2181290.

[47] Herlina, R. Setiabudy, and A. Rahardjo, “Cogging torque reduction by modifying stator teeth and permanent magnet shape on a surface mounted PMSG,” *International Seminar on Intelligent Technology and Its Applications (ISITIA)*, Aug. 2017, doi: https://doi.org/10.1109/isitia.2017.8124085.

[48] K. Kamiev, J. Nerg, J. Pyrhonen, and V. Zaboin, “Hybrid excitation synchronous generators for island operation,” *International Conference on Electrical Machines (ICEM)*, Sep. 2010, doi: https://doi.org/10.1109/icelmach.2010.5608243.

[49] Y. Amara, L. Vido, M. Gabsi, E. Hoang, A. Ahmed, and M. Lecrivain, “Hybrid Excitation Synchronous Machines: Energy-Efficient Solution for Vehicles Propulsion,” *IEEE Transactions on Vehicular Technology*, vol. 58, no. 5, pp. 2137–2149, Jan. 2009, doi: https://doi.org/10.1109/tvt.2008.2009306.

[50] B. Kou, Y. Jin, H. Zhang, L. Zhang, and H. Zhang, “Analysis and Design of Hybrid Excitation Linear Eddy Current Brake,” *IEEE Transactions on Energy Conversion*, vol. 29, no. 2, pp. 496–506, Jun. 2014, doi: https://doi.org/10.1109/tec.2014.2307164.

[51] M. Amrhein and P. T. Krein, “Induction Machine Modeling Approach Based on 3-D Magnetic Equivalent Circuit Framework,” *IEEE Transactions on Energy Conversion*, vol. 25, no. 2, pp. 339–347, Jun. 2010, doi: https://doi.org/10.1109/tec.2010.2046998.

[52] E. Yildiriz, M. Gulec, and M. Aydin, “An Innovative Dual-Rotor Axial-Gap Flux-Switching Permanent-Magnet Machine Topology With Hybrid Excitation,” *IEEE Transactions on Magnetics*, vol. 54, no. 11, pp. 1–5, Nov. 2018, doi: https://doi.org/10.1109/tmag.2018.2848878.

[53] Y. Liu and X. Zhang, “Design and Optimization of Hybrid Excitation Synchronous Machines With Magnetic Shunting Rotor for Electric Vehicle Traction Applications,” *IEEE Transactions on Industry Applications*, vol. 53, no. 6, pp. 5252–5261, Nov. 2017, doi: https://doi.org/10.1109/tia.2017.2720671.

[54] K. Berkoune, E. Ben Sedrine, L. Vido, and S. Le Ballois, “Robust control of hybrid excitation synchronous generator for wind applications,” *Mathematics and Computers in Simulation*, vol. 131, pp. 55–75, Jan. 2017, doi: https://doi.org/10.1016/j.matcom.2015.10.002.

[55] M. Cheraghi and M. Karimi, “Optimal design of a Hybrid Excited Doubly Salient Permanent Magnet generator for wind turbine application,” *7th Power Electronics, Drive Systems & Technologies Conference (PEDSTC)*, Jan. 2017, doi: https://doi.org/10.1109/pedstc.2017.7910344.

[56] S. Asfirane, S. Hlioui, Y. Amara, and M. Gabsi, “Study of a Hybrid Excitation Synchronous Machine: Modeling and Experimental Validation,” *Mathematical and Computational Applications*, vol. 24, no. 2, p. 34, Mar. 2019, doi: https://doi.org/10.3390/mca24020034.

[57] Y. Wang and Z. Deng, “A Controllable Power Distribution Strategy for Open Winding Hybrid Excitation Generator System,” *IEEE Transactions on Energy Conversion*, vol. 32, no. 1, pp. 122–136, Mar. 2017, doi: https://doi.org/10.1109/tec.2016.2616414.

[58] A. Nasr, S. Hlioui, M. Gabsi, M. Mairie, and D. Lalevee, “Design Optimization of a Hybrid-Excited Flux-Switching Machine for Aircraft-Safe DC Power Generation Using a Diode Bridge Rectifier,” *IEEE Transactions on Industrial Electronics*, vol. 64, no. 12, pp. 9896–9904, Dec. 2017, doi: https://doi.org/10.1109/TIE.2017.2726974.

[59] E. Sulaiman, T. Kosaka, and N. Matsui, “Design and analysis of high-power/high-torque density dual excitation switched-flux machine for traction drive in HEVs,” *Renewable and Sustainable Energy Reviews*, vol. 34, pp. 517–524, Jun. 2014, doi: https://doi.org/10.1016/j.rser.2014.03.030.

[60] W. Hua, M. Cheng, and G. Zhang, “A Novel Hybrid Excitation Flux-Switching Motor for Hybrid Vehicles,” *IEEE Transactions on Magnetics*, vol. 45, no. 10, pp. 4728–4731, Sep. 2009, doi: https://doi.org/10.1109/tmag.2009.2022497.

[61] J. T. Chen, Z. Q. Zhu, S. Iwasaki, and R. Deodhar, “A Novel Hybrid-Excited Switched-Flux Brushless AC Machine for EV/HEV Applications,” *IEEE Transactions on Vehicular Technology*, vol. 60, no. 4, pp. 1365–1373, May 2011, doi:

https://doi.org/10.1109/tvt.2011.2132811.

[62] H. Hua and Z. Q. Zhu, “Novel Parallel Hybrid Excited Machines With Separate Stators,” *IEEE Transactions on Energy Conversion*, vol. 31, no. 3, pp. 1212–1220, Sep. 2016, doi: https://doi.org/10.1109/tec.2016.2553149.

[63] Q. Wang and S. Niu, “A Novel Hybrid-Excited Dual-PM Machine With Bidirectional Flux Modulation,” *IEEE Transactions on Energy Conversion*, vol. 32, no. 2, pp. 424–435, Jun. 2017, doi: https://doi.org/10.1109/tec.2017.2649574.

[64] J. Druant, H. Vansompel, F. De Belie, J. Melkebeek, and P. Sergeant, “Torque Analysis on a Double Rotor Electrical Variable Transmission With Hybrid Excitation,” *IEEE Transactions on Industrial Electronics*, vol. 64, no. 1, pp. 60–68, Jan. 2017, doi: https://doi.org/10.1109/tie.2016.2608768.

[65] Y. Wang and Z.-Q. Deng, “A Position Sensorless Method for Direct Torque Control With Space Vector Modulation of Hybrid Excitation Flux-Switching Generator,” *IEEE Transactions on Energy Conversion*, vol. 27, no. 4, pp. 912–921, Dec. 2012, doi: https://doi.org/10.1109/tec.2012.2210718.

[66] F. Xinghe and Z. Jibin, “Numerical Analysis on the Magnetic Field of Hybrid Exciting Synchronous Generator,” *IEEE Transactions on Magnetics*, vol. 45, no. 10, pp. 4590–4593, Oct. 2009, doi: https://doi.org/10.1109/tmag.2009.2023625.

[67] C. D. Syverson, “Hybrid alternator.” [Online]. Available: https://patents.google.com/patent/US5397975A/en (accessed Mar. 28, 2024).

[68] Y. Wu, L. Sun, Z. Zhang, Z. Miao, and C. Liu, “Analysis of Torque Characteristics of Parallel Hybrid Excitation Machine Drives With Sinusoidal and Rectangular Current Excitations,” *IEEE Transactions on Magnetics*, vol. 54, no. 11, pp. 1–5, Nov. 2018, doi: https://doi.org/10.1109/tmag.2018.2828642.

[69] M. Shi, B. Zhou, J. Wei, Z. Zhang, Y. Mao, and C. Han, “Design and Practical Implementation of a Novel Variable-Speed Generation System,” *IEEE Transactions on Industrial Electronics*, vol. 58, no. 11, pp. 5032–5040, Nov. 2011, doi: https://doi.org/10.1109/tie.2011.2148677.

[70] Z. Zhang, S. Ma, J. Dai, and Y. Yan, “Investigation of Hybrid Excitation Synchronous Machines With Axial Auxiliary Air-Gaps and Non-Uniform Air-Gaps,”

IEEE Transactions on Industry Applications, vol. 50, no. 3, pp. 1729–1737, May 2014, doi: https://doi.org/10.1109/tia.2013.2282937.

[71] Z. Zhang, J. Dai, C. Dai, and Y. Yan, "Design Considerations of a Hybrid Excitation Synchronous Machine with Magnetic Shunt Rotor," *IEEE Transactions on Magnetics*, vol. 49, no. 11, pp. 5566–5573, Nov. 2013, doi: https://doi.org/10.1109/tmag.2013.2262000.

[72] W. Han, "Control method for electric vehicle hybrid excitation type internal combustion power generation range extending system," Accessed: Mar. 28, 2024. [Online]. Available: https://eureka.patsnap.com/patent-CN108407624A.

[73] M. Hendijanizadeh, S. M. Sharkh, and A. A. Qazalbash, "Comparison of PM and Hybrid Excited Machines for Marine Vessel Hybrid-Electric Propulsion," *2018 International Conference on Electrical Machines (ICEM)*, Sep. 2018, doi: https://doi.org/10.1109/icelmach.2018.8507207.

[74] K. Kamiev, A. Parviainen, and J. Pyrhönen, "Hybrid excitation synchronous generators for small hydropower plants," *International Conference on Electrical Machines (ICEM)*, Sep. 2016, doi: https://doi.org/10.1109/icelmach.2016.7732877.

[75] R. Mbayed, "Contribution to the Control of the Hybrid Excitation Synchronous Machine for Embedded Applications," 2012. Accessed: Mar. 28, 2024. [Online]. Available: https://theses.hal.science/tel-00837741.

[76] P. J. Schubel and R. J. Crossley, "Wind Turbine Blade Design," *Energies*, vol. 5, no. 9, pp. 3425–3449, Sep. 2012, doi: https://doi.org/10.3390/en5093425.

[77] J. G. Njiri and D. Söffker, "State-of-the-art in wind turbine control: Trends and challenges," *Renewable and Sustainable Energy Reviews*, vol. 60, pp. 377–393, Jul. 2016, doi: https://doi.org/10.1016/j.rser.2016.01.110.

[78] A. Yahdou, "Commande hybride par mode glissant d'ordre 2 d'un système eolien à double rotor," *repository.enp.edu.dz*, 2017. [Online]. Available: http://repository.enp.edu.dz/xmlui/handle/123456789/987 (accessed Jun. 20, 2024).

[79] S. Kadi, H. Benbouhenni, E. Abdelkarim, K. Imarazene, and E. M. Berkouk, "Implementation of third-order sliding mode for power control and maximum power point tracking in DFIG-based wind energy systems," *Energy Reports*, vol. 10, pp. 3561–

3579, Nov. 2023, doi: https://doi.org/10.1016/j.egyr.2023.09.187.

[80] M. Rapin and J. M. Noël, *L'énergie éolienne: Principes, Etudes de cas*, Accessed: Jun. 20, 2024. [Online]. Available: https://www.decitre.fr/livres/l-energie-eolienne-9782100508013.html.

[81] M. A. Salman and S. K. Kadhim, "Optimal Backstepping Controller Design for Prosthetic Knee Joint," *Journal Européen des Systèmes Automatisés*, vol. 55, no. 1, pp. 49–59, Feb. 2022, doi: https://doi.org/10.18280/jesa.550105.

[82] B. Bossoufi *et al.*, "DSPACE-based implementation for observer backstepping power control of DFIG wind turbine," *IET Electric Power Applications*, vol. 14, no. 12, pp. 2395–2403, Sep. 2020, doi: https://doi.org/10.1049/iet-epa.2020.0364.

[83] G. Tao and W. Li, "Higher-order tracking properties of adaptive backstepping control systems," *Automatica*, vol. 153, p. 111019, Jul. 2023, doi: https://doi.org/10.1016/j.automatica.2023.111019.

[84] W. M. Kacemi, E. Bounadja, A. B. Djilali, A. Iqbal, and K. Fettah, "Enhanced Backstepping Control for HESG-Based Wind Conversion Systems in MPPT Applications," *Journal Européen des Systèmes Automatisés*, vol. 57, no. 1, pp. 273–280, Feb. 2024, doi: https://doi.org/10.18280/jesa.570126.

[85] R. Rathi and K. S. Sandhu, "Comparative analysis of MPPT algorithms using wind turbines with different dimensions & ratings," *International Conference on Power Electronics, Intelligent Control and Energy Systems (ICPEICES)*, Jul. 2016, doi: https://doi.org/10.1109/icpeices.2016.7853107.

[86] Z. Li, B. Li, M. Yu, C. Yu, and P. Shen, "Amorphous metallic ultrathin nanostructures : A latent ultra-high-density atomic-level catalyst for electrochemical energy conversion," *International Journal of Hydrogen Energy*, vol. 47, no. 63, pp. 26956–26977, Jul. 2022, doi: https://doi.org/10.1016/j.ijhydene.2022.06.049.

[87] N. Khezami, *Commande multimodèle optimale des éoliennes : application à la participation des éoliennes au réglage de la fréquence*, PhD thesis, Ecole Centrale de Lille; École supérieure des sciences et techniques, Tunis, 2011. [Online]. Available: https://theses.hal.science/tel-00675623.

[88] N. Laverdure, *Sur l'intégration des générateurs éoliens dans les réseaux faibles ou insulaires*, PhD thesis, Institut National Polytechnique de Grenoble - INPG, 2005. [Online]. Available: https://theses.hal.science/tel-00170128.

[89] H. Kim, H. Choi, H. Kang, J. An, S. Yeom, and T. Hong, "A systematic review of the smart energy conservation system: From smart homes to sustainable smart cities," *Renewable and Sustainable Energy Reviews*, vol. 140, p. 110755, Apr. 2021, doi: https://doi.org/10.1016/j.rser.2021.110755..

[90] S. El Aimani and B. Robyns, "Modélisation des différentes technologies d'éoliennes intégrées dans un réseau de moyenne tension," *theses.fr*, Jan. 01, 2004. [Online]. Available: https://theses.fr/2004ECLI0004 (accessed Jun. 20, 2024).

[91] B. Yan *et al.*, "A Novel, Stable, and Economic Power Sharing Scheme for an Autonomous Microgrid in the Energy Internet," *Energies*, vol. 8, no. 11, pp. 12741–12764, Nov. 2015, doi: https://doi.org/10.3390/en81112338.

[92] D. Ikni, M. S. Camara, M. B. Camara, B. Dakyo, and H. Gualous, "Permanent Magnet Synchronous Generators for Large Offshore wind farm connected to Grid - Comparative study between DC and AC configurations," *International Journal of Renewable Energy Research*, vol. 4, no. 2, pp. 519–527, Jun. 2014. [Online]. Available: https://dergipark.org.tr/en/pub/ijrer/issue/16075/168122 (accessed Jun. 20, 2024).

[93] S. Li, T. A. Haskew, K. A. Williams, and R. P. Swatloski, "Control of DFIG Wind Turbine With Direct-Current Vector Control Configuration," *IEEE Transactions on Sustainable Energy*, vol. 3, no. 1, pp. 1–11, Jan. 2012, doi: https://doi.org/10.1109/TSTE.2011.2167001.

[94] S. Li, T. A. Haskew, R. P. Swatloski, and W. Gathings, "Optimal and Direct-Current Vector Control of Direct-Driven PMSG Wind Turbines," *IEEE Transactions on Power Electronics*, vol. 27, no. 5, pp. 2325–2337, May 2012, doi: https://doi.org/10.1109/tpel.2011.2174254.

[95] H. Benbouhenni and N. Bizon, "Improved Rotor Flux and Torque Control Based on the Third-Order Sliding Mode Scheme Applied to the Asynchronous Generator for the Single-Rotor Wind Turbine," *Mathematics*, vol. 9, no. 18, p. 2297,

Sep. 2021, doi: https://doi.org/10.3390/math9182297.

[96] H. Benbouhenni and N. Bizon, “Third-Order Sliding Mode Applied to the Direct Field-Oriented Control of the Asynchronous Generator for Variable-Speed Contra-Rotating Wind Turbine Generation Systems,” *Energies*, vol. 14, no. 18, p. 5877, Sep. 2021, doi: https://doi.org/10.3390/en14185877.

[97] H. Benbouhenni and N. Bizon, “A Synergetic Sliding Mode Controller Applied to Direct Field-Oriented Control of Induction Generator-Based Variable Speed Dual-Rotor Wind Turbines,” *Energies*, vol. 14, no. 15, p. 4437, Jul. 2021, doi: https://doi.org/10.3390/en14154437.

[98] I. Sami, S. Ullah, Z. Ali, N. Ullah, and J.-S. Ro, “A Super Twisting Fractional Order Terminal Sliding Mode Control for DFIG-Based Wind Energy Conversion System,” *Energies*, vol. 13, no. 9, p. 2158, May 2020, doi: https://doi.org/10.3390/en13092158.

[99] A. Susperregui, J. M. Herrero, M. I. Martinez, G. Tapia-Otaegui, and X. Blasco, “Multi-Objective Optimisation-Based Tuning of Two Second-Order Sliding-Mode Controller Variants for DFIGs Connected to Non-Ideal Grid Voltage,” *Energies*, vol. 12, no. 19, p. 3782, Oct. 2019, doi: https://doi.org/10.3390/en12193782.

[100] W. Kantas, S. Mendaci, H. Benbouhenni, H. Gasmi, and T. Es-saadi, “Application of third-order sliding mode controller to improve the maximum power point for the photovoltaic system,” *Energy Reports*, vol. 9, pp. 5372–5383, Dec. 2023, doi: https://doi.org/10.1016/j.egyr.2023.04.366.

[101] E. Bounadja, A. B. Djilali, and A. Yahdou, “Modified third-order sliding mode control with adaptive gains for a multiphase PMSG wind turbine under double-phase open fault,” *International Journal of Circuit Theory and Applications*, 2024. doi: https://doi.org/10.1002/cta.4253.

[102] W. Kacemi, E. Bounadja, A. B. Djilali, *et al.*, “Enhancing Wind Energy Conversion Efficiency with Parallel Hybrid Excitation Synchronous Generators based on Second Order Sliding Mode Control,” *Przegląd Elektrotechniczny*, vol. 1, no. 4, pp. 39–44, 2024, doi: https://doi.org/10.15199/48.2024.04.08.

Appendix

Table 1 represents the HESG-based WECS parameter used in this work.

Table 1: *Parameters of HESG-based WECS*

Parameter	Value
Grid parameters	
R_g	0.00095Ω
L_g	0.000303H
DC-link	
C	0.01F
V_{dc}	1800V
HESG	
P_t	1.5 MW
M	1.9 mH
L_d	0.1 mH
L_q	0.18 mH
R_s	0.024 Ω
R_f	0.049 Ω
L_f	0.19 Ω
p	6
φ_{PM}	0.21 Wb
Turbine	
R	55m
rho	1.22Kg/m^3
C_p-max	0.35
J	10000
λ_{opt}	7.07

Table 2 represents the gain values for the controls used in this work.

Table 2 *Parameters of the three controllers*

PI	STC	ASTC
Generator speed		
$K_p = 4.8e^{+09}$	$k_I = 100$	$k_l = 50$
$K_i = 9.8e^{+106}$	$k_2 = 50$	$k_2 = 10$
		$k_3 = 500$
Generator excitation currents		
$K_p = 0.2$	$k_I = 35$	$k_l = 5$
$K_i = 14.6$	$k_2 = 5.3$	$k_2 = 1.49$

		$k_3 = 2.36$
Grid currents		
$k_p = 3.5$	$k_{\mathrm{k}} = 22.35$	$k_t = 14.22$
		$k_2 = 2.5$
$k_i = 246.74$	$k_2 = 1.39$	$k_3 = 22.4$
DC-Link voltage		
$K_p = 61.63$	$k_l = 1000$	$\mathrm{k_I} = 3000$
$K_i = 5900$	$k_2 = 250$	$k_2 = 250$
		$k_3 = 532$